

Dipl.-Ing. Pavel Shcheglov

**Study of Vapour-Plasma Plume during
High Power Fiber Laser Beam
Influence on Metals**

Die vorliegende Arbeit entstand an der BAM Bundesanstalt für Materialforschung und -prüfung.

Impressum

**Study of Vapour-Plasma Plume during
High Power Fiber Laser Beam
Influence on Metals**

2012

Herausgeber:

BAM Bundesanstalt für Materialforschung und -prüfung

Unter den Eichen 87

12205 Berlin

Telefon: +49 30 8104-0

Telefax: +49 30 8112029

E-Mail: info@bam.de

Internet: www.bam.de

Copyright © 2012 by

BAM Bundesanstalt für Materialforschung und -prüfung

Layout: BAM-Referat Z.8

ISSN 1613-4249

ISBN 978-3-9815134-3-1

STUDY OF VAPOUR-PLASMA PLUME DURING HIGH POWER FIBER LASER BEAM INFLUENCE ON METALS

Faculty of Experimental and Theoretical Physics
National Research Nuclear University "MEPhI", Moscow, Russia

Thesis for obtaining academic degree Candidate of Science
(Physics and Mathematics)

Speciality: 01.04.21 Laser Physics

Dipl.-Ing. **Pavel Shcheglov**
from Divnomorskoe, Russia

Supervisors: Dr. Viktor Petrovskiy,
National Research Nuclear University "MEPhI",
Moscow, Russia

Prof. Dr.-Ing. Michael Rethmeier,
BAM Federal Institute for Materials Research and Testing,
Berlin, Germany

Date of defence: 29 February 2012

Berlin 2012

Table of Contents	
List of Figures	VIII
List of Tables	XI
Symbols and Abbreviations	XII
Introduction	1
Einleitung	9
Chapter 1. Interaction between laser radiation and matter during high power laser welding of metals	16
1.1. High power high brightness solid state lasers	17
1.1.1. Thin disc lasers	18
1.1.2. Fiber lasers.....	19
1.1.3. Characteristics of the high power laser beam.....	20
1.1.4. Applications of high power high brightness solid state lasers.....	22
1.1.5. Peculiarities of metal welding processes with high power high brightness solid state lasers	25
1.2. Vapour-plasma plume in high power laser metal welding processes	26
1.2.1. Welding plasma formation	27
1.2.2. Welding plasma state during CO ₂ - and solid state laser welding	29
1.3. Mechanism of metal vapour condensation in welding plume.....	32
1.3.1. Theoretical preconditions	32
1.3.2. Indirect experimental confirmations	36
1.3.3. Optical diagnostics of condensed particles in the welding plume	37
1.3.4. Direct measurement of particle parameters.....	39
1.3.5. Scattering and absorption of laser radiation by condensed metal vapour particles	40
Summary of Chapter 1	42
Chapter 2. Welding plume spectroscopy	44
2.1. Structure of the welding plume	45
2.2. Welding plasma spectroscopy.....	46
2.2.1. Experimental technique.....	46
2.2.2. Emission spectra of the welding plasma.....	48

2.3.	Welding plasma state and its influence on the laser radiation	49
2.3.1.	Interaction with atoms of ambient medium	50
2.3.2.	Absorption by free electrons in plasma	52
2.4.	Influence of the shielding gas on the welding plume	54
2.5.	Welding plume study in the upper part	56
2.5.1.	Spectral pyrometry method	56
2.5.2.	Plume temperature in the upper part.....	57
2.5.3.	High-speed video observation	59
Summary of Chapter 2		61
Chapter 3. Measurement of the probe radiation extinction in the welding plume.....		63
3.1.	Thermal refraction measurement of the transversally propagated probe beam	64
3.1.1.	Thermal refraction effect formation in the welding plume	64
3.1.2.	Determination of the thermal refraction influence degree on the extinction of probe radiation	66
3.2.	Measurement of the 1.3 μm wavelength IR-laser radiation extinction	68
3.2.1.	Experimental technique.....	69
3.2.2.	Temporal dynamics of the probe beam extinction	70
3.2.3.	Spatial distribution of the probe beam extinction	71
3.2.4.	Spatial distribution of the extinction coefficient.....	72
Summary of Chapter 3		76
Chapter 4. Metal vapour condensation effect in fiber laser welding plume medium.....		77
4.1.	Measurement of the condensed particle parameters in the welding plume	78
4.1.1.	Experimental technique.....	79
4.1.2.	Multi-wavelength method.....	80
4.1.3.	Transmission spectra of the welding plume.....	82
4.1.4.	Measurement of the averaged condensed particle parameters.....	84
4.2.	Estimation of the welding plume influence on the high power fiber laser radiation.....	87

4.2.1.	Metal vapour condensation under the influence of high power laser radiation.....	87
4.2.2.	Estimation of the high power fiber laser beam attenuation when propagating through the welding plume medium.....	90
Summary of Chapter 4	92
Conclusions	94
Zusammenfassung	95
Literature	97
Acknowledgments	108
Curriculum Vitae	109

List of Figures

Fig. 1.1:	Schemes of diode pumped solid state lasers [13].....	17
Fig. 1.2:	Thin disc laser design (left) [5] and principle of power scaling by the number of discs (right) [13].....	18
Fig. 1.3:	Scheme of the clad-pumped fiber laser [13].....	19
Fig. 1.4:	Longitudinal cross-section of an axially symmetric laser beam propagating along the z axis.....	20
Fig. 1.5:	Process of deep penetration laser metal welding [89]	23
Fig. 1.6:	Characteristic view of the welding defects appeared during 16 mm mild steel plate welding with fiber laser [90].....	24
Fig. 1.7:	Schematical view of the keyhole during deep penetration laser welding [28].....	27
Fig. 1.8:	Plasma emission spectral lines during 10 kW fiber laser welding under Ar-shielding [97]	31
Fig. 1.9	Temperature (a) and Fe mass concentration (b) fields in the vapour-gas plume during the outflow in Ar- (left) or He- (right) medium [48].....	33
Fig. 1.10:	Thermodynamical state of the metal vapour inside and outside the keyhole [48].....	35
Fig. 1.11:	Condensed metal vapour cluster growth in the welding plume; r – cluster radius, h – plume height [52].....	36
Fig. 1.12:	Welding plume during CO₂- (a) and fiber (b) laser welding and luminescence of a carbon aerosol under the influence of a CO₂-laser beam (c) [43],[63],[97].....	37
Fig. 1.13:	Picture of the condensed metal vapour particles sedimented on a glass plate [69].....	39
Fig. 1.14:	Dependency of extinction, absorption and scattering efficiency on particle radius for the radiation wavelength of 1.06 μm [48]	42
Fig. 2.1:	High-speed video observation of different parts of the welding plume	45
Fig. 2.2:	Plume front dynamics: front height vs. time (left) and front speed vs. plume height (right).....	46
Fig. 2.3:	Experimental setup of welding plume emission spectra measurement	47
Fig. 2.4:	Characteristic emission spectra of the lower welding plume part during the welding in air (a), under Ar- (b) and He-shielding (c) atmosphere as well as corresponding Boltzmann plots (d)	49

Fig. 2.5:	Dependency of welding plasma temperature and electron density on laser beam power; plume height is 2 mm	53
Fig. 2.6:	Dependency of the welding plasma temperature on the plume height (calculated from the Boltzmann plotting method; incident laser radiation power 4 kW)	54
Fig. 2.7:	Disappearance of the welding plasma by Ar-supply: (a-c) – welding in air, (d-f) – welding under Ar.....	55
Fig. 2.8:	Panoramic emission spectra of the upper welding plume part in case of welding in air, under Ar and He shielding atmosphere in normal (a) and Wien (b) coordinates.....	58
Fig. 2.9:	Plume temperature in the lower part (determined using Boltzmann plots) and the upper part (measured with spectral pyrometry)	59
Fig. 2.10:	Images of the upper part of the welding plume during welding with front-exhaust (a) and rear-exhaust (b) (original images); (c,d) – highly contrasted images.....	60
Fig. 3.1:	Scheme of the experiment for probe beam thermal refraction measurement when transmitting transversally through the welding plume.....	66
Fig. 3.2:	Deviation of the probe beam spot position on the target surface due to the thermal refraction in the welding plume.....	66
Fig. 3.3:	Dependency of the relative thermal refraction angle on the radiation wavelength	67
Fig. 3.4:	Scheme of the experiment for the measurement of IR probe radiation extinction in the welding plume	69
Fig. 3.5:	Typical form of the probe beam transmission signal during welding	70
Fig. 3.6:	Temporal parameters of the extinction signal	71
Fig. 3.7:	Spatial distributions of the probe beam extinction in longitudinal (a) and transversal (b) direction for different plume heights	72
Fig. 3.8:	Parameters of spatial distribution of the probe radiation extinction over the keyhole.....	74
Fig. 3.9:	Spatial distribution of the probe radiation extinction coefficient above the keyhole; hatched area corresponds to the lower part of the welding plume (welding plasma)	75
Fig. 4.1:	Scheme of experimental setup for welding plume extinction measurement in continuous frequency spectrum.....	79

Fig. 4.2:	Characteristic dependency of the iron particle extinction efficiency ratio on the average particle diameter a_0 for the wavelengths of $\lambda_1 = 300$ nm and $\lambda_2 = 400$ nm on the average particle diameter a_0	83
Fig. 4.3:	Characteristic transmission spectra of the welding plume in near-UV and visible wavelength ranges	84
Fig. 4.4:	Statistical set of transmission spectra (a) and corresponding logarithmic extinction functions (b) during a single welding process	85
Fig. 4.5:	Comparison of the extinction amplitude in continuous (condensed particles) and in linear (metal vapour) spectrum for a measurement series 1-7	86
Fig. 4.6:	Values of the average particle diameter a_0 at different plume height	87
Fig. 4.7:	Logarithmic extinction function spectra corresponding to Fig. 4.9 and extinction efficiency spectra calculated for different particle diameter values a_0 (measured a_0 value is about 80 nm)	88
Fig. 4.8:	Spatial distribution of the condensed metal particle concentration in welding plume at a height of 10 mm	89
Fig. 4.9:	Scheme of probe laser radiation coupling into the optical tract of a high-power fiber laser	90
Fig. 4.10:	Scheme of the scattered probe radiation registration	91
Fig. 4.11:	Emission spectrum of the welding plume with the scattered probe laser radiation line (left) and spectrum of registered signal after monochromator (right)	91
Fig. 4.12:	Characteristic form of the scattered probe laser radiation signal at plume height of 25 mm; A – peaks in the time interval 2.6-3.0 seconds with a high temporal resolution	92

List of Tables

Table 1.1:	Beam quality characteristics for different industrial laser types	22
Table 4.1:	Chemical composition of sedimented particles from the welding plume [69].....	40
Table 4.2:	Values of the complex refractive index for iron particles at different wavelengths [128],[129]	82

Symbols and Abbreviations

$A(h)$	spatial extinction distribution function amplitude	
A_{ij}	transition probability	s^{-1}
a	condensed metal vapour particle diameter	nm
a_0	average condensed metal vapour particle diameter	nm
α	beam asymptotic angle	mrad
α_i	ionisation degree	
α_{max}	maximal metal vapour condensation degree	
B	weld width	mm
BPP	beam parameter product.....	mm·mrad
C_{abs}	absorption cross-section	cm^2
C_{ext}	extinction cross-section	cm^2
C_n	volume particle number density.....	cm^{-3}
C_{sca}	scattering cross-section	cm^2
c	speed light in vacuum	m/s
D	collimated beam diameter.....	mm
d	active cylindrical laser rod diameter	cm
$\delta(a)$	delta-function	
$\delta\lambda$	spectrometer measurement accuracy	μm
E_i, E_j	electron energy levels in atom	eV
E_F	electric field intensity	V/m
E	probe beam extinction	
E_0	characteristic internal atom field intensity.....	V/m
E_L	total high-power fiber laser beam attenuation	
e	electron charge.....	C
ε	emittance	
ε_{kin}	free electron kinetic energy	eV
ε_0	vacuum dielectric permittivity	$F \cdot m^{-1}$

f	lens focal distance.....	mm
FM	few-mode laser generation	
G	particle geometrical cross-section.....	cm ²
g_i	energy level statistical weight	
H	penetration depth	mm
h	welding plume height	mm
h_p	Planck constant	J·s
$h_p \nu_{ij}$	quantum energy for transition $E_i \rightarrow E_j$	eV
I	radiation intensity	W/cm ²
I_0	initial beam intensity	W/cm ²
I_1^{Fe}	first-order ionisation potential for Fe-atoms	eV
I_{ij}	emission intensity	W
$I_s(\lambda, T)$	emission spectral intensity.....	W/cm ² ·nm
I_t	transmitted beam intensity	W/cm ²
K_{ib}	inverse Bremsstrahlung absorption coefficient	m ⁻¹
K_{ext}	extinction coefficient.....	m ⁻¹
k_w	weld formation coefficient	
k_b	Boltzmann constant	J·K ⁻¹
k	particle imaginary refractive index	
L	probe beam path length	cm
LM	laser module	
L_{pl}	characteristic length of plasma plume	cm
L_s	plume-screen distance.....	m
l	active cylindrical laser rod length	cm
λ	radiation wavelength	μm
λ_{ij}	quantum wavelength for transition $E_i \rightarrow E_j$	μm
λ_p	probe laser radiation wavelength.....	μm
M^2	beam quality parameter	
MM	multi-mode laser generation	

m_e	electron mass kg
m_{Fe}	Fe-vapour mass concentration
N	total particle number
$N(a)$	size distribution function
N^+, N^{++}, \dots	singly-, doubly-, etc ionized atom number density cm^{-3}
N_i	energy level population
n	refractive index
n_0	neutral Fe-atom volume concentration cm^{-3}
n_{air}	air refractive index in normal conditions
n_{cond}	condensed atom number density cm^{-3}
n_e	free electron volume concentration cm^{-3}
n_m	refractive ambient medium index
n_p	particle complex refractive index
$n(r)$	refractive index spatial distribution function
ν	light wave frequency s^{-1}
ν_c	total electron collision frequency s^{-1}
ν_{ea}	electron-atom collision frequency s^{-1}
ν_{ei}	electron-ion collision frequency s^{-1}
OFC	optical fiber combiner
P	air pressure torr
P	atom polarisation $\text{V}\cdot\text{m}^2$
PL	probe laser
p	gas pressure Pa
Q_{ext}	single particle extinction efficiency
R	beam wave front curvature radius mm
$R(H)$	calculated keyhole outlet radius mm
$R(\lambda, T)$	Planck-function
SM	single-mode laser generation
s	coordinate along the beam trajectory m

σ_c	classical collision cross-sectionm ²
$\sigma_{\omega,\omega}$	Rayleigh light scattering cross sectioncm ²
T	thermodynamical plasma temperatureK
T_0	threshold plasma temperatureK
T_a	actual vapour temperatureK
T_p	saturated vapour temperatureK
t	time s
t_{air}	air temperature °C
\mathcal{G}	vapour supercooling degree
θ, r	polar coordinates
θ_r	thermal refraction anglemrad
V	ionisation potentialeV
$W(h)$	spatial extinction distribution function width mm
w	beam waist radius mm
w_0	focus spot radius mm
ω	light wave circular frequency rad/s
ω_p	Langmuir plasma frequency rad/s
x, y, z	Cartesian coordinates
X_w, Y_w	Wien-coordinates
$\chi^{(1)}(\omega, \omega)$	linear atom susceptibilitym ³
ψ_n, ζ_n	Rikatti-Bessel functions
$\text{Yb}^{3+}:\text{YAG}$	ytterbium ion in yttrium-aluminium garnet crystal
$Z(T)$	partition function of element
z_R	Rayleigh-length mm

Introduction

In the last 5-10 years, thick metal processing technology has obtained a great development potential owing to the creation of principally new types of high power laser radiation sources. A class of high-power high-brightness solid state lasers has appeared which is today composed of fiber lasers based on ytterbium ions [1],[2] and thin disc lasers based on Yb^{3+} :YAG crystals [3],[4],[5]. Principally both of these laser types originated from solid-state lasers with an open optical cavity. As an active element in such systems a crystal or a glass rod doped with rare-earth alloying elements is used. Normally, the active rod is optically pumped by flash-lamps (lamp pump) or by high-power light-emitting diodes (diode-pump). One of the main problems in such lasers which limit their maximal output radiation power is the thermal lensing effect [6]. Since in this case a relatively small active medium volume and a limited heat abstraction possibility basically do not allow effective cooling of the laser active element, essential worsening of the output laser beam quality is unavoidable when the pumping power is increased.

In case of a fiber laser the active rod “narrows” to the size of an optical fiber which owing to a few cores with different refraction index provides total internal radiation reflection at both the laser generation and the pumping wavelengths. Thereby, since the pumping radiation is absorbed in the optical fiber for a distance of some tens meters, the cooling requirements become minimal, whereas the output beam quality is maintained by the optical fiber waveguide properties [7],[8],[9].

In a thin disc laser the contrary occurs, i.e. the active rod “shrinks” to the form of a thin disc. Here, heat is not abstracted from the cylindrical rod surface, but from the plane disc side. Such cooling way avoids temperature drops in the wave front plane of generated radiation and consequently reduces the thermal lensing effect [10],[11]. In order to increase the radiation generation efficiency, a method of multiple pumping radiation passage through the active medium is applied. In design of both the thin disc and the fiber lasers a module principle is actively used where the radiation from a few independent single-mode laser modules of the same type is coupled in a common multi-mode optical fiber [12]. Physical limitations of the output laser beam power in this case are the influence of non-linear optical effects and the optical damage threshold of the output fiber.

Beside the number of economical advantages of fiber and thin disc lasers [10],[13], the high brightness of their radiation allows it to obtain very high power density simultaneously with a high Rayleigh length [14],[15],[16]. This peculiarity is the most important advantage when using such radiation as an energy source in application to deep penetration metal welding [17],[18]. Thick plate laser metal welding technology has a great application potential in some heavy-industry areas like high pressure pipe production, pipe-line construction [19],[20], manufacture of some fusion reactor parts [21],[22] and also shipbuilding [23],[24].

Before the first high-power fiber lasers were developed, high-thickness metal welding was mainly carried out with radiation of CO_2 -gas lasers [25],[26]. As the principle physical differences between high-power high-brightness solid state lasers and CO_2 -lasers, the following features can be highlighted from the point of view of only deep penetration laser

metal welding. First, the radiation of both fiber and thin disc lasers has wavelengths in the near-IR spectral range (1.07 μm and 1.03 μm respectively) which is almost ten times shorter than the IR-radiation of CO₂-gas lasers (10.6 μm). It should be noted in this context that the absorption coefficient of the most steel types is essentially higher for the short-wavelength solid-state laser radiation than for the long-wavelength CO₂-laser radiation [7]. Second, the spatial power density distribution in the laser beam cross-section for the solid-state lasers has a rectangular form [27], whereas the CO₂-gas laser beam has a more Gauss-like power density distribution. Both of the mentioned factors offer an unquestionable advantage in technologies of laser hardening, laser surface modification or laser heat conduction welding of thin metal plates where no keyhole is created [25]. However, in deep penetration laser metal welding they can play a negative role as well. For example, a sharply rectangular distribution of the laser beam power density can lead to abrupt temperature gradients in the weld pool and on the keyhole metal walls which is a destabilizing factor due to the intensification of the Marangoni effect [28],[29],[30]. On the other hand, high absorptivity of the laser beam by metal during keyhole welding can be a hindrance to the effect of laser radiation channelling by multiple reflections from the narrow keyhole metal walls [31],[32],[33].

However, the most differences between the two laser types appear in the process of vapour-plasma welding plume formation and development as well as in the influence of this plume on laser radiation [34],[35],[36],[37]. In a long-term investigation of the deep penetration welding process with CO₂-laser radiation, effects of welding plasma formation and its influence on laser radiation were studied and described in detail [38],[39],[40],[41]. According to the most frequent instance, a cloud of metal vapour is formed over the metal surface when the metal intensively evaporates by high-power laser radiation. The vapour in this cloud has a low free electron concentration, but due to the so-called inverse Bremsstrahlung absorption during collisions with heavy vapour and ambient gas particles, this small number of free electrons absorb some part of the laser beam energy and increase their kinetic energy. When the kinetic energy of the original free electrons becomes high enough for collisional ionisation of iron atoms, they begin to kick out the secondary electrons from the excited states in atoms, i.e. the ionisation and an avalanche increase of the number of free electrons and ions (optical breakdown) occurs [42]. Since in the optical breakdown state almost the whole laser radiation energy is absorbed by plasma, the maximal power density deposited into material is limited by the optical breakdown threshold in high-power CO₂-laser beam welding. This is a considerable limitation, though in many particular cases it was possible to increase the threshold power density value by using some special shielding gases or additional gas supply devices. The optimal mode of CO₂-laser beam metal welding is given in the so-called sub-threshold optical discharge state, where some small part of the laser radiation is absorbed by the free electron cloud, but the electron concentration and the kinetic energy are not high enough to produce an electron avalanche [43]. In this case the welding plasma can exert even some positive stabilizing influence on the welding process.

In case of fiber laser radiation which has a ten times shorter wavelength the inverse Bremsstrahlung absorption coefficient by the free electron cloud is almost a hundred times lower [44]. For this reason, even with essentially higher power densities of the laser beam,

the vapour cloud over the metal surface is not heated up and optical breakdown does not occur [45],[46],[47]. At the same time, the hot metal vapour flowing out of the keyhole becomes strongly supersaturated due to the low temperature of the medium above the metal surface, as it was shown in thermodynamical state simulation of metal vapour inside and outside the keyhole during deep-penetration high power fiber laser welding [48],[49]. Therefore, the possibility of metal vapour volume condensation and of small condensed phase particle formation should be considered. Theoretical estimations based on kinetical description of condensed cluster growth gave the cluster size values ranging from 10 nm to 100 nm [50],[51],[52]. If the volume concentration of such particles in the welding plume medium is high enough, absorption or scattering of a considerable part of the high power fiber laser beam can happen [48],[53],[54],[55]. However, in contrast to the welding plasma plume studied in detail during many-years investigation of high power CO₂-laser metal welding, both the small condensed metal vapour particle parameters and their influence on the welding quality are not known in full at the moment.

Presence of some small absorbing or scattering objects in the welding plume medium was indirectly detected in a few investigations where the plume transparency was measured for probe laser radiation transmitting through the plume in transversal direction parallel to the metal surface [56],[57],[58]. In such configuration, some extinction of the probe laser beam was registered. The reason was however not clear. The possible mechanisms of probe laser radiation extinction in this case are thermal refraction, welding plasma absorption, influence of the small condensed metal vapour particles and of the macroscopic liquid metal drops spattering from the weld pool. Since the measurements were carried out with a low temporal resolution, the extinction dynamics was not described. It is obvious that the character of the temporal extinction changing plays a very important role in understanding the influence of the extinction effect on welding process stability [59],[60]. Beside probe radiation extinction measurement, a high-power solid state laser radiation scattering from the welding plume was examined experimentally [61]. Results revealed the occurrence of laser radiation scattering which was probably caused by some small particles. However, no quantitative description of the observed effect was made. The welding plume form itself gives evidence of the presence some small particles in it. In contrast to the case of high power CO₂-laser metal welding, the geometrical form of the light emitting area characteristically differs from that of the welding plasma plume by looking more like a high-power beam trace propagating through a dusty medium [43],[62],[63],[64].

Direct measurements of the condensed metal vapour particle size and of the chemical composition were carried out in a few experiments by means of particle sedimentation from the welding plume volume on a cold glass plate. Average size and concentration of particles were measured also with different optical diagnostic methods [67],[68],[69], particularly with the multi-wavelength method [65],[66]. Nevertheless, in such arrangement the experiments did not provide sufficient measurement locality and could not give information about the temporal dynamics of the metal vapour condensation effect. This is the reason why the previously obtained data are insufficient to answer the following questions: how the metal vapour condensation process takes place in the area close to the keyhole outlet; which parameters are valid for the small condensed particle cloud (first of all

particle size and concentration) over the metal surface, and how strongly this cloud influences the high-power solid-state laser radiation propagating through it.

These issues have motivated **the present investigation aimed at determining the characteristics of the vapour-plasma welding plume medium generated during high power ytterbium fiber laser welding of low-alloyed mild steel plates and at detecting new physical effects which are able to cause a welding plume influence on the fiber laser beam.**

Scientific novelty of the investigation

A wide complex study of the vapour-gas plume generating during deep penetration ytterbium fiber laser welding of low-alloyed mild steel plates was carried out:

- For the first time, the influences exerted by all possible laser-matter interaction mechanisms (such as absorption and refraction in welding plasma or in metal vapour, thermal refraction on the refractive index gradients, macroscopic liquid metal drop spattering from the weld pool and absorption or scattering on the small condensed metal vapour particles) were determined experimentally in one and the same condition;
- The structure of the vapour-plasma welding plume medium over the keyhole was described and characteristics of laser-induced welding plasma in air or argon shielding atmosphere were measured;
- The average condensed metal vapour particle parameters (particle size and particle volume concentration) were determined by means of optical diagnostics methods;
- For the first time, the presence of small condensed particles was proved experimentally inside the high-power fiber laser beam caustics;
- High-power fiber laser beam attenuation by the cloud of small condensed metal vapour particles during the welding process was estimated.

Scientific and practical importance

The main significance of the investigation lies in the expansion of knowledge about the welding plume state as well as about the interaction mechanisms between laser radiation and welding plume matter during deep-penetration high-power high-brightness fiber laser welding of low-alloyed mild steel. Results of the investigation can be used in the development of thick metal laser welding technologies and in the construction or optimisation of industrial laser welding equipment.

Information about metal vapour condensation processes in a laser-induced plume can find application also in such technologies as deposition of thin layers or formation of nanoscale powders.

Main results and propositions of the investigation

1. During deep-penetration high-power fiber laser welding of low-alloyed mild steel the vapour-plasma welding plume divides into two different parts – the welding plasma and the cloud of small condensed metal vapour particles.

2. The welding plasma occupies the area close to the keyhole outlet and, due to its low electron temperature and free electron density, does not influence the propagating laser radiation and the welding process in whole.
3. The small metal particle cloud is situated over the welding plasma and is created owing to cooling and condensation of hot metal vapour flowing out of the keyhole.
4. The condensed particles have sub-micron sizes (about 60-80 nm) and volume concentration value on the plume axis near 10^{10} cm^{-3} . They are able to absorb laser radiation propagating through the particle cloud.
5. Under the high-power fiber laser beam influence condensed metal particles warm up and generate thermal light emission in the upper part of the welding plume, however, they are not totally evaporated.
6. High-power fiber laser beam attenuation by a small condensed metal vapour particle cloud does not occur uniformly over the welding time and can lead to a significant worsening of the radiation power stability when it reaches the metal surface (in comparison to the initial output fiber laser beam power stability).
7. The oscillation amplitude of the total high-power fiber laser beam attenuation value can reach more than 10% when the beam propagates through the whole condensed metal vapour particle cloud during the welding process. This effect can negatively influence the final thick metal welding quality.

Structure of the dissertation

The dissertation consists of an introduction, four chapters and a conclusion. It is expounded in 107 pages including 45 figures, 3 tables, 55 formulae and a literature index of 130 items.

Brief outline of the dissertation

The first chapter contains a literature review on the subject of interaction between high power laser radiation and matter during deep-penetration laser welding of thick metals. General working principles of high-power high-brightness solid state lasers as well as peculiarities of thick metal welding with these lasers are described. Mechanisms of vapour-plasma formation and development are examined and a comparative analysis of the welding plasma state during high-power CO₂- and solid state laser welding processes is carried out. The mechanism of metal vapour condensation in the welding plume during laser welding is described in detail and a review of the previously used methods of condensed metal particle diagnostics and parameters measurement is given.

In the second chapter results of the welding plasma investigation generated during high-power fiber laser welding of low-alloyed steel plates with different thicknesses are presented. On the basis of high-speed video observation data, a description of the whole welding plume structure is made showing that the welding plume is characterized by the welding plasma (the lower part) and the condensed metal vapour particle emission (the upper part). From the experimentally measured welding plasma emission spectra the parameters of the plasma state (like electron temperature and free electron volume

concentration) are determined in different welding conditions. The inverse Bremsstrahlung absorption coefficient for the fiber laser radiation wavelength is calculated with the obtained plasma parameters and the conclusion is drawn that, due to low temperature and small size, the welding plasma cannot influence laser radiation and welding quality.

In the third chapter a measurement of the probe IR-laser radiation extinction at a wavelength of 1.3 μm when the probe beam propagates transversally through the welding plume during the welding process is described. Before that, the thermal refraction effect of probe radiation on thermal refractive index gradients in the welding plume medium is investigated. It is ascertained that for the configuration used in this experiment the thermal refraction effect is not able to significantly contribute to the total probe beam extinction. Then, measurements of temporal dynamics of the probe beam extinction signal as well as of spatial distributions of the extinction at different welding plume heights are described. With the measured results the full spatial distribution of the extinction coefficient is rebuilt. From the character of the observed extinction signals it is concluded that the extinction cannot be caused by welding plasma absorption, thermal refraction and macroscopic liquid metal drops. The only possible reason of the observed phenomena is a presence of some small metal particles in the welding plume which absorb or scatter the propagating laser radiation.

The fourth chapter is devoted to the average parameters measurement of the condensed metal vapour particles. The measurements of the welding plume wavelength transmission spectra (in transversal direction) are made. Using the multi-wavelength method, the condensed metal particle average size and their volume concentration in the welding plume are determined to be about 60-80 nm and up to 10^{10} cm^{-3} , respectively. It is shown that these parameters correspond to the extinction coefficient measured in chapter 3. By coupling the probe laser radiation directly to the optical tract of the high-power fiber laser particle diagnostics inside the fiber laser beam caustics is carried out. Assuming the particle parameters inside the fiber laser beam caustics being the same with the measured average parameters, the high-power fiber laser beam attenuation is estimated when it propagates through the whole welding plume height.

Author's personal contribution

All presented results and propositions of the investigation were obtained and developed by the author either personally or with his direct participation. The author participated in the arrangement and implementation of all measurements as well as in the processing of all experimental results.

Approval of the presented results

The main results of the dissertation were presented and discussed in the following workshops or conferences:

- 5th International Conference "Laser technologies in welding and materials processing", Katsiveli, Ukraine, 2011;

- 20th International Laser Physics Workshop (LPHYS'11), Sarajevo, Bosnia and Herzegovina, 2011;
- XXII International Science and Technology Conference „Lasers in Science, Technology and Medicine“, Gelendzhik, Russia, 2011;
- 30th International Congress on Applications of Lasers & Electro-Optics (ICALEO-2011), Orlando, FL, USA, 2011;
- Scientific colloquium in the “Institute of laser and information technology problems RAS”, Shatura, Russia, 2012.

Publications

Subjects of this dissertation were presented in 14 publications, of which 4 papers were published in journals and 10 papers or extended abstracts in conference proceedings [70] - [83].

Einleitung

Seit der Entwicklung in der letzten 5 bis 10 Jahren eines grundsätzlich neuen Quelltyps für Hochleistungslaserstrahlung hat die Technologie der Laserbearbeitung von dicken Metallblechen ein großes Entwicklungspotential erhalten. Damit wurde eine neue Klasse der sogenannten Hochleistungsfestkörperlaser mit hoher Strahlqualität geschaffen, zu der derzeit die Faserlaser (in Yb^{3+} -dotierten Glasfasern) [1],[2] und die Scheibenlaser (im Yb^{3+} :YAG-Krystall) [3],[4],[5] gehören. Prinzipiell beruhen diese beiden Lasertypen auf dem Prinzip des Festkörperlasers mit einem offenen optischen Resonator, in dem ein Kristall- bzw. ein Glasstab unter Zusatz eines Seltenerdenmetalls als aktives Element genutzt wird. Das optische Pumpen erfolgt entweder mit Blitzlampen oder mit Hochleistungsdioden. Eines der größten Probleme, welches die Ausgangsleistung der Strahlung solcher Laser begrenzt, ist der Effekt der thermischen Linse [6]. In diesem Fall lässt ein relativ kleines Volumen des Aktivmediums sowie ein eingeschränkter Wärmeentzug eine effektive Abkühlung des aktiven Elements des Lasers nicht zu. Bei einer höheren Pumpleistung führt dieser Umstand unvermeidlich zu einer wesentlichen Verschlechterung der Strahlqualität.

Im Fall des Faserlasers wird der Aktivstab zu den Dimensionen einer optischen Faser „gezogen“. Die Faser hat mehrere optische Schichten mit unterschiedlichen Brechzahlen und sichert die Totalreflexion sowohl für die Wellenlänge der Lasergeneration als auch für die Pumpwellenlänge. Da die Pumpstrahlung in der Faser auf einer Strecke von mehreren Dutzend Metern absorbiert wird, werden die Abkühlanforderungen minimiert und die Strahlqualität durch die Lichtleitereigenschaften der Faser bleibt erhalten [7],[8],[9].

In einem Scheibenlaser geschieht das Gegenteil, d.h. der Aktivstab wird zu einer dünnen Scheibe „zusammengedrückt“. Dabei wird die Wärme nicht mehr von der zylindrischen Oberfläche des Stabes, sondern von der flachen Ebene der Scheibe entzogen, was räumliche Temperaturgradienten in der Wellenfront-Ebene der generierten Strahlung ausschließt und den Effekt der Thermorefraktion verkleinert [10],[11]. Um die Effektivität der Lasergenerierung zu steigern, wird das Verfahren des mehrfachen Durchgangs der Pumpenstrahlung durch das aktive Medium genutzt. Bei der Produktion von sowohl Scheiben- als auch Faserlasern wird auch das Modul-Prinzip verwendet, in dem die Strahlung von mehreren unabhängigen gleichartigen Einmodenlasermodulen in einer gemeinsamen Vielmodenfaser gesammelt wird [12]. Die physikalischen Beschränkungen der Leistung des Ausgangsstrahls sind in diesem Fall die Entwicklung der nichtlinearen optischen Effekte sowie die Grenze der optischen Beständigkeit der Vielmodenfaser.

Neben mehreren ökonomischen Vorteilen der Faser- bzw. Scheibenlaser ermöglicht die hohe Qualität seines Strahls eine hohe Leistungsdichte und zudem eine größere Rayleigh-Länge [10],[14],[13],[15],[16]. Diese Eigenschaften zählen zu den größten Vorteilen bei der Anwendung solcher Strahlung als Energiequelle zum Schweißen von dickeren Metallblechen [17],[18]. Die Technologie des Laserschweißens von Metallen mit hoher Blechdicke hat ein großes Anwendungspotential im Maschinenbau, bei der Herstellung von Hochdruckrohre bzw. beim Pipelinebau [19][20], beim Aufbau der unterschiedlichen Komponenten eines Fusionsreaktors [21],[22] sowie im Schiffbau [23],[24].

Bevor die Hochleistungsfaserlaser mit hoher Strahlqualität entwickelt wurden, wurde für das Laserschweißen von dicken Metallblechen die Strahlung von CO₂-Lasern genutzt [25],[26]. Aus Sicht des Tiefschweißens sind prinzipielle physikalische Unterschiede zwischen dem Faser- und dem CO₂-Laser die kürzere Wellenlänge der Strahlung und die verschiedenen Leistungsdichteverteilungen in den Querschnitten des Laserstrahls, welche im Falle des Faserlasers eine nahezu rechteckige Form aufweisen [27]. Der Absorptionskoeffizient der meist verwendeten Stähle ist für die Strahlung eines Ytterbium-Faserlasers mit einer kürzeren Wellenlänge von 1,07 µm wesentlich höher als für die CO₂-Laserstrahlung mit einer Wellenlänge von 10,6 µm [7]. Beide genannten Faktoren bieten unbestreitbare Vorteile für Technologien wie Laserhärtung, Laseroberflächenbearbeitung oder Wärmeleitungslaserschweißen von dünnen Blechen [25]. Beim Schweißen von dicken Metallblechen können sie aber auch eine negative Rolle spielen. Eine scharfe räumliche Intensitätsverteilung im Laserstrahl kann zu höheren Temperaturgradienten im Schmelzbad und an den Wänden der Dampfkapillare führen, was als ein destabilisierender Faktor infolge des erhöhten Einflusses des Marangoni-Effekts wirkt [28],[29],[30]. Andererseits kann eine hohe Absorption der Laserstrahlung an der Metalloberfläche ein Hindernis für den Tiefschweißeffekt der Laserstrahlung sein, wenn der Laserstrahl von den Metallwänden der schmalen Dampfkapillare reflektiert wird [31],[32],[33].

Aber die bedeutendsten Unterschiede zeigen sich in den Prozessen der Bildung und der Entwicklung der Dampf-Plasma-Schweißfackel sowie im Einfluss dieser Fackel auf die Laserstrahlung [34],[35],[36],[37]. In der langen Forschung bezüglich des Tiefschweißprozesses mit der Strahlung von CO₂-Lasern wurden sowohl der Effekt der Entstehung des Schweißplasmas als auch sein Einfluss auf die Laserstrahlung detailliert untersucht und in der Literatur beschrieben [38],[39],[40],[41]. Laut der Hauptmeinung wird während der intensiven Metallverdampfung in der Dampfkapillare eine Wolke des Metaldampfes mit einer geringeren Konzentration freier Elektronen über der Metalloberfläche gebildet. Anschließend absorbieren die Elektronen einen gewissen Teil der Laserstrahlenergie infolge des sogenannten inversen Bremsstrahlungseffektes während der Kollisionen mit schweren Partikeln (Atome und Ionen des Metaldampfes bzw. der Umgebung). Dadurch wird die kinetische Energie der freien Elektronen gesteigert bis sie schnell genug sind, um die Schlagionisation der Eisenatome auszulösen. Wenn solche beschleunigten Elektronen die sekundären Elektronen aus den angeregten Eisenatomen herauszuschlagen beginnen, steigt die Anzahl freier Elektronen lawinenartig an, d.h. es findet ein optischer Durchbruch statt [42]. Da beim optischen Durchbruch fast die gesamte Energie der Laserstrahlung vom Plasma absorbiert wird, ist die maximale Leistungsdichte der CO₂-Laserstrahlung, die beim Tiefschweißen in das Metall hineingeleitet werden kann, durch die Schwelle des optischen Durchbruchs begrenzt. In einigen konkreten Fällen kann der Schwellwert der Leistungsdichte durch Anwendung technologischer Schutzgase bzw. einer speziellen Ausrüstung für die Schutzgaszufuhr wesentlich erhöht werden. Optimale Bedingungen für das Tiefschweißen mit der Strahlung eines CO₂-Lasers liegen gering unter diesem Schwellwert. In diesem Zustand wird bereits ein geringer Teil der Energie der Laserstrahlung von der Wolke der freien Elektronen absorbiert, aber die Elektronenkonzentration und ihre Energie sind noch nicht hoch genug, um eine

Elektronenlawine zu produzieren [43]. Als ein Energiepuffer kann das Schweißplasma in diesem Fall sogar stabilisierend für den Prozess wirken.

Im Falle der Faserlaserstrahlung, die im Vergleich zur CO₂-Laserstrahlung eine um etwa eine Größenordnung kürzere Wellenlänge besitzt, ist der Koeffizient der inversen Bremsstrahlungsabsorption von den freien Elektronen im Metaldampf bereits um fast zwei Größenordnungen kleiner [44]. Dementsprechend wird die Wolke aus dem Metaldampf über der Metalloberfläche nicht erwärmt und der optische Durchbruch findet nicht statt, auch wenn die Leistungsdichte wesentlich höher als beim CO₂-Laserschweißen ist [45],[46],[47]. Wie die Simulation des thermodynamischen Zustandes des Metaldampfes innerhalb und außerhalb der Dampfkapillare gezeigt hat [48],[49], wird unterdessen der heiße Metaldampf, der aus der Dampfkapillare herausströmt, wegen der relativ geringeren Temperatur über dem Metall stark übersättigt. Deshalb muss in diesem Bereich die Möglichkeit der Volumenskondensation des Metaldampfes sowie der Entstehung einer Wolke aus den Partikeln der kondensierten Phase berücksichtigt werden. Laut den theoretischen Bewertungen, die auf einer kinetischen Beschreibung des Wachstums von einem Kondensat-Cluster basieren, können die Clustergrößen der kondensierten Phase in der Nähe der Metalloberfläche im Bereich von 10 nm bis 100 nm liegen [50],[51],[52]. Im Fall dass die Partikelkonzentration in der Schweißfackel hoch genug ist, kann die Absorption bzw. die Streuung eines beträchtlichen Teiles des Laserstrahles erfolgen, der durch die Schweißfackel transmittiert wird [48],[53],[54],[55]. Abgesehen von der Plasmafackel, die in zahlreichen Untersuchungen zum Schweißprozess mit der Strahlung eines CO₂-Lasers detailliert erforscht wurde, sind jedoch sowohl die Parameter der kondensierten Partikel als auch ihr Einfluss auf die Schweißnahtqualität heutzutage noch so gut wie unbekannt.

Indirekt wurde die Existenz kleiner absorbierender bzw. streuender Objekte in der Schweißfackel beim Tiefschweißen mit einem Hochleistungsfestkörperlaser in einigen Untersuchungen registriert, in denen die Fackeltransparenz für eine parallel zur Metalloberfläche transmittierten Prüfstrahlung gemessen wurde [56],[57],[58]. Dabei wurde eine Abschwächung der Leistung (Extinktion) des Prüfstrahls entdeckt. Jedoch ist der Beitrag zur totalen Extinktion von den in diesem Fall möglichen unterschiedlichen Effekten (wie die Thermorefraktion, die Absorption und die Refraktion im Schweißplasma, der Einfluss kleiner kondensierter Partikel bzw. aus dem Schmelzbad gespritzter makroskopischer flüssiger Metalltropfen) unklar geblieben. Außerdem wurde die Extinktionsdynamik aufgrund der geringen zeitlichen Auflösung der Messungen nicht beschrieben, obwohl offensichtlich ist, dass für die Beantwortung der Frage des Einflusses des Extinktionseffektes auf die Schweißprozessstabilität der Charakter der zeitlichen Wechsel des Extinktionswertes eine sehr wichtige Rolle spielt [59],[60]. Neben der Extinktionsmessung der Prüfstrahlung wurde die gestreute Strahlung des Hochleistungsfestkörperlasers aus der Schweißfackel registriert [61]. Damit wurde experimentell die Existenz der Streuung gezeigt, welche wahrscheinlich von den kleinen kondensierten Partikeln verursacht wird. Jedoch wurde keine qualitative Beschreibung präsentiert. Selbst das Aussehen der Schweißfackel zeugt vom Vorhandensein der kleinen Partikel, da die Form des leuchtenden Bereiches sich stark von der beim CO₂-

Laserschweißen entstehenden Plasmafackelform unterscheidet und mehr an die Spur des Laserstrahles erinnert, der sich durch ein verstaubtes Medium propagiert [43],[62],[63],[64].

In einer Reihe von Untersuchungen wurden direkte Messungen der Größe und der chemischen Zusammensetzung der kondensierten Partikel durchgeführt. Dabei wurden die Partikel aus der Schweißfackel auf einen kalten Glasträger sedimentiert. Außerdem wurde ein optisches Diagnostikverfahren angewendet (das Multi-Wellenlänge-Verfahren [65],[66]), um die Partikelgröße und die Partikelkonzentration zu messen [67],[68],[69]. Die erhaltenen Daten geben dennoch keine ausführliche Antwort auf die Fragen, wie der Prozess der Metaldampfkondensation in unmittelbarer Nähe des Dampfkapillaren-Ausgangs verläuft, welche Parameter (in erster Linie Größe und Konzentration) die Wolke aus kondensierten Partikeln über der Metalloberfläche aufweist und wie diese Wolke die durch sie sich verbreitete Strahlung des Hochleistungsfestkörperlasers beeinflusst.

Aus den dargestellten Fragestellungen ergab sich **die Zielstellung – Bestimmung der Charakteristik des Dampf-Plasma-Mediums der Schweißfackel, die durch Einwirkung der Hochleistungsstrahlung eines Faserlasers auf das Metall entsteht, sowie Feststellung der neuen physikalischen Effekte, durch welche die Schweißfackel einen großen Einfluss auf die Laserstrahlung ausüben kann.**

Wissenschaftliche Neuartigkeit der Arbeit

Zum ersten Mal wurde eine breite komplexe Untersuchung der Dampf-Plasma-Fackel durchgeführt, die durch Einwirkung der Hochleistungsstrahlung eines Ytterbiumfaserlasers auf das Metall entsteht:

- Erstmals wurde der Einfluss aller möglichen Mechanismen der Wechselwirkung zwischen Hochleistungslaserstrahlung und Medium der Dampf-Plasma-Fackel (wie Absorption und Refraktion im Schweißplasma und im Metaldampf, Thermorefraktion an den Gradienten der Brechzahl, Einfluss von aus dem Schmelbad herausgespritzten flüssigen makroskopischen Mealltropfen, Streuung und Absorption an den kleinen Partikeln aus dem kondensierten Metaldampf) experimentell unter ein und derselben Bedingungen bestimmt;
- Die Struktur des Mediums der Dampf-Plasma-Fackel über der Dampfkapillare wurde beschrieben und die Charakteristik des laserinduzierten Schweißplasmas wurde in Luft sowie unter Ar-Schutzgas gemessen;
- Mittels optischer Diagnoseverfahren wurden die durchschnittlichen Parameter (Größe und Konzentration) der Wolke aus kondensierten Partikeln gemessen;
- Zum ersten Mal wurde experimentell die Existenz kleiner kondensierter Partikel innerhalb der Kaustik des Hochleistungsstrahls eines Faserlasers gezeigt;
- Die Leistungsabschwächung des Hochleistungsstrahls eines Faserlasers durch Absorption in der Wolke kleiner kondensierter Partikel wurde beurteilt.

Wissenschaftliche und praktische Bedeutung

Die Hauptbedeutung der Arbeit besteht in der Erweiterung der Kenntnisse über den Zustand der Schweißfackel sowie über die Mechanismen der Wechselwirkung zwischen

der Laserstrahlung und der Schweißfackel beim Schweißen von Baustählen mit der Strahlung eines Hochleistungsfaserlasers hoher Strahlqualität. Die Ergebnisse der Untersuchung können für die Entwicklung der Technologie des Laserschweißens von Metallen mit großer Blechdicke und für die Konstruktion bzw. Optimierung der Laseranlagen benutzt werden.

Die Erkenntnisse über die Prozesse der Metaldampfkondensation in der laserinduzierten Fackel können auch in der Technologie der Bedampfung dünner Schichten und in der Produktion nanodimensionalen Pulvers Anwendung finden.

Hauptergebnisse und -thesen der Arbeit

1. Beim Metallschweißen mit Hochleistungsfaserlasern teilt sich die Dampf-Plasma-Fackel in zwei unterschiedliche Teile – das Schweißplasma und die Wolke kondensierter Metallpartikel.
2. Das Schweißplasma befindet sich in nächster Nähe des Dampfkapillar-Ausgangs und übt infolge der geringen Werte der Elektronendichte und der Temperatur keinen Einfluss auf die transmittierte Laserstrahlung und den gesamten Schweißprozess aus.
3. Die Wolke der kleinen kondensierten Partikel befindet sich über dem Schweißplasma und entsteht infolge der Abkühlung und der Kondensation des heißen Metaldampfs, der aus der Dampfkapillare herausströmt.
4. Die kondensierten Metallpartikel haben eine Größe von etwa 60 nm bis 80 nm. Die Partikelwolke mit der Konzentration von ca. 10^{10} cm^{-3} kann die transmittierte Laserstrahlung absorbieren.
5. Unter dem Einfluss des Hochleistungsfaserlaserstrahls werden die kondensierten Partikel erwärmt, wodurch die Lichtemission des oberen Teils der Schweißfackel entsteht. Eine vollständige Verdampfung der Partikel findet dennoch nicht statt.
6. Die Leistungsabschwächung des Faserlaserstrahls verläuft unregelmäßig über die Zeit und kann dazu führen, dass die Leistungsstabilität der Strahlung, welche die Metalloberfläche erreicht, wesentlich schlechter wird als die ursprüngliche Stabilität der Ausgangsleistung des Faserlasers.
7. Die Schwingungsamplitude des vollen Absorptionswertes des Hochleistungsfaserlaserstrahls, der während des Schweißens durch die gesamte Wolke der kondensierten Partikel transmittiert wird, kann bis 10% groß sein, was einen negativen Einfluss auf die Qualität von gefügten Bauteilen mit großer Blechdicke ausüben kann.

Aufbau der Dissertation

Die vorliegende Dissertation besteht aus einer Einleitung, vier Kapiteln und einer Zusammenfassung sowie einem Literaturverzeichnis mit 130 Quellen. Auf 107 Seiten werden die Ergebnisse mit 45 Bildern, 3 Tabellen und 55 Formeln erläutert.

Kurze Inhaltsangabe der Dissertation

Das erste Kapitel enthält eine Literaturübersicht zum Thema der Wechselwirkung zwischen der Hochleistungslaserstrahlung und der Materie während des Laserschweißens von dicken Metallblechen. Die allgemeine Funktionsweise der Hochleistungsfestkörperlaser hoher Strahlqualität sowie die Besonderheiten des Schweißprozesses für dicke Metallbleche werden beschrieben. Außerdem werden die Mechanismen der Bildung und der Entwicklung der Dampf-Plasma-Fackel betrachtet und eine Vergleichsanalyse des Schweißplasmazustandes beim Einsatz von CO₂- und Faserlasern durchgeführt. Der Kondensationsmechanismus des Metaldampfes während des Schweißprozesses wird detailliert beschrieben. Zudem wird eine Übersicht über die früher genutzten Verfahren der Partikel Diagnostik bzw. Messung der Partikelparameter präsentiert.

Im zweiten Kapitel werden die Ergebnisse der Untersuchung des Schweißplasmas während des Hochleistungsfaserlaserschweißens von niedriglegierten Stählen unterschiedlicher Blechdicke präsentiert. Mittels High-Speed-Videobeobachtung wird die Struktur der Schweißfackel gezeigt. Hierbei wurde festgestellt, dass die gesamte Schweißfackel aus dem Schweißplasma (im unteren Teil) und aus der Lichtemission der kleinen kondensierten Partikel (im oberen Teil) besteht. Die Parameter des Schweißplasmazustandes (Temperatur und Konzentration freier Elektronen) wurden mittels experimenteller Messung der Plasmaemissionsspektren für unterschiedliche Schweißparameterfenster ermittelt. Der Wert der inversen Bremsstrahlungsabsorption für die gemessenen Plasmaparameter und die Wellenlänge des Faserlasers wurden berechnet. Die Ergebnisse führten zu der Schlussfolgerung, dass das Schweißplasma aufgrund seiner niedrigen Temperatur und kleinen Größe keinen maßgeblichen Einfluss auf die Laserstrahlung bzw. auf die Schweißnahtqualität ausüben kann.

Im dritten Kapitel wird eine Messung der Extinktion der Prüflaserstrahlung im IR-Wellenlängenbereich (1,3 µm) dargestellt. Dabei wurde der Prüfstrahl quer durch das Medium der Schweißfackel geleitet. Zuvor wurde der Effekt der Thermorefraktion der Prüfstrahlung an den thermischen Gradienten der Brechzahl im Medium der Schweißfackel untersucht. Es wurde festgestellt, dass in der genutzten Konfiguration der Effekt der Thermorefraktion keinen wesentlichen Beitrag zur vollen Extinktion der Prüfstrahlung leisten kann. Anschließend wird die zeitliche Dynamik des Extinktionssignals beschrieben. Die räumlichen Verteilungen der Extinktion wurden in unterschiedlichen Fackelhöhen gemessen. Aus den Messergebnissen wurde die volle räumliche Verteilung des Extinktionskoeffizienten rekonstruiert. Vom Charakter des Extinktionssignals wurde der Schluss gezogen, dass der Extinktionseffekt nicht mit der Absorption bzw. der Refraktion der Prüfstrahlung im Schweißplasma, ebenso wenig wie mit der Thermorefraktion und auch nicht mit dem Einfluss der makroskopischen flüssigen Metalltropfen zusammenhängt. Der einzige mögliche Grund dieses Phänomens ist die Existenz der kleinen Metallpartikel in der Schweißfackel, welche die transmittierte Laserstrahlung absorbieren bzw. streuen.

Das vierte Kapitel ist der Messung der durchschnittlichen Parameter der kondensierten Metallpartikel gewidmet. Die Frequenzspektren des Durchlasses der Schweißfackel (in Querrichtung) wurden experimentell ermittelt. Dabei wurde mit Hilfe des Multi-Wellenlängen-Verfahrens festgestellt, dass die kondensierten Metallpartikel in der Fackel

eine durchschnittliche Größe von 60 nm bis 80 nm und eine räumliche Konzentration an der Fackelachse von ca. 10^{10} cm^{-3} haben. Es wird gezeigt, dass diese Partikelparameter mit dem im dritten Kapitel gemessenen Extinktionskoeffizienten übereinstimmen. Durch direkten Anschluss eines Prüflasers an das optische System des Hochleistungsfaserlasers wurde die Diagnose der kleinen kondensierten Partikel unmittelbar innerhalb der Kaustik des Faserlaserstrahls durchgeführt. Nach der Vermutung, dass die Partikelparameter innerhalb der Kaustik des Faserlaserstrahls mit den früher gemessenen durchschnittlichen Parametern übereinstimmen, erfolgte eine Beurteilung der Leistungsabschwächung des Hochleistungsfaserlaserstrahls, der die gesamte Höhe der Schweißfackel durchläuft.

Persönlicher Beitrag des Autors

Alle Ergebnisse und Thesen der Dissertationsuntersuchung wurden vom Autor selbst oder unter dessen unmittelbarer Mitwirkung von ihm ermittelt und entwickelt. Der Autor hat beim Versuchsaufbau, bei der Versuchsdurchführung sowie bei der Auswertung aller experimenteller Ergebnisse teilgenommen.

Wissenschaftliche Diskussion der präsentierten Ergebnisse

Die wichtigsten Ergebnisse der Dissertation wurden auf den folgenden Konferenzen präsentiert und diskutiert:

- Annual conference „Scientific session MEPhI“, Moscow, Russia, 2009, 2010, 2011, 2012;
- The 5th International Conference “Laser technologies in welding and materials processing”, Katsiveli, Ukraine, 2011;
- 20th International Laser Physics Workshop (LPHYS'11), Sarajevo, Bosnia and Herzegovina, 2011;
- XXII International Science and Technology Conference „Lasers in Science, Technology and Medicine“, Gelendzhik, Russia, 2011;
- 30th International Congress on Applications of Lasers & Electro-Optics (ICALEO-2011), Orlando, FL, USA, 2011;
- Scientific colloquium in the “Institute of laser and information technology problems RAS”, Shatura, Russia, 2012.

Veröffentlichungen

Die Thematik der Dissertation wurde in 14 Veröffentlichungen präsentiert. Davon erschienen 4 Artikel in Zeitschriften und 10 Artikel in Konferenzbänden [70] - [83].

Chapter 1.

Interaction between laser radiation and matter during high power laser welding of metals

1.1. High power high brightness solid-state lasers

1.1.1. Thin disc lasers

1.1.2. Fiber lasers

1.1.3. Characteristics of the high power laser beam

1.1.4. Applications of high power high brightness solid state lasers

1.1.5. Peculiarities of metal welding process with high power high brightness solid-state lasers

1.2. Vapour-plasma plume in high power laser metal welding process

1.2.1. Welding plasma formation

1.2.2. Welding plasma state during CO₂- and solid-state laser welding

1.3. Mechanism of metal vapour condensation in welding plume

1.3.1. Theoretical preconditions

1.3.2. Indirect experimental confirmations

1.3.3. Optical diagnostics of condensed particles

1.3.4. Direct measurement of particle parameters

1.3.5. Scattering and absorption of laser radiation by condensed metal vapour particles

Summary

1.1. High power high brightness solid state lasers

After the advent of high power emitting diodes, the traditionally used lamp pumping of solid state lasers was replaced with the diode pumping, which sharply increased the efficiency of material processing systems. Numerous advantages have been gained by this replacement. First, owing to the more effective conversion of electrical energy to the optical radiation, the total efficiency of the laser equipment increases by a factor of five and more. Second, due to the decreasing energy deposition on the active laser crystal, the thermal lens effect becomes considerably lower, which increases the beam quality. Third, the long operating time of the pumping diodes (more than 10 000 hours) increases the laser reliability and reduces the service costs. Finally, simple electrical control of the pumping diode generation mode as well as its short response time allow it to realize any temporal pulse shape of the laser radiation in a broad spectral band [84].

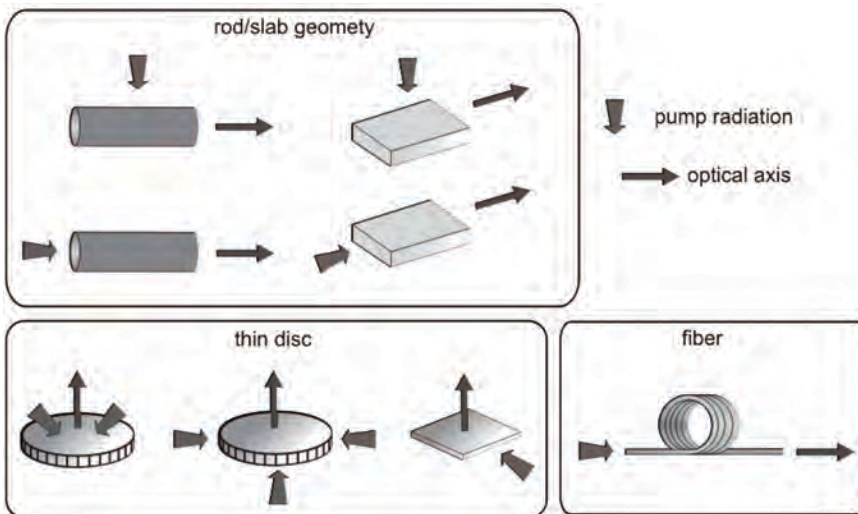


Fig. 1.1. Schemes of diode pumped solid state lasers [13]

In addition, the high pumping intensity allows it to use as the active medium not only Nd-ions, but also the ions of other rare-earth elements. This opens up the possibility of increasing the quantum efficiency of the generation as well as getting the radiation with other wavelength for different applications. But the main advantage of such systems for the deep penetration laser welding process is the combination of high radiation power and high beam quality [14], i.e. the high brightness of the radiation (the term “brightness” is defined as the ratio between the radiation power density and the solid angle in which the radiation is focused).

The geometry of the active laser medium, the orientation of the optical axis as well as the pumping direction are shown for three main types of high power high brightness solid state lasers in Fig. 1.1 [13]. In the first generation systems the geometrical orientation of the

active crystal, pumping and cooling units was principally the same as in traditional solid state lasers with the lamp pumping. Therefore, the temperature gradient in the direction normal to the optical axis and subsequent formation of the refractive index gradient were unavoidable. Thereby, it was not possible to suppress the thermal lens effect completely, although it was essentially reduced. This was one of the reasons why new laser construction principles were explored which would solve this problem. Examples of such solutions are the disc and fiber lasers of the new generation.

The characteristic peculiarities of the high brightness solid state lasers, which attract considerable interest for application in the deep penetration metal welding technology, will be described below. Also the physical differences between the welding processes with CO₂- and fiber lasers will be shown.

1.1.1. Thin disc lasers

When a length of the active cylindrical rod l decreases and becomes much smaller than the rod diameter d (i.e. $l/d \ll 1$), cooling from the cylindrical surfaces is not possible. Instead, the heat energy must be removed from the plane disc surface. If the thermal conductivity is high, the isotherms of the temperature field on the whole disc surface in the crystal are directed normally to the optical axis. At the same time there is almost no change in the refractive index along the disc radius. Therefore, the plain wave propagating along the disc axis acquires no additionally phase shifts and such generation scheme must provide a high beam quality independently of the output radiation power.

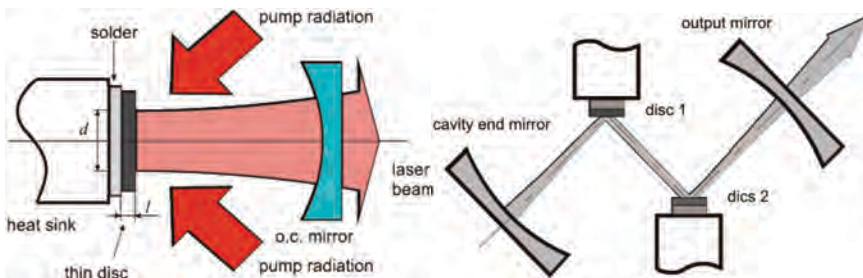


Fig. 1.2. Thin disc laser design (left) [5] and principle of power scaling by the number of discs (right) [13]

The design of the thin disc laser is shown in Fig. 1.2 (left). When the crystal is placed on the heat-removing mount, both the axial and the radial pumping direction are possible. This construction has two important peculiarities, which were observed from the experience of the work with the thin disc lasers. First, if the cavity configuration is fixed, the beam quality parameter M^2 (see Sec. 1.1.3) is almost independent of the output power level, i.e. there is no thermal lens effect. Second, the beam quality can be improved by optimising the cavity configuration without decreasing the output power or the efficiency [13].

Technically available methods for output power increase are in this case either increasing of the pumping area diameter on the disc surface or using of the several discs which are situated along the break cavity axis (see Fig. 1.2 right). In order to receive a power of

several kilowatts and more, the radiation from few identical modules is combined in the single general optical fiber.

At the present time disc lasers are available based on ytterbium ions in the yttrium-aluminium garnet crystal ($\text{Yb}^{3+}:\text{YAG}$) with $1.03\ \mu\text{m}$ wavelength and power levels up to 16 kW. The beam parameter product BPP of such systems is near $8\ \text{mm}\cdot\text{mrad}$ and the full efficiency is more than 20% [10],[11]. The length of the radiation delivery fiber can reach up to 200 m [25].

1.1.2. Fiber lasers

Fiber lasers normally have a multi-clad single-mode active fiber, which is doped with rare-earth elements and is several meters long. It is pumped in the butt by multi-mode diodes. Depending on the doping element, the spectral composition of the fiber laser radiation is in the range of $1\div 2\ \mu\text{m}$. But for deep penetration welding ytterbium fiber lasers with a wavelength of $1.07\ \mu\text{m}$ are used mainly. The full efficiency of the ytterbium fiber laser is more than 20%, which allows it to use in such devices a simple air cooling system. Fig. 1.3 shows the scheme of the clad-pumped fiber laser.

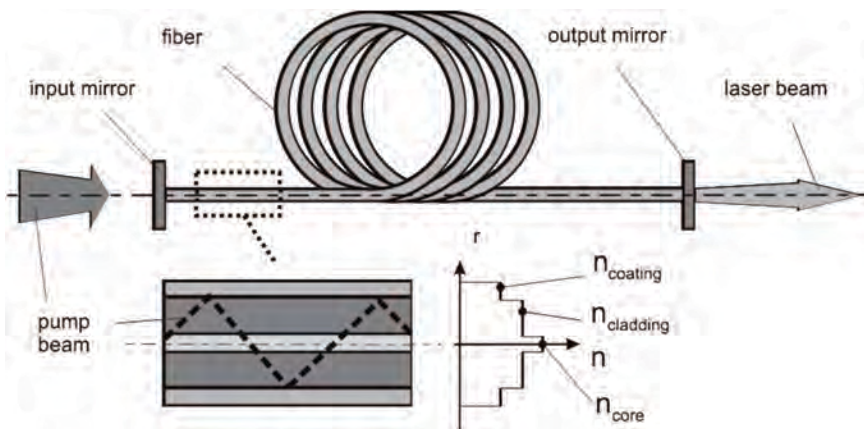


Fig. 1.3. Scheme of the clad-pumped fiber laser [13]

The radiation of the diode lasers is focused on the relative broad non-active part of the fiber-clad. During propagation through this clad, the pump beam is absorbed in the central fiber core (see Fig. 1.3) and excites the active medium over the length of several meters. The generated laser radiation leaves the cavity area through a single mode passive fiber, which can be up to 50 meters long. The beam quality, corresponding to the diffractive limit, is a function of only optical fiber properties, and is independent of the temperature and of the output power level [7].

The fiber lasers as well as the thin disc lasers have the advantage that the power can easily be increased, as the output power in kW-range is obtained by the combination of few fiber laser modules with a general multi-mode output fiber. Such systems give high beam quality, which is not lower than for the CO_2 -lasers, although their radiation is no more single-mode. Thanks to such module construction, the reliability of the whole system remains high with

any output power, as there is no additional load imposed on the components [8]. In our days multi-mode fiber lasers with more than 50 kW power and single-mode laser with up to 10 kW power are in use. The full efficiency of such systems is about 30% [9].

1.1.3. Characteristics of the high power laser beam

The laser beam has an axially symmetric shape, which is shown in *Fig. 1.4*. The beam boundary (at the $1/e^2$ level) is a hyperboloid of rotation with the asymptotic angle α , which determines the beam divergence in the far field.

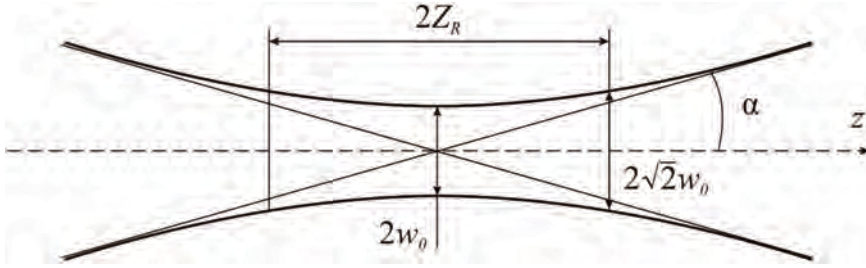


Fig. 1.4. Longitudinal cross-section of an axially symmetric laser beam propagating along the z axis

In this case the dependencies of the laser beam radius w and of the wave front curvature radius R on the longitudinal coordinate z are described as follows [85]:

$$w(z) = w_0 \left[1 + \left(\frac{M^2 \lambda z}{\pi w_0^2} \right)^2 \right]^{1/2} \quad (1.1)$$

$$R(z) = z \left[1 + \left(\frac{\pi w_0^2}{M^2 \lambda z} \right)^2 \right] \quad (1.2)$$

where λ is the radiation wavelength; $M^2 \geq 1$ is a dimensionless parameter which showing the deviation of the laser beam from the ideal Gaussian beam with $M^2 = 1$. The parameter M^2 shows the possibility of laser beam focusing (beam “focusability”), i.e. it determines the radius w_0 in the beam waist point (in the focal plane) and the divergence angle α in the far-zone:

$$w_0 \alpha = \frac{M^2 \lambda}{\pi} \quad (1.3)$$

The value $w_0 \alpha$ is called the beam parameter product *BPP*. It allows to compare different laser beams with each other. However, when lasers with the same wavelength are compared (e.g. ytterbium fiber and thin disc lasers) for beam quality characterization only the M^2 parameter is often used. From *Eq. (1.3)* it follows that the value $w_0 \alpha$ is invariant in any laser beam transformation. Particularly, when focusing a collimated beam with diameter D using a lens with focal distance f , the focal beam radius w_f is:

$$w_f = D/2 \cdot \alpha \frac{f}{D/2} = \frac{M^2 \lambda}{\pi} \cdot \frac{2f}{D} = BPP \cdot \frac{2f}{D} \quad (1.4)$$

The depth of focus or, as it is often called, the Rayleigh length z_R of the beam is defined as the distance where the beam diameter changes in factor of $\sqrt{2}$. This parameter also appears to be dependent on the BPP parameter:

$$z_R = \frac{\pi w_0^2}{M^2 \lambda} = \frac{w_0^2}{BPP} \quad (1.5)$$

The length of the beam waist is thereby equal to the doubled z_R value.

From the equations given above it follows that a laser source with the smaller BPP value should have the following advantages for application in the deep-penetration metal welding process [13],[86]:

- the lower BPP value allows it to get the lower value of the focal spot diameter w_f ; thereby, the higher radiation power density and the more effective energy deposition in the material (narrow weld, lower thermal conductivity losses) are achieved,
- when the focal spot diameter is fixed (or the permissible power density on the metal surface is limited) the radiation with the lower BPP parameter allows it to use the focal lenses with the higher focal distances f ; thereby, the technological flexibility of the treatment process is increased and the probability of working optics damage by liquid melt drops and other objects from the welding area is reduced,
- a decreased BPP parameter leads to an increase of the beam waist length $2z_R$, thereby, the process becomes less sensitive to small variations of the working distance between welding optics and metal surface, and the irregularity of the radiation power density distribution along the metal thickness is reduced (especially important for thick material welding),
- when the realization of the welding process with low focal distance f is possible, the lower BPP value allows it to decrease the collimated laser beam diameter D ; thereby, size and mass of the welding optics are reduced, which can be important for some high-speed metal treatment processes or for the use of technological robots.

Table 1.1 compares the beam quality characteristics for different types of laser sources used in metal welding (CO_2 -, disc and fiber lasers). It is seen that the CO_2 -lasers generally exhibit quite good mode composition of their radiation (low M^2) even with high output power. This is connected with the fact that the generation of their radiation takes place in gas medium in contrast to the generation in solid-state medium in the case of the fiber or disc lasers. In addition, power scaling in CO_2 -laser is produced not through the module scheme but only in the single open cavity. At the same time, as the wavelength of the CO_2 -laser radiation is almost ten times greater than that of solid state laser radiation, the beam parameter product BPP is worse as a rule.

Table 1.1. Beam quality characteristics for different industrial laser types

Laser type	Generation mode*	Power, kW	Fiber diameter, μm	BPP , $\text{mm}\cdot\text{mrad}$	Source
CO ₂	SM	1.0	–	3.55	[26]
	FM (1.2 kW)		–	5.64	[10]
Disc	FM		50	2.0	[87]
Fiber	SM		20	0.37	[15]
	MM		100	4.0	[16]
CO ₂	SM		5.0	–	3.55
	FM	–		6.14	[10]
Disc	FM	100		4.0	[87]
	MM (5.3 kW)	200		8.0	[10]
Fiber	SM	20		0.37	[2]
	MM	100		6.0	[16]
CO ₂	FM	10.0	–	6.41	[10]
Disc	MM		200/300	8.0/12.0	[10]
Fiber	SM (P)		20	0.37	[17]
	MM		200	8.0	[16]
CO ₂	MM	20.0	–	15.19	[10]
Disc	MM	16.0	200/300	8.0/12.0	[10]
Fiber	MM (P)	50.0	100	4.5	[17]

*SM – single-mode; FM – few-mode; MM – multi-mode; (P) – in project

Among the commercially available multi-mode lasers, the fiber and the thin disc lasers exhibit similar beam quality and correspondingly offer approximately the same technological application possibilities. However, fiber lasers can be produced also in the single-mode (up to 10 kW power). In this case they possess the minimal possible BPP value. Some of the data refer to about the technical possibility of creating unique fiber laser units with up to 50 kW power (100 kW in project) and a $BPP \leq 4.5$ [17].

From this comparison it can be concluded that at the moment the beam quality of fiber lasers in the few kW power range is higher than that of thin disc lasers. Furthermore, high power (up to 20 kW) thin disc lasers have been developed quite recently, while corresponding fiber lasers have been existing since 2005. Accordingly, the overwhelming number of thick metal welding applications of the new generation solid state lasers concerns the fiber lasers today. On the other hand, very active work for the improvement of the thin disc laser characteristics is being carried out now and in the near future the described situation can be changed. However, within the scope of this study the main attention will be paid to welding with the radiation of high power fiber lasers.

1.1.4. Applications of high power high brightness solid state lasers

Solid-state lasers with high radiation brightness are used nowadays in a number of material treatment tasks where they often replace CO₂-lasers traditionally used for these purposes before. Besides a number of economical advantages of such replacement [88], particular attention must be given to some principal physical aspects of high power solid-state laser treatment which promote the efficiency and improve the processing quality.

This study addresses solid-state laser application to the deep penetration metal welding process. In this process the laser radiation is directed to the high-power focusing system where it is formed into a convergent beam passing the components joined. While some part of the beam is reflected back the main part is absorbed or penetrates into the material. The absorption causes metal heating and melting of the adjoining surfaces (see Fig. 1.5). As a result, the weld is formed during the relative movement of the laser beam and of the metal specimen. This process is characterised by a low molten material volume as well as by high heating and cooling rates of the weld and the heat-affected zone. These peculiarities of thermal exposure predetermine minimal deformations of the joined components, specific physico-chemical and metallurgical processes in the weld metal as well as high technological and constructional strength of the joined components.

Deep penetration laser welding is one of the processes which quite clearly shows the technical advantages of the high-brightness solid-state lasers. Owing to the shorter wavelength these lasers, their radiation is better absorbed by metals than the long-wavelength radiation of CO₂-lasers. In contrast, absorption in the laser-induced plasma is at the same time by almost two orders of magnitude lower. Therefore, in the welding process using a few kilowatts of fiber laser power the problems associated with plasma shielding and plasma refraction of the radiation traditionally encountered in gas-laser welding are considerably alleviated (for more details see Sec. 1.2.1.). In addition, the higher beam quality allows it to focus the radiation very sharply and to produce in this way a very high power density (see Sec. 1.1.3).

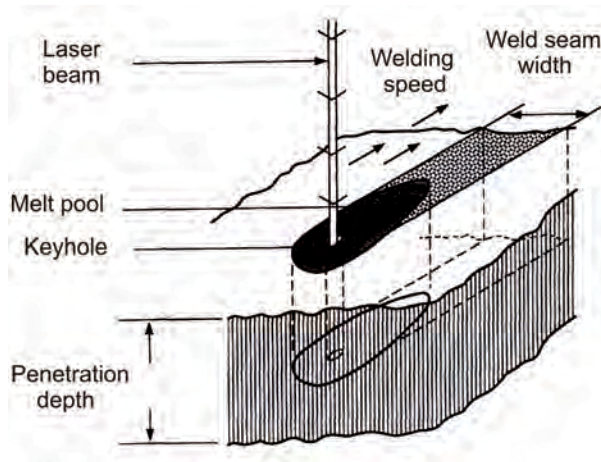


Fig. 1.5. Process of deep penetration laser metal welding [89]

With the full laser power of 10 kW the power density can be by two orders of magnitude higher than the achievable limit with the CO₂-lasers (see Sec. 1.1.3). In this case the power density becomes comparable with that in the electron beam vacuum welding process.

Power density is a key parameter in the process of the deep penetration welding. As can be seen from the comparison made in [18] between the spatial energy distributions for different

types of welding sources from one side and the corresponding weld geometry from another side, the sharper focusing of high power fiber laser radiation should provide deeper metal penetration than CO₂-laser welding.

However, in real practical work welding with such deep penetration involves significant problems. They are first of all the process instability, the necessity of developing some complicated shielding gas supply systems, the narrow parameter window and the impossibility of creating some applicable universal methods for several welding technologies. Some of these problems were solved during many years of studying the CO₂-laser welding process. But it appeared that the high power solid-state laser welding process has its own peculiarities which do not allow it to use the previous gained experience in full.

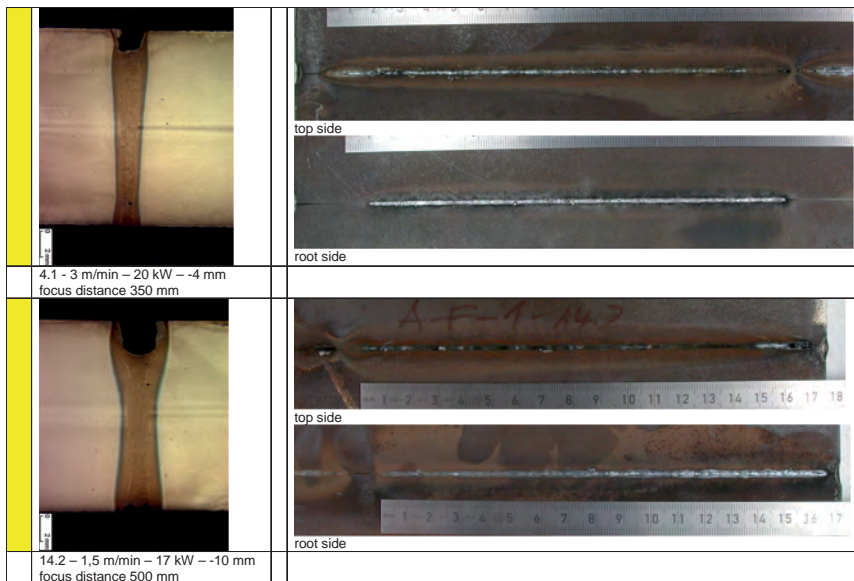


Fig. 1.6. Characteristic view of the welding defects appeared during 16 mm mild steel plate welding with fiber laser [90]

There are some problems with humping formation (i.e. quasi-periodical waves of crystallized metal in the weld) which can be explained by the hydro-dynamical effects in the melt pool most likely connected with increasing melt pool size (as well as keyhole diameter), since the focus spot size becomes much smaller in welding with fiber laser [45],[91]. Nevertheless, these effects are generally not connected with a concrete type of laser source. A fundamental problem, which is not characteristic of the CO₂-laser welding process, is the presence of macroscopic melt pool oscillations. Such oscillations lead to liquid metal spattering from the melt pool and form undercuts (see Fig. 1.6) [90],[92].

Significantly, when pure laser welding is replaced by hybrid laser-arc welding (using the laser beam in combination with a melting electrode arc) the process grows noticeably more stable and its real technological application potential becomes apparent [93][94][95].

1.1.5. Peculiarities of metal welding processes with high power high brightness solid state lasers

Between the three mentioned processes (CO₂-laser welding and hybrid laser welding on the one hand and high power high brightness solid-state laser welding on the other hand) there are few fundamental differences which can cause the situation described above.

- First, the welding plasma plume difference. In CO₂-laser welding the plasma plume arises due to absorption of laser radiation by the low-ionized metal vapour erosion jet. As far as the vapour-gas medium is heated up and the free electron density increases, a hot plasma plume with the temperature of $(6\div 15)\cdot 10^3$ K is formed. When the laser radiation intensity is high enough, an optical breakdown of the gas medium can occur [34],[35],[36],[37]. In spite of the fact that this limits the maximal available laser radiation power density, the plasma plume radiation absorption takes some useful action. It is considered that the hot plasma inside the keyhole is some kind of energy buffer when the energy is transmitted from the radiation to the metal keyhole walls (the “plasma fur coat” effect) [43]. Thereby not only more uniformly transmitted energy distribution along the keyhole height, but also “smoothing” of the short-time oscillations of the laser radiation power or of the spatial beam position are achieved. During laser-arc hybrid welding with a high power solid-state laser the plasma plume is formed and maintained mainly due to the burning of electric arc. The plasma temperature in this case accounts for about $(5\div 8)\cdot 10^3$ K. Such plasma remains almost fully transparent for the short-wavelength laser radiation. In the process of laser-arc hybrid welding, like in CO₂-laser welding, simultaneous energy transmission from both the laser radiation and the electric arc plasma to the metal takes place. However, in this case, owing to the possibility of the independent control of these two processes (as well as owing to the filler material supply) the welding efficiency is considerably increased. In welding with high power solid-state lasers the welding plume offers low-ionized gas rather than plasma. Due to the low absorption coefficient for the short-wavelength laser radiation the erosive jet of evaporated metal is almost not heated and the plume temperature reaches only the value of $(3\div 6)\cdot 10^3$ K [45],[46]. The welding plasma formation mechanism as well as the plasma state analysis during the welding processes with CO₂- and solid-state lasers are given in detail in *Sec. 1.2.1*. Apart from the absence of the “plasma fur coat” stabilizing influence, the low welding plume temperature may lead to condensation of metal vapour which escapes the keyhole. This means that a cloud of small condensed metal particles can be formed (see *Sec. 1.1*) which have a negative influence on the transmitting laser radiation.
- Second, the absorption coefficient by iron is about five times higher for ytterbium solid-state laser radiation with a wavelength of 1.07 μm than for CO₂-laser long-wavelength radiation [7]. On the one hand, this favours the more effective energy deposition on the metal specimen and eliminates the necessity of depositing special absorbing layers on the surface of the components to be joined (especially in welding of such high-reflective materials like aluminium or copper). However, it is believed that during the CO₂-laser welding process, the more stable and deeper penetration of the laser beam into the material is promoted by the multiple reflections

from the keyhole walls (Fresnel absorptions). This effect can partially compensate the defocusing and the refraction effects in the welding plasma plume [31],[32],[33],[43]. In this case, this effect will be less pronounced for the short-wavelength radiation of the fiber or disc lasers, since when the beam impinges on the metal keyhole wall due to some short-time beam trajectory deviation almost the whole beam power can be absorbed in one or two reflections still in the upper part of the keyhole.

- Third, in the multi-mode fiber lasers the radiation of several single-mode lasers is collected in a single delivery fiber. As a result of this constructive peculiarity the energy distribution in the fiber laser beam cross-section exhibits a characteristic difference from the CO₂-laser beam. Since the CO₂-laser radiation is generated in the open cavity and by the gas medium, the spatial power density distribution form is qualitatively similar to the Gaussian beam. But for the high power fiber laser the form of this distribution looks more like rectangular [27]. Such type of energy source leads to higher temperature gradients on the metal surface and can intensify the influence of the thermal capillary instability (Marangoni-effect) [28],[29],[30]. The temperature gradients are enlarged in this case also due to the absence of a full-blown hot plasma plume, which in case of CO₂- or arc-laser hybrid welding heats up the peripheral areas of the keyhole and the melt pool, i.e. the areas, where there is no direct laser beam irradiation.

It is evident that all three aspects described above are closely connected with each other and each of them deserves individual detailed investigation. However, in this study the attention will be paid only to the first problem, i.e. to the peculiarities of the welding plume formation and development as well as to the formation of the condensed metal particle cloud and to its influence on the transmitting laser radiation.

1.2. Vapour-plasma plume in high power laser metal welding processes

In this study the welding process in the so-called deep penetration mode is examined. This process produces a narrow weld with high weld formation coefficient (up to 10 and more) which is determined as the ratio $k_w = H/B$, where H – penetration depth and B – weld width. The power density of the laser beam focused on the surface of the metal to be welded which is necessary to maintain such evaporation mode, should be not less than 10^5 W/cm^2 [39].

The physical model of the deep metal penetration effect under the continuous-wave laser radiation influence can be formulated based on the following considerations. After the laser radiation with a certain threshold power density has hit the metal surface, the metal is heated up at a heating rate much higher than the heat extraction rate due to heat conduction deep into the metal, convection and back reflection mechanisms. During this process the metal is not only melted by the laser, but is also heated locally up to temperatures higher than the boiling temperature. This leads to intensive metal evaporation and dispersion of the metal vapour. Intensive evaporation causes a reactive force which bends the liquid melt surface [39],[50]. As a result, a deep narrow keyhole is formed in the

melt pool, which is filled by metal vapour. When the laser beam is moved at a certain speed relative to the metal specimen, the keyhole acquires dynamic stability and propagates through the material. On the front keyhole wall the metal is melted and the melt is transported along the side walls to the back keyhole wall where it crystallizes (see Fig. 1.7).

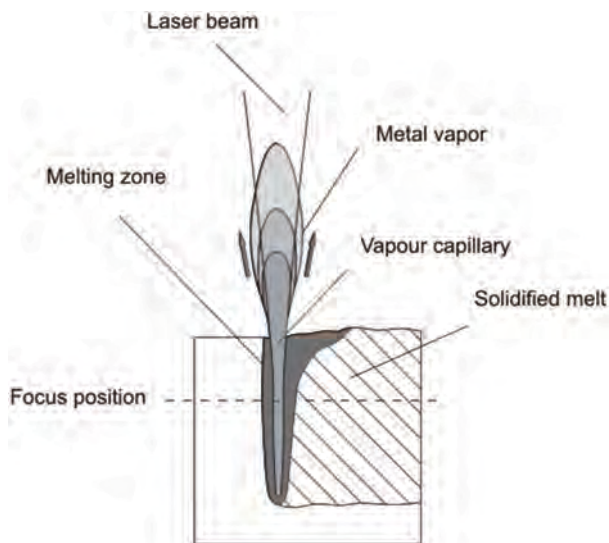


Fig. 1.7. Schematic view of the keyhole during deep penetration laser welding [28]

In the next sections the process of plasma plume formation and development under the laser radiation influence will be examined. The most prevailing theories will be described which explain the causes of metal vapour ionisation as well as the characteristic plasma states. The plasma plume parameters in the processes of CO₂-laser beam welding with the wavelength of 10.6 μm and solid-state laser beam welding with the wavelength of 1.07 μm will be compared.

1.2.1. Welding plasma formation

Different notions and theoretical approaches are used to describe plasma plume formation mechanisms. In the fundamental research of the origin of laser-induced optical breakdown in gases made by Raizer [40] the conditions of a laser-induced arc generation and subsequent spread of this discharge were established. The investigation in [41] gives a theoretical conception of the plasma formation, which is based on metal evaporation from the irradiated surface followed by absorption of the laser radiation by the vapour at rapidly increasing temperature and ionisation degree.

It is known that efficient heating of the vapour can take place only due to the inverse Bremsstrahlung absorption, i.e. by the interaction with the free electrons. There are also some suppositions about the origin of the free electrons in the vapour cloud during evaporation. First, the evaporated metal vapour is already partially ionized. The electrons can be pulled out from the metal surface owing to the photoelectric emission under the influence of the laser radiation and to the thermoelectronic emission from the heated metal

surface. Second, the critical free electron density, which is necessary for the electron avalanche generation, is much lower than the density of some admixtures with a low ionisation potential (in the first place the hydrocarbonic molecules). Therefore, the free electrons can be produced as a result of the multi-photon ionisation of these admixtures.

Considerable influence on the plasma formation is exerted by oxidized layers, structure defects and micro heterogeneities on the workpiece surface as well as by chemical reactions between the vapour and the ambient gas.

It should be noted, that the metal vapour assists over the surface almost at all kinds of laser processing connected with metal heating up to fusion temperature. Thus, at the beginning of plasma plume formation, the ionisation should be considered taking account of the concentration of the metal vapour particles having a low ionisation potential. The mechanism of electron avalanche formation and development in an easy-ionized admixture is imagined as the ionisation, conditioned by the electrons which acquire the energy owing to the photon absorption. An electron, which has sufficient energy, can cause ionisation by collision with an atom. As a result, two free electrons with low energy are produced. Then, the photon absorption by these two electrons and the following ionisation due to the collisions with atoms are repeated. This process leads to the avalanche ionisation, i.e. to the plasma plume generation.

The process of the plasma generation has a three-stage character [96]. At the first stage the metal is evaporated and a cloud from the metal vapour with a low free electron concentration with kinetic energy $\varepsilon_{kin} \leq 1$ eV is formed above the surface. Then, the vapour is heated owing to the inverse Bremsstrahlung absorption of the laser radiation by electrons in the heavy particle field. Finally, when the kinetic energy of the electrons becomes high enough to trigger the ionisation of the iron vapour atoms, they start to knock out the secondary electrons from the excited atoms and produce the avalanche increasing number of the free electrons and ions, i.e. the electrical discharge. Preliminary atom excitation up the stairs of metastable energy levels takes place also due to the collisions with electrons [40].

In this process the plasma plume experiences some characteristic phases which have each differences in temperature, free electron concentration, velocity of the plasma front propagation and threshold power density of the radiation necessary for the transition and the maintenance of the plume state. These phases were referred to in [42] as three burning modes of the plasma plume:

- **The light burning mode.** The heating of the gas due to the inverse Bremsstrahlung absorption takes place more intensively in the focal area of the laser beam. With increasing temperature, the energy from the space occupied with the plasma is slowly transmitted to the undisturbed gas in the opposite direction to the laser beam, i.e. the plasma broadens. The free electron concentration increases slightly and the plasma front velocity is in the range from 1 m/s to 100 m/s. Due to the laser beam divergence and the decrease in power density the plasma temperature falls down with and the plasma front moves away from the focal point. As the plasma can exist only at a minimal temperature level T_0 , which secures a sufficient charged particle

concentration, the moving of the plasma front ends when the temperature falls down to values $T < T_0$. The calculation in [43] for CO₂-laser beam welding in Ar medium gives a value of $\sim (0.1 \div 1)$ MW/cm² for a stable burning mode threshold.

- **The subsonic radiation wave mode.** When the power density of the laser radiation increases, optical discharge occurs. It is accompanied by a transition to the so called subsonic radiation wave mode. The plasma front velocity rises up to the value from 1 km/s to 4 km/s. In this mode a characteristic sharp increase in free electron density as well as in temperature and in plasma plume size takes place. The plasma optical transparency for the CO₂-laser radiation decreases down to several dozens of percent. Also, the refraction mechanism of the radiation passing through the plasma plume becomes more active.
- **The light-detonation wave mode.** Further growth of the radiation intensity causes appearance of light-detonation waves which have front velocities from 5 km/s to 20 km/s. The plasma in this mode is not transparent for the laser radiation. The whole radiation energy is consumed only to maintain the plume.

The plasma plume evolving during laser welding passes sequentially through the three described stages, when the radiation power density exceeds the threshold for each of them. When the power density is moderate, the plasma plume can stop at the subsonic radiation wave mode or at the light burning mode. Analyse of the plasma plume state in real deep penetration CO₂ and fiber laser welding processes in terms of the described regimes, as well as of the plasma influence on the welding quality will be given in Sec. 1.2.2.

The reasons for plasma plume formation near the metal surface during laser irradiation can also be seen from a somewhat different point of view. It is on a reasonable basis that the physical nature of the breakdown origin can be similar to the "ignition" by a hot surface as a result of chemical burning reactions. That means that the breakdown takes place due to the thermal ionisation of the metal vapour, though the evaporation of the metal can be inconsiderable. The threshold power density value, which ensures the breakdown, generally depends on such parameters of the treated surface like thermal conductivity, light absorption coefficient, evaporation energy and ionisation potential of the vapour atoms. According to this theory, properties of the ambient gas and its pressure do not influence significantly the threshold power density value.

In addition, the gas breakdown mechanism by laser radiation near the metal surface was studied also as a result of the considerable increase in electromagnetic field intensity near the micro roughness node points. Small areas of micro protuberances are heated up to boiling temperature much faster than macro sections of the surface under the laser beam spot. Above such micro surface protuberances, areas with fully ionized plasma are generated. When the power density is high enough, these areas can be a source of the light-explosive waves which propagate through the whole laser irradiated surface in some fractions of a millisecond.

1.2.2. Welding plasma state during CO₂- and solid state laser welding

In numerous studies investigating the deep penetration welding process using CO₂-laser radiation it was experimentally ascertained that the threshold power density, which is

necessary for the creation and maintenance of the plasma plume in the light burning mode, lies in the range of $(0.1\div 1)$ MW/cm² [43]. Depending on the pressure and on the type of ambient atmosphere, on the material as well as on the laser radiation focusing conditions, the plasma plume can reach temperatures ranging from 8000 K to 17000 K [28]. Under these conditions the welding plume absorbs only a small part of the laser radiation energy which passes through into the vapour channel. Experimentally measured values of the full laser beam energy absorption account from several units to several tens of percent in this case [34],[35],[36],[37],[62]. Real energy loss of the laser radiation in the welding process takes place mainly owing to the near-surface plasma absorption with consequent dissipation due to the thermal radiation as well as the dispersion of the plasma in the ambient medium. At the same time, the most part of the energy absorbed in the plasma inside the keyhole is fully passed on to the metal keyhole walls. As opposed to the near-surface plasma absorption, this effect plays a positive role in the deep penetration metal welding process.

First, in this case the energy transmission onto the metal walls along the whole channel height occurs more uniformly compared to separate narrowly focused laser beam. This implies that owing to the constantly high temperature and to the intensive metal evaporation from the keyhole walls the maintenance of the narrow and deep channel becomes easier, since reactive forces are generated during the evaporation.

Second, the keyhole plasma is a sort of stabilizing energy buffer when the energy is transmitted from the laser radiation to the metal. Such partially stepped kind of energy transformation allows it to smooth out the influence of short-term parameter variations of the focused laser beam under the near-surface plasma influence. In [43] it was noted that the interrupted character of the weld becomes stable when the power density crosses the lower threshold limit of the light burning mode.

This is to say that the light burning mode offers the optimal situation for CO₂-laser welding in the power range of $(1\div 5)$ kW. In this case the power density of the radiation allows it not to go out of the light burning mode limits, but at the same time the focal spot size on the metal surface is still small enough.

When the power density increases, the welding plasma changes to the subsonic radiation wave mode. The influence of the near-surface plasma on the laser radiation increases as well. The absorption can reach up to $(40-80)\%$. The thermal refraction effect, which in the light burning mode is negligibly low, becomes apparent. The metal penetration efficiency is decreased and the further laser power rise does not lead to the deeper keyhole. The melt pool is widened due to the refraction and the intensive heating of the peripheral metal surface by the near-surface plasma. Finally, when the welding plasma transforms to the light-detonation wave mode, almost the whole energy of the laser radiation is absorbed in the plume. Effective metal welding in this case becomes impossible.

Though investigations of the laser-induced plasma parameters during high power high brightness solid-state laser metal welding are not so numerous as in case of CO₂-laser welding, the obtained data is valuable enough to create a general picture of the plasma

formation process as well as to trace the fundamental differences of this process from one described above.

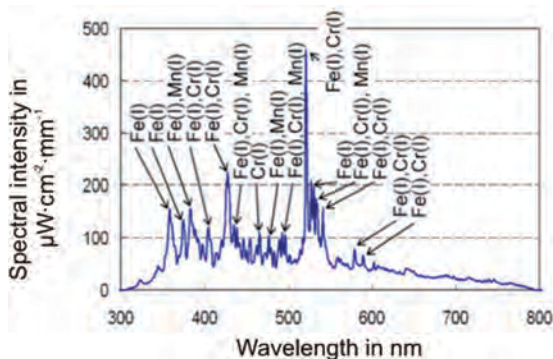


Fig. 1.8. Plasma emission spectral lines during 10 kW fiber laser welding under Ar-shielding [97]

Spectral diagnostics of the plasma plume produced during the high power fiber laser welding process [45],[97],[98],[99] showed that the temperature of the plasma free electrons ranges from 3500 K to 6000 K, i.e. it is much lower than in the CO₂-laser welding process. Moreover, as measured in [97], spectra of the plasma plume emission showed only neutral iron atom lines as well as a few lines of some neutral alloying element atoms (see Fig. 1.8), while the ionisation degree α , as calculated from Saha's equation, was only 0.02. This means that the induced plasma has a very weakly-ionized state. It is necessary also to note that these measurements were carried out at an extremely high power density value (about 10^8 W/cm²), which is not typical for deep penetration laser metal welding. As a rule, in real thick metal laser welding processes, when the laser radiation power is about 10 kW, it is desirable to have a high beam waist length. But when the beam parameter product *BPP* of the laser source is limited the increasing waist length follows to the broadening focal spot as well as to the decreasing power density down to 10^6 – 10^7 W/cm². Therefore, the data given above can be used as a reference for the maximal possible values. In real deep penetration welding conditions the plasma plume temperature as well as the ionisation degree should be far lower.

Actually, it is not correct to call the laser-induced welding plume “plasma”, since it offers rather only the hot weakly-ionized gas consisting of metal and alloying element vapour. Understanding that, some authors use the word “plasma” or “plasma plume” only as a term which became conventional during the many-years study of the CO₂-laser welding process. In the next Chapter it will be showed that the medium above the keyhole during high-power fiber laser metal welding consists of two parts. The lower one is an erosive laser-induced low-ionized vapour jet from the keyhole. The second one is formed by small condensed particles and cold metal vapour. Thereby, the words “plume” or “welding plume” mean from this point “plasma” + condensed particles, whereas “plasma” or “welding plasma” is only the lower part of the “welding plume”. This is not conventional terminology and used only in scope of the thesis, since such plume differentiation is only a new suggestion of the presented study.

The reason for such low welding plume temperature is low absorption of laser radiation. At the beginning stage of plasma plume formation, which was described in detail in *Sec. 1.2.1*, the warming up of the plasma takes place owing to the inverse Bremsstrahlung absorption of the photons with a small number of free electrons. However, since the effect of the inverse Bremsstrahlung absorption in plasma is proportional to the double incident radiation wavelength degree, the short-wavelength radiation of solid-state lasers is absorbed by the free electrons in plasma almost a hundred times less than the long-wavelength radiation of CO₂-lasers. When the plasma temperature is from 3000 K to 7000 K, the inverse Bremsstrahlung absorption coefficient K_{ib} for the radiation with 1.07 μm wavelength was experimentally measured to change between 0 and 0.4 m^{-1} [45],[100]. Thereby, when the typical welding plume height is about 1 cm, the maximal value of the absorbed laser beam energy is approximately 0.1% of the incident beam energy. It is evident that such low energy is insufficient for a significant warming up of the metal vapour as well as for the development of a full-blown plasma plume.

1.3. Mechanism of metal vapour condensation in welding plume

During the influence of high power laser radiation on the metal surface the jet of the evaporated atoms mixes with the ambient gas. The subsequent expansion of this mixture leads to its cooling and supersturation. As a result, generation and subsequent growth of the condensed phase clusters become possible. The presence of the condensed phase in the plasma plume can exert a considerable influence on the kinetic processes in the plasma as well as on the macroscopic characteristics of the plasma itself. In addition, the condensed metal clusters can absorb or scatter laser radiation, which impairs the beam focusing quality and the temporal power stability.

A detailed description of the small metal particle condensation effect in the welding plume as well as the results of its direct experimental confirmation under real welding conditions are given in the next sections of this chapter.

1.3.1. Theoretical preconditions

Numerical calculation results [48],[49] of the spatial distributions of the vapour-plasma mixture parameters over the metal surface are shown in *Fig. 1.9*.

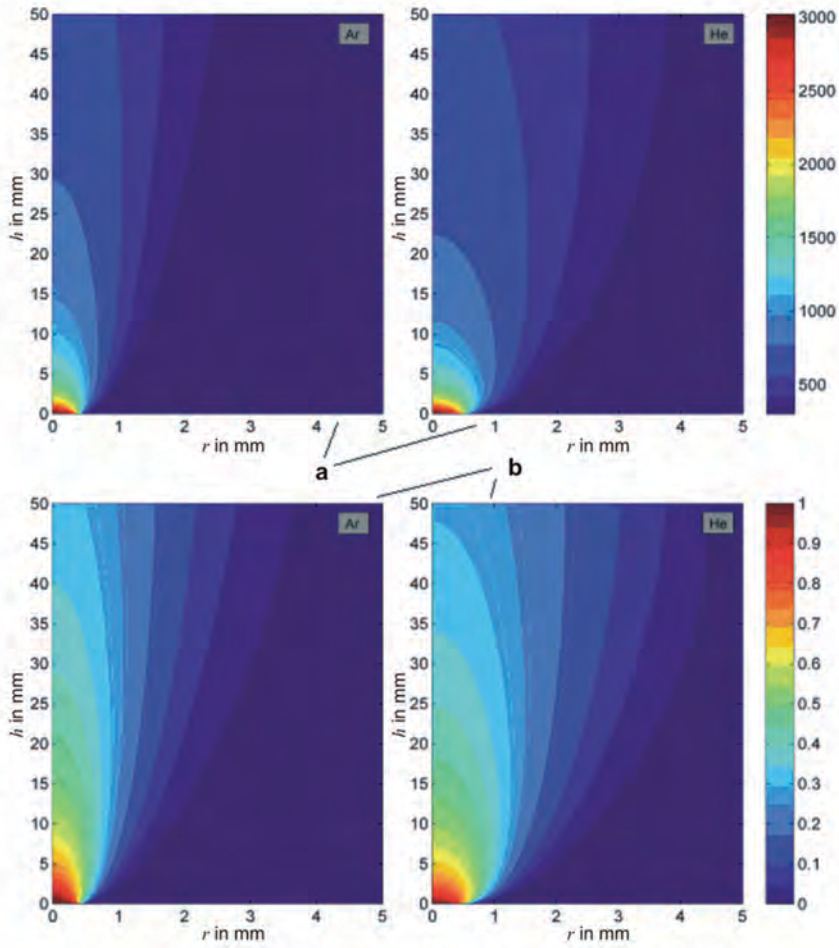


Fig. 1.9. Temperature (a) and Fe mass concentration (b) fields in the vapour-gas plume during the outflow in Ar- (left) or He- (right) medium [48]

Within the scope of this study it was assumed that the ambient medium consists of inert gas Ar or He, i.e. it does not enter into chemical reaction with the metal atoms and its ionisation degree is negligibly low. The spatial distribution of the metal vapour mass concentration m_{Fe} on the boundary between the metal and the ambient medium was defined in the following way:

$$\begin{cases} m_{Fe} = 1, & \text{when } 0 \leq r \leq R(H) \\ m_{Fe} = 0, & \text{when } r > R(H) \end{cases} \quad (1.6)$$

where $R(H) \approx 0.4$ mm is the calculated radius of the keyhole outlet.

The spatial distributions of the vapour atom mass concentration indicate that the rectangular profile from Eq. (1.6) diffuses gradually with increasing height above the metal

surface. When the plume height $h = 30$ mm, the value of m_{Fe} in the whole vapour flow becomes less than 0.4, and the radius of the area where the metal vapour concentration reduces down to zero reaches 4 mm. The temperature and the axial velocity of the vapour-gas mixture show a similar behaviour, except that the areas of the thermal and the gas-dynamical disturbance of the ambient gas are much narrower.

In order to describe the thermodynamical state of the metal vapour both inside and outside the keyhole, a dimensionless parameter ϑ can be used. This parameter characterizes the vapour supercooling degree as following [48]:

$$\vartheta = \frac{T_p - T_a}{T_p} \quad (1.7)$$

where T_p and T_a are the saturated vapour temperature corresponding to a given vapour density and to the actual vapour temperature, respectively. In terms of such description, the supercooling degree $\vartheta > 0$ or $\vartheta < 0$ corresponds to the supersaturated (supercooled) or to the superheated vapour state, respectively. In the former case volume condensation of the metal vapour can happen and small clusters of condensed metal vapour can be produced. Calculation results [48] of the metal vapour supersaturation degree inside and outside the keyhole are presented in *Fig. 1.10*. From the picture it can be seen that the whole keyhole volume can be divided into three zones with each a different vapour state.

In the areas where evaporation of the keyhole walls occurs, the vapour is supersaturated. By contrast, in the areas where surface condensation on the metal channel walls takes place the vapour is superheated. The supersaturation degree of the metal vapour inside the keyhole is small giving a value of about a few hundredths only. However, the situation changes significantly in the vapour-gas plume above the keyhole. When the vapour leaves the keyhole, it becomes strong supersaturated (see *Fig. 1.10*). Therefore, the possibility of its volume condensation as well as of condensed phase cluster formation has to be considered in this area.

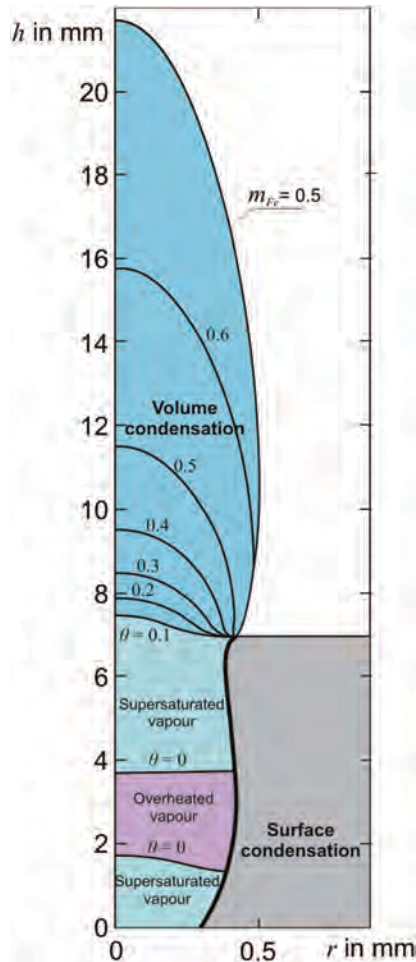


Fig. 1.10. Thermodynamical state of the metal vapour inside and outside the keyhole [48]

A theoretical possibility of metal vapour condensation during the solid-state laser metal welding process was shown in some other studies as well. For example, in [51],[52] the evolution of condensed metal clusters in the vapour-plasma medium was described by a growth equation which includes the atom flow on the cluster surface as well as the evaporation atom flow away from the surface. As a result of the calculations, a maximal cluster size of about 80 nm (see Fig. 1.11) was obtained.

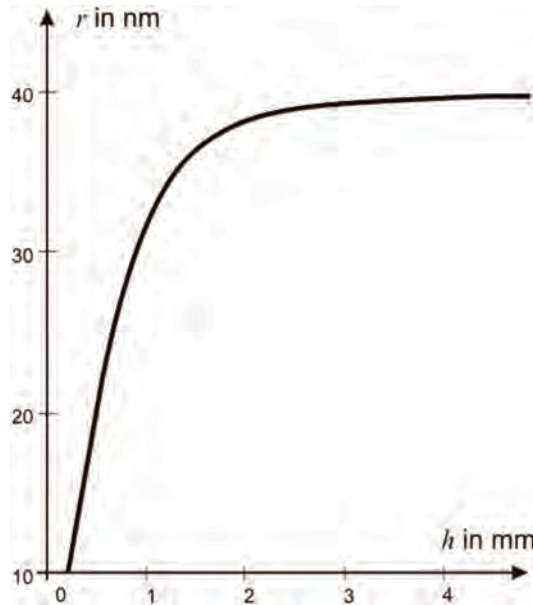


Fig. 1.11. Condensed metal vapour cluster growth in the welding plume; r – cluster radius, h – plume height [52]

The maximal degree of condensation α_{\max} , i.e. the ratio between the number of atoms in condensed state n_{cond} and the total number of atoms in volume unit n_0 , was calculated in [50]: $\alpha_{\max} = \left(\frac{n_{\text{cond}}}{n_0} \right)_{\max} \approx 0.5$. The maximal cluster size in these conditions was calculated to be less than 100 nm.

1.3.2. Indirect experimental confirmations

There are a number of experimental results showing the existence of condensed metal particles in the plume during solid-state and fiber laser welding. Measurements revealed [56],[57],[58] that a probe beam with 1.07 μm radiation wavelength is diminished by its passage through the welding plume transversally to the plume axis (parallel to the metal surface). The extinction coefficient increased with increasing power density of the laser radiation and decreased with increasing plume height. At the maximal achievable power density the extinction near the metal surface was measured to be about 4%. By using a high-speed video camera the position of the probe beam spot on the target plate was observed for different wavelengths of the probe radiation. The dependency of the refraction angle on the wavelength indicated a scattering effect like the Rayleigh scattering on small particles. Such particles must be much smaller than the used probe radiation wavelength. Therefore the observed extinction cannot be caused by macroscopic drops from the liquid metal, but only by nanoparticles from the condensed metal vapour.

Radiation scattering caused by the plume during 2 kW power Nd:YAG laser welding of mild steel with overpressure was detected in [61]. Besides the absorption in the welding plume, a considerable growth of back-reflection radiation signals (see Fig.3.2.1) as well as a

decrease of the penetration depth was registered. The authors drew a conclusion about the radiation scattering on the metallic vapour cloud above the keyhole without considering the possibility of its condensation. However, as the increasing ambient pressure obviously favours more intensive vapour condensation, the scattering reason is probably also the presence of condensed metal particles in the welding plume.

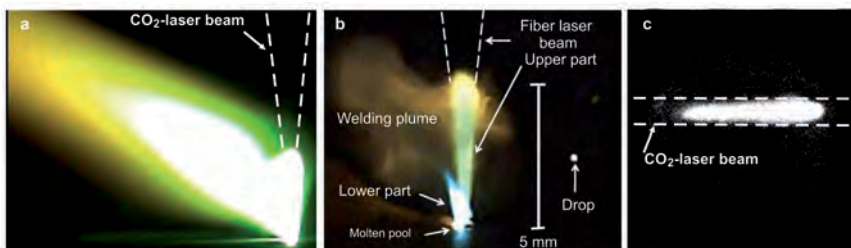


Fig. 1.12. Welding plume during CO₂- (a) and fiber (b) laser welding and luminescence of a carbon aerosol under the influence of a CO₂-laser beam (c) [43],[63],[97]

Other experimental confirmation of the appearance of small particles above the keyhole during welding was provided by the results of high-speed photo and video observation of the glowing plume. The plume form differs strongly from the erosion plasma plume in case of CO₂-laser welding, but it looks like a trace of the laser beam propagating through dusty medium, where the radiation is absorbed by small particles. Due to the radiation energy absorption the particles warm up and vaporize. Fig. 1.12 shows the characteristic form of the CO₂-laser welding plasma plume (Fig. 1.12.a) [43], the fiber laser welding plume (Fig. 1.12.b) [97] and the glowing trace of a CO₂-laser beam in the carbon aerosol medium (Fig. 1.12.c) [63].

In [101] a comparison between the penetration depths in stainless steel by high-power fiber laser radiation with different welding parameter sets was made in case of welding with and without using a fan which blew the upper part of the welding plume away. Besides registration of scattered fiber laser radiation on the welding plume medium, a negative influence of this effect on the metal penetration depth was shown.

Increasing penetration depth, more stable welding process as well as reducing spattering were received in some investigation during deep-penetration metal welding in vacuum or in low-pressure atmosphere [102],[103]. Since the condensation process should be less intensive with decreasing pressure over the keyhole, the most probably explanation of these effects is also a reducing influence of the small condensed metal vapour particles.

1.3.3. Optical diagnostics of condensed particles in the welding plume

There are a number of different natural mediums consisting of small scattering particles which are distributed in homogeneous matter (e.g. fog, interstellar dust etc.). Examples of such desirable or undesirable mediums produced by human technical activity are much more various (industrial smokes, colloidal solutions etc). For the most of these examples, light scattering appears to be the easiest way of small particle detection and the evident

method of its consequent study. Experiments and observations can be interpreted simpler when the particles are distributed in the medium not too close to each other and when the studied samples are small enough to ignore multiple scattering events. Previous theoretical estimations of condensed particle parameters have shown that both of these two conditions are fulfilled more than enough in case of radiation scattering on small condensed metal vapour clusters in the welding plume during the deep penetration laser welding process.

Plasma containing small particles inside is called dusty plasma. There are some methods for dusty plasma investigation in certain laboratory conditions [104],[105],[106]. However, most of them seem to be inapplicable in conditions of real deep penetration welding due to the following reasons:

- plume formation process is unstable,
- direct control of the plume parameters is impossible,
- arrangement of measuring devices in the welding plume is technically difficult,
- presence of hot metal vapours and other constituents in the plume,
- complicated gas flows owing to the shielding gas supply.

One of the suitable methods in this case which is able to give some information about the particle cloud parameters is laser light scattering (LLS) [65] by using probe laser sources.

An application example of the LLS method in condensed metal particle diagnostics is described in [67]. The investigation of the welding plume was carried out during stainless steel welding with a 3 kW power thin disc laser. The average particle size and the particle concentration were determined from the relation between the extinction coefficients for three different probe radiation wavelengths (so called multi-wavelength method) [66] when the probe beams propagated transversally through the plume. Assuming all particles in the plume being uniformly distributed in the space and having the same size, the cluster diameter and the concentration were calculated to be $a \approx 115 \text{ nm}$ and $C_n = (5 \div 7) \cdot 10^7 \text{ cm}^{-3}$, respectively. The full plume attenuation of the disc laser radiation was estimated to be about 5%. Authors drew the conclusion that such low attenuation level does not influence considerably the final welding quality. However, when it is supposed that this process runs not continuously, but quasi-periodically in time, it can lead to full laser beam power modulation with an amplitude of some hundreds of Watt. The impact of small radiation power oscillations on the formation of weld imperfections in CO₂-laser beam welding was theoretically shown in [59],[60], where the eigenfrequency spectra of the liquid weld pool oscillations were simulated. It was concluded that due to some resonance effects between the frequency oscillations of the weld pool and of the laser power such process can destabilize the quasi-stationary welding process as well as favour the formation of weld imperfections. Therefore, besides giving more precise measurement results concerning the spatial characteristics of the condensed metal vapour particle cloud, determination of its generation and movement dynamics is important to be described as well. All this will allow it to understand the temporal characteristics of the welding plume influence on the laser radiation and finally on the weld quality.

1.3.4. Direct measurement of particle parameters

In [68] measurement of the probe laser radiation extinction was carried out in different probe beam positions relative to the welding plume. In the same study small condensed metal vapour particles were sedimented on a cold glass plate. By consequent observation with a TEM-microscope the particle size distribution was measured.

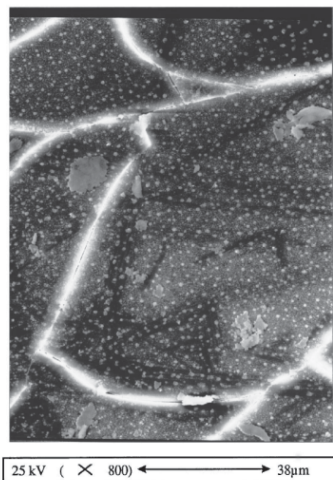


Fig. 1.13. Picture of the condensed metal vapour particles sedimented on a glass plate [69]

The average particle size was obtained to be a little bit more than 40 nm, and 82% of the sedimented particles were no bigger than 55 nm. The character of this distribution was almost independent of the type of ambient atmosphere (Ar, He, N₂). The extinction of the probe laser radiation with 1.06 µm wavelength in the welding plume was detected to be much higher than in all other previous work. During Nd:YAG-laser beam welding with 8 kW power the extinction in the area situated close to the keyhole outlet was measured to be about 27%. However, at a plume height of 3 mm over the metal surface the extinction value was only 11%.

The authors were not able to give an explanation of the fact that with lower laser beam power (4.5 kW) at the same plume height the probe beam extinction was much higher (near 38%). Attenuation recalculation of the Nd:YAG-laser beam when it propagates through the whole welding plume height gave results from 10% to 70% depending on some conditions.

In work [69] a detailed research of particles was carried out which were sedimented from the welding plume on a cold glass plate during Nd:YAG-laser beam welding of stainless steel specimens. An electron microscope picture of the glass plate with sedimented condensed metal vapour particles is shown in Fig. 1.13. The chemical composition of the sedimented particles was studied as well. As can be seen from Table 4.1, more than half of the condensed phase consists of iron oxide FeO.

Table 4.1. Chemical composition of sedimented particles from the welding plume [69]

Chemical composition	FeO	Cr ₂ O ₃	MnO	NiO	SiO ₂
Relative concentration in %	57.43	24.11	7.14	6.59	4.73

The characteristic size of the sedimented particles was observed to be near 1 μm. However, using a microscope with a higher resolution, it became clear that the particles seen in Fig. 1.13 correspond to agglomerates with a great number of much smaller particles with diameters of about 50 nm. Based on this finding it was concluded that such sedimentation method is not able to give precise information about the condensed metal vapour particles in the welding plume, since the metal vapour condensation conditions on the glass plate surface differ from those in the welding plume volume.

1.3.5. Scattering and absorption of laser radiation by condensed metal vapour particles

To characterize the interaction between electro-magnetic radiation and small particles the value of the extinction cross-section is used. The full extinction cross-section is composed of the cross-sections of scattering and absorption: $C_{ext} = C_{sca} + C_{abs}$. The physical principle involved in these cross-sections is that the total energy absorbed or scattered in all directions equals to the energy falling on the square C_{abs} or C_{sca} , respectively. For spherical particles with diameter a it is more convenient to use dimensionless parameters of the extinction, scattering or absorption efficiency:

$$Q_{ext} = \frac{C_{ext}}{G}, \quad Q_{sca} = \frac{C_{sca}}{G}, \quad Q_{abs} = \frac{C_{abs}}{G} \quad (1.8)$$

where $G = \pi a^2 / 4$ is the geometrical cross-section of the particle.

In the approximation of only single scattering events, the intensity of light which is transmitted through a particle cloud is given by the Lambert-Beer law:

$$I = I_0 \exp\left(-\int_0^L K_{ext} dl\right) \quad (1.9)$$

where: I_0 is the initial light intensity; K_{ext} is the extinction coefficient which is a property of the scattering medium; L is the beam path length.

According to the light scattering theory [53],[54], the radiation extinction coefficient of a particle cloud is connected with its density, size and optical properties in the following way:

$$K_{ext} = \frac{\pi}{4} C_n \int_0^\infty Q_{ext} N(a) a^2 da \quad (1.10)$$

where: C_n is the number density of particles; Q_{ext} is the extinction efficiency for a single particle; $N(a)$ is the particle size distribution function which is normalized to provide the condition $\int N(a)da = 1$.

The extinction efficiency value Q_{ext} for every particle is a complicated function of its size and its complex refractive index. With the exception of some special cases, there is no precise analytical expression which allows it to calculate Q_{ext} in arbitrary conditions. However, the most important case of light scattering on particles with spherical form (with arbitrary size and complex refractive index) is described by the Mie-scattering theory [107]:

$$Q_{ext} = \frac{2}{x^2} \sum_{n=1}^{\infty} (2n+1) \operatorname{Re}(a_n + b_n), \quad (1.11)$$

$$Q_{sca} = \frac{2}{x^2} \sum_{n=1}^{\infty} (2n+1) (|a_n|^2 + |b_n|^2) \quad (1.12)$$

where:

$$a_n = \frac{m \psi_n(mx) \psi_n'(x) - \psi_n(x) \psi_n'(mx)}{m \psi_n(mx) \xi_n'(x) - \xi_n(x) \psi_n'(mx)} \quad (1.13)$$

$$b_n = \frac{\psi_n(mx) \psi_n'(x) - m \psi_n(x) \psi_n'(mx)}{\psi_n(mx) \xi_n'(x) - m \xi_n(x) \psi_n'(mx)} \quad (1.14)$$

$x = \pi m a / \lambda$ is the particle size parameter; λ is the radiation wavelength; m is the ratio between the complex refractive particle index $n_c = n + ik$ and the refractive medium index around the particle n_m which in our case can be considered as 1; ψ_n , ξ_n are Ricatti-Bessel functions; character strokes mean the derivative.

Dependencies of the extinction, absorption and scattering efficiencies on the scattering particle radius which were calculated for the radiation wavelength of 1.06 μm are shown in *Fig. 1.14*. From this picture it is seen that when the particle size is small (less than 100 nm), radiation extinction generally takes place due to its absorption, whereas by contrast, when the particle radius is 100 nm and more, the scattering effect dominates over the absorption. Therefore, for the characteristic condensed metal vapour particle size of 50-100 nm (see *Sec. 1.3.1*) the extinction coefficient can reach a few units per centimetre already with a cluster density of about $10^9 \div 10^{10} \text{ cm}^{-3}$. Hence, radiation with quite high energy will be mainly absorbed by the particles, which will inevitably cause their warming up and perhaps even evaporation.

The detailed numerical absorption and scattering calculations of the radiation with a wavelength of 1.07 μm on a particle cloud consisting of pure iron particles as well as of oxide Fe_3O_4 -particles during deep-penetration laser metal welding were carried out in [124]. The extinction of laser beam intensity which passes 1 cm through the particle cloud with a particle radius from 10 nm to 100 nm was shown to be about 4%, while the particle density was about $C_n = 1.9 \cdot 10^9 \text{ cm}^{-3}$ (according the average particle diameter $a = 100 \text{ nm}$).

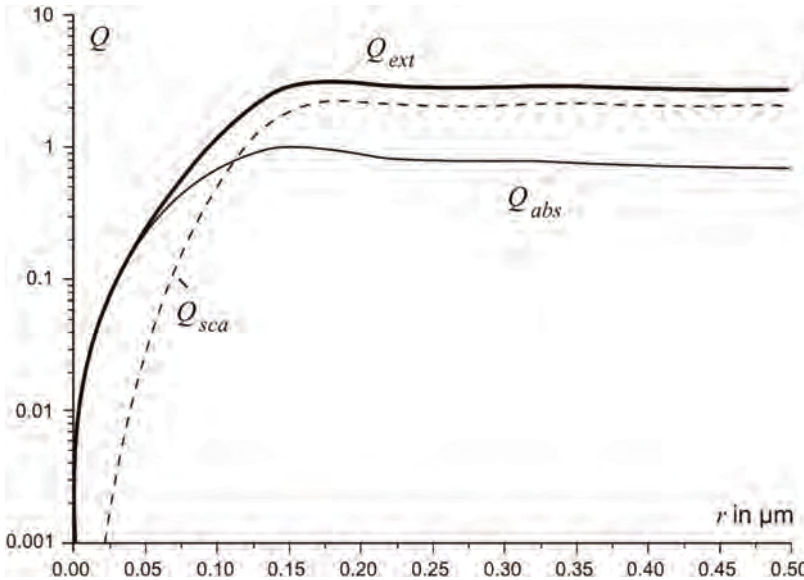


Fig. 1.14. Dependency of extinction, absorption and scattering efficiency on particle radius for the radiation wavelength of $1.06 \mu\text{m}$ [48]

In addition, it should be noted that besides the considerable reduction of the full welding laser beam power, such warming up or evaporation of the condensed metal particles under the laser radiation favours the increase of the general welding plume temperature and, as a consequence, the intensification of the influence of the negative thermal refraction effect (see Sec. 3.1.1).

Summary of Chapter 1

1. Besides the economical advantages, high power solid-state lasers with high radiation brightness like fiber or thin disc lasers have as a rule a lower BPP parameter value; this allows it to obtain sharper radiation focusing simultaneously with a longer Rayleigh length.
2. In the deep penetration metal welding process the tightly focused laser beam provides a higher density of energy deposition into the material; the longer Rayleigh length lowers the requirements for accurate maintenance of the working distance between the welding head and the metal surface; therefore high power fiber (or thin disc) lasers attract great interest as energy sources for this technology.
3. In comparison to the traditionally used CO_2 -laser radiation, the peculiarities of the high power fiber laser radiation, which cause the physical differences of the deep penetration welding process, are the shorter radiation wavelength and the sharper profile of the spatial power density distribution in the beam cross-section.

4. The coefficient of the inverse Bremsstrahlung light absorption by plasma electrons in the heavy-particle field for radiation with $1.07 \mu\text{m}$ wavelength is approximately a hundred times lower than for radiation with $10.6 \mu\text{m}$ wavelength. In the process of deep penetration laser metal welding the plasma formation at the beginning stage takes place due to the warming up of the low-ionized metal vapour which absorbs the laser radiation energy by the inverse Bremsstrahlung absorption mechanism. As a consequence, the temperature and the concentration of the free electron in the welding plasma during high power solid-state laser welding should be much lower than during high power CO_2 -laser welding.
5. From the theoretical estimations and the presented experimental data it follows that the plasma plume should not influence the transmitting laser radiation.
6. When the hot vapour-gas jet escapes the keyhole in the welding plume area with a lower temperature, supersaturation of the metal vapour takes place which can lead to vapour volume condensation and to the generation of a small condensed metal vapour particle cloud.
7. Theoretical calculations of the condensed metal vapour cluster formation kinetics give cluster size values of about 50-100 nm.
8. Cloud of condensed metal particles can cause considerable extinction of a fiber laser beam during welding. Therefore, the metal vapour condensation effect should be taken into account and the condensed particle parameters should be measured experimentally.

Chapter 2. Welding plume spectroscopy

- 2.1. Structure of the welding plume**
- 2.2. Welding plasma spectroscopy**
 - 2.2.1. Experimental technique**
 - 2.2.2. Emission spectra of the welding plasma**
- 2.3. Welding plasma state and its influence on the laser radiation**
 - 2.3.1. Interaction with atoms of ambient medium**
 - 2.3.2. Absorption by free electrons in plasma**
- 2.4. Influence of the shielding gas on the welding plume**
- 2.5. Welding plume study in the upper part**
 - 2.5.1. Spectral pyrometry method**
 - 2.5.2. Plume temperature in the upper part**
 - 2.5.3. High-speed video observation**

Summary

Spectral analysis of the welding plume emission was carried out to determine the welding plasma state and to measure its influence on fiber laser radiation. The aim of this experiment was to check the validity of the supposition made in Sec. 1.2.2 that the welding plasma influence is negligibly low due to its low temperature. To simplify the interpretation of the measurement results as well as to account for the welding plume dynamics the emission spectra measurements were combined with high-speed video recording (up to 20000 fps) carried out in both the plasma light only and with the help of an external illumination lamp. The measurements were made in cases of welding in ambient air as well as under shielding gas atmosphere (Ar, He).

2.1. Structure of the welding plume

The Fig. 2.1 shows the results of the high-speed video observation of the different welding plume areas during the welding process.

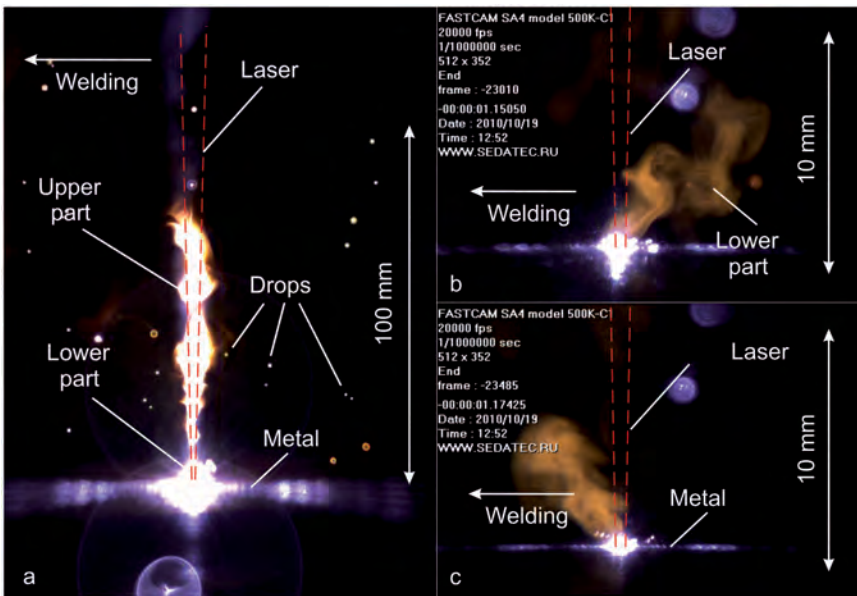


Fig. 2.1. High-speed video observation of different parts of the welding plume

These pictures were made in the light of the welding plasma, i.e. without external illumination sources. Video recording of the full welding plume size (see Fig. 2.1.a) was carried out at a frame rate of 10000 fps and a frame exposure of about $33 \mu\text{s}$ each. The lower part of the welding plume adjoins directly the keyhole outlet and its brightness is much higher than that of the other welding plume areas. Therefore in order to record this part in more detail (see Fig. 2.1.b-c) the exposure time was decreased down to $1 \mu\text{s}$. In addition, smooth metal plates were placed at three sides of the welding plume, which reflected part of the plasma emission light back and illuminated the interaction zone. As the oscillation in the lower part of the welding plume occurred much faster than in the upper part, the recording speed was also increased up to 20000 fps.

From the obtained results it was ascertained that the whole welding plume consists of two parts with different dynamics, brightness and geometrical form. The lower part (“welding plasma”) corresponds to a small area (near 3-4 mm in height) of bright emission with sharp borders and has fast oscillations (up to few kHz) in the welding plane which, however, decline mainly in the direction opposite to welding (see Fig. 2.1.b-c). The upper part emission can reach an area of more than 50 mm in height and has a geometrical form very similar to the caustic form of the fiber laser beam. The light area is observed to move relatively slowly upward from the metal surface showing a simultaneous decrease in emission intensity in the upper part.

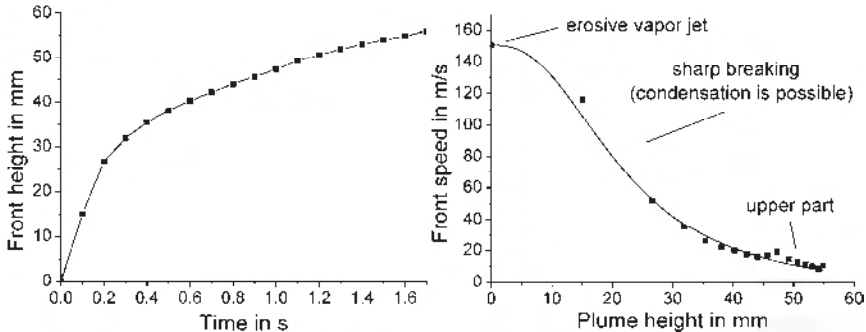


Fig. 2.2. Plume front dynamics: front height vs. time (left) and front speed vs. plume height (right)

Temporal dynamics of the plume front in the first moments after starting the laser influence is shown in Fig. 2.2. As seen, the front speed near the metal surface corresponds to the characteristic values for an erosive vapor jet from keyhole (about 100 m/s). But than the vapour is broken drastically, i.e. its condensation at height from ca. 20 mm is probable (the condensation effect is discussed in Chapter 4). The upper part of the welding plume moves up from the metal surface with a speed of only a few meters per second, whereas its boundary becomes fuzzy.

Beside the welding plume emission a great number of liquid metal drops produced due to weld pool spattering can be seen in all presented pictures.

2.2. Welding plasma spectroscopy

2.2.1. Experimental technique

The welding plasma study was carried out in conditions similar to the real conditions of the deep penetration metal welding process with high power solid-state laser radiation. The penetration of the low-alloyed mild steel specimen was provided by a high power fiber laser with a radiation power of 20 kW. The laser beam was focused on the metal surface into a spot with 560 μm diameter. The principal scheme of the experimental setup, which allowed it to register the welding plasma plume emission spectra, is shown in Fig. 2.3. An echelett-grating (11) with the resolution ratio $\frac{\lambda}{\Delta\lambda} > 10^4$ was used for the spectral diagnostics of the

welding plasma emission radiation. The scanning mirror (8) in the spectrometer performs the re-turning of the echelett-grating spectral range and at the same time shifts the diffraction peaks in the direction orthogonal to the direction of the spectral factorization. Such 2D-factorized spectra were registered with a video camera (14) and consequently processed with a PC (15). This technique gave an opportunity of simultaneous observation of a number of spectral lines in the broad spectral range, whereas the spectral resolution remained high enough.

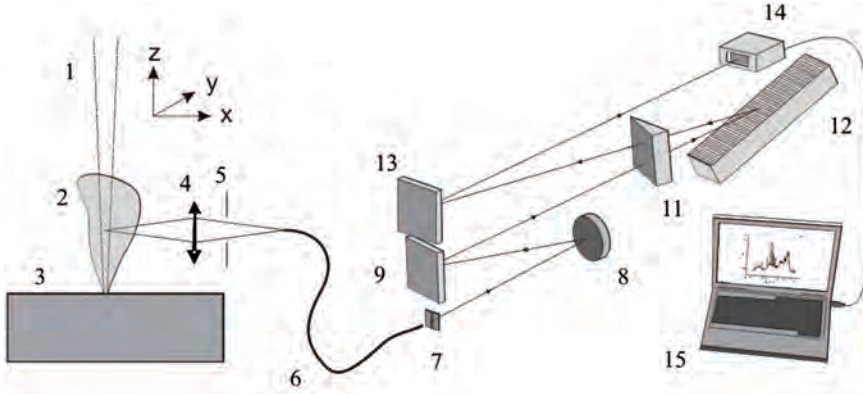


Fig. 2.3. Experimental setup of welding plume emission spectra measurement: 1 – laser beam; 2 – plasma plume; 3 – specimen; 4 – focusing lens; 5 – slit; 6 – optical fiber; 7 – inlet spectrometer slit; 8 – scanning mirror; 9, 13 – rotating mirrors; 11 – prism; 12 – echelett; 14 – video camera; 15 – PC

In the local thermodynamical equilibrium condition the intensity of the radiation, which is emitted due to the electron transition between the energy levels E_i and $E_j < E_i$, respectively, is given by the equation:

$$I_{ij} = N_i A_{ij} h_p \nu_{ij} \quad (2.1)$$

where N_i is the population of the upper energy level; A_{ij} is the transition probability; $h_p \nu_{ij}$ is the energy of the emitted light quantum. In the equilibrium state the distribution of the number of electrons along the electron energy levels in atom is given by the Boltzmann law:

$$\frac{N_i}{N} = \frac{g_i}{Z(T)} \exp\left(-\frac{E_i}{k_b T}\right) \quad (2.2)$$

where N is the full number of particles; g_i is the statistical weight of the upper energy level; $Z(T)$ is the partition function of the chemical element; k_b is the Boltzmann constant.

Using Eq. (2.1), Eq. (2.2) can be rewritten to read:

$$\ln\left(\frac{I_{ij} \lambda_{ij}}{A_{ij} g_i}\right) = -\frac{E_i}{k_b T} + \ln\left(\frac{N h_p c}{Z(T)}\right) \quad (2.3)$$

As the exact values of the transition probabilities, of the partition functions as well as of the full number of atoms are in general case unknown, the temperature is normally determined by the ratio of two or more spectral line intensities, where all lines must correspond to the same ionisation degree. In this case, measurement of the absolute spectral line intensity values can be abandoned. Graphical dependencies of the values of $\ln\left(\frac{I_{ij}\lambda_{ij}}{A_{ij}g_i}\right)$ on different energy levels E_i are called Boltzmann plots, whereas the method of the temperature calculation based on the inclination angle of the Boltzmann plot lines is often called as the method of Boltzmann plots.

When the electron temperature value is measured, the ionisation degree of the plasma plume α_i can be obtained from Saha's equation which, by taking only the first-order ionisation into account, has the following form:

$$\frac{\alpha_i^2}{1-\alpha_i} = \left(\frac{2\pi m_e k_b T}{h_p^2}\right)^{3/2} \frac{k_b T}{p} \exp\left(-\frac{eV}{k_b T}\right) \quad (2.4)$$

where m_e , e are the mass and the charge of electron, respectively; V is the ionisation potential; p is the gas pressure.

Then, the concentration of free electron in the plasma can be calculated from the perfect gas equation:

$$n_e = \alpha_i n_0 = \alpha \frac{p}{k_b T} \quad (2.5)$$

where n_0 is the Fe-atom concentration (it is supposed that near the metal surface the erosive jet consists of 100% iron atoms).

2.2.2. Emission spectra of the welding plasma

The characteristic spectra of welding plasma emission in case of welding in air (a), under Ar (b) and He (c) shielding atmosphere as well as the Boltzmann plots corresponding to these spectra with the linear approximation are shown in *Fig. 2.4*.

Against the background of continuous radiation all spectra show a few strongly marked lines which correspond mainly to the electron transitions in the neutral iron atom. Depending on the chemical composition of the steel to be welded, the emission spectra also show a small number of lines identified as corresponding to the electron transitions in the neutral atoms of the alloying elements (Cr, Mn, Ni and other). However, neither electron transitions in the iron ion nor lines of the shielding gas atoms were found. This indicates a plasma temperature which is too low for both the iron atom ionisation and for the excitation of high-energy levels.

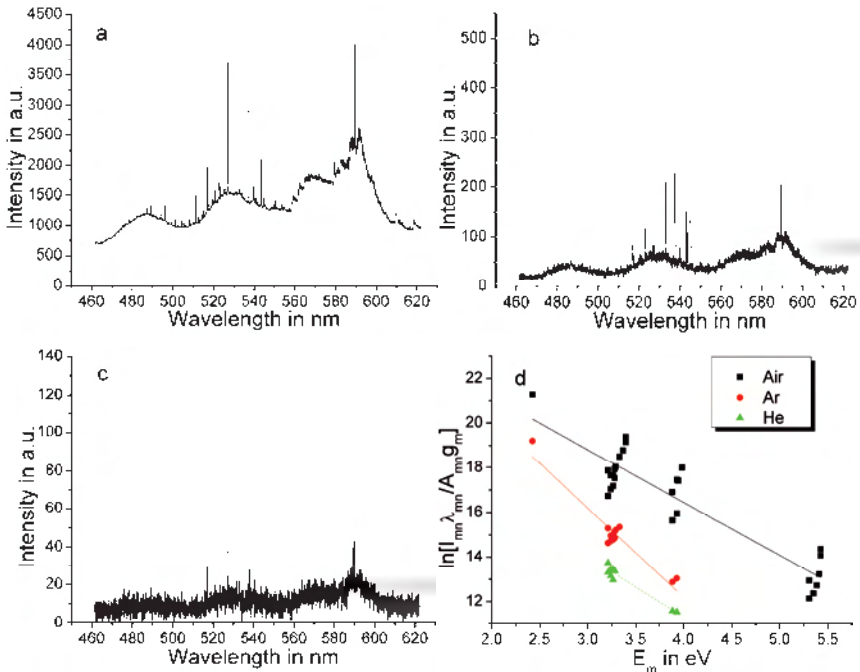


Fig. 2.4. Characteristic emission spectra of the lower welding plume part during the welding in air (a), under Ar- (b) and He-shielding (c) atmosphere as well as corresponding Boltzmann plots (d)

From the spectra shown in Fig. 2.4 a strong reduction in emission intensity can be observed when Ar or especially He shielding is used. In case of Ar-supply the average intensity decreases approximately by the factor of 20 in comparison with the welding in air. The supply of He reduces it even more (almost by the factor of 80). At the same time a reduction in the number of spectral lines is seen. Nevertheless, in case of welding in air and under Ar-shielding a sufficient number of lines was registered to build corresponding Boltzmann plots and to measure the equilibrium plasma temperature.

2.3. Welding plasma state and its influence on the laser radiation

Deep penetration laser metal welding is an operation typically involving not only the useful process of energy transmission from the laser radiation to the metal, but also a number of other interaction processes which can change energetic, geometric and dynamical characteristics of the laser beam and impede high-quality weld formation to a greater or lesser degree.

In general case the medium above the keyhole during the deep penetration laser metal welding consists of atoms and molecules of the ambient atmosphere (air or shielding gas like Ar or He) as well as of metal vapour atoms or ions (Fe and alloying elements). The plasma plume is formed by ions (with different ionisation degree) of iron, alloying elements

and ambient gas (air, Ar, He) as well as by free electrons. Besides direct interaction of the mentioned matters with the laser radiation, diffraction effects are also possible in the presence of some gradient in the refraction index of the medium inside the laser beam caustic due to the sharp spatial changes of different medium properties (like temperature, pressure, concentration, chemical composition etc.). The diffractive effects will be studied and described in *Chapter 3*.

In this section, the interaction between the matters mentioned above and laser radiation will be described focusing only on the details necessary for studying the deep penetration laser metal welding process. In addition, conclusions will be drawn about the degree of influence exerted by each of these matters on the laser welding process for two types of technological lasers (solid-state lasers with 1.07 μm wavelength and CO_2 -lasers with 10.6 μm wavelength).

2.3.1. Interaction with atoms of ambient medium

Atmospheric air has practically no influence on the laser radiation (except the case of optical breakdown), since the wavelengths of both the solid-state laser and the CO_2 -laser lie in the so-called atmospheric transparency window [109]. The same is true of all shielding gases which are used in laser welding technology. The only possible mechanism of interaction between laser radiation and atmospheric air is thermal refraction (or the mirage-effect), i.e. refraction of the bounded beam due to the gradients of the temperature distribution field. This mechanism will be discussed further below together with the refraction of the free electron cloud in the plasma plume. Here only the interaction of high-power laser radiation with atoms and ions of the metal vapour is considered.

Line absorption. Metal vapour can absorb laser radiation only in the case when the energy of the incident photons coincides with the corresponding electron or vibronic transition energy in the molecules, atoms or ions. Therefore, this absorption mechanism is strongly dependent on distribution of the energy levels in the vapour matter. The corresponding absorption bands of the iron atoms and ions are as a rule very narrow and seldom overlap the wavelength of lasers which are used for materials processing [108]. This implies that this mechanism does not play any considerable role in the deep penetration welding process with both solid-state and CO_2 -laser radiation.

Multi-photon absorption. Multi-photon absorption or multi-photon ionisation can happen when the number of photons is high enough to interact during the lifetime of some virtual particle energetic levels and when the total energy of all these photons is high enough to cause particle ionisation. The probability of a transition with absorption of n photons is approximately proportional to the intensity to the n -th power.

The ionisation potential of iron atom is $I_1^{\text{Fe}} = 7.87$ eV. Therefore, direct multi-photon ionisation of the iron vapour by the high power solid-state laser at the energy of one light quantum of $h_p\nu = 1.3$ eV requires extremely high laser light intensity. In this case, absorption of the light quanta is the more probable, when the atom goes upstairs the consecutive quantum energy levels (step-by-step excitation) [110]. The resonance character of these transitions is partly diffused by the Boltzmann energy distribution,

therefore the ionisation probability increases with increasing temperature (like in the common photo-ionisation process). This mechanism can have a significant influence in technologies where an extremely high radiation power density is used (e.g. surface modification with laser pulses of pico- and femtosecond duration). However, in the processes of deep penetration laser metal welding such mechanism is neither capable of causing significant absorption of the laser radiation energy nor of generating a developed plasma plume.

Scattering. When the light propagates through a gas medium consisting of atoms and ions of air, shielding gas and metal vapour, it can be not only absorbed, but also scattered. The process of scattering can be considered to take place in two steps. First, an atom absorbs one light quantum and an electron in the atom transits from the ground state to one of the excited levels. Then, the excited electron spontaneously relaxes returning either back to the same ground energy level or to another level with lower energy. In this process, some other “scattered” light quantum is emitted. The scattering cross-section is described in this case by the well-known Rayleigh equation [111]:

$$\sigma_{\omega,\omega} = \frac{16\pi}{3} \omega^4 c^{-4} |\chi^{(1)}(\omega; \omega)|^2 \quad (2.6)$$

where: ω is the light wave frequency; $\chi^{(1)}(\omega; \omega)$ is linear susceptibility of the atom which defines the relationship between the atom polarization and the electro-magnetic field intensity: $\mathbf{P} = \chi^{(1)} \mathbf{E}_F$. The expressions for the scattering cross-sections in case of the combinational scattering (Raman scattering) can be obtained by means of the substitution $\omega \rightarrow \nu$, $\chi^{(1)}(\omega; \omega) \rightarrow \chi^{(1)}(\nu; \omega)$.

As the non-resonant linear susceptibility values as well as the concentrations of the scattering particles are small, the scattering cross-sections for the radiation of the fiber laser at both the air and the metal vapour atoms appear to be also negligibly low. In comparison with other scattering mechanisms in the process of deep penetration fiber laser metal welding they can be completely ignored.

Generally, not only linear, but also non-linear scattering processes should be taken into account. Such processes are conditioned by absorption of a few photons and described by non-linear susceptibilities. The acceptability of the linear approximation depends on the ratio between the amplitudes of the electric light wave field and of the characteristic internal field E_0 . This internal field defines the connection forces which act on the optical electron in the medium. For atoms in gases the characteristic value of the internal field is $E_0 \approx 10^9$ V/cm. However, when the power density of the fiber laser radiation is about 10^9 W/cm², the intensity of the light wave field is only $E_F = 10^6$ V/cm. Therefore, all non-linear processes of the interaction between radiation and matter in case of such low intensities ($10^6 \div 10^9$ W/cm²) are also negligible.

2.3.2. Absorption by free electrons in plasma

It is well known that a free electron cannot absorb a photon, as the energy and impulse conservation laws can not be satisfied simultaneously [112]. For the absorption of a photon by an electron the third body is necessary. It may be a neutral atom, a molecule or the crystal lattice in the solid. During the collision with the third body the electron can absorb a photon, and the photon energy would be passed then to the kinetic energy of the colliding particles, i.e. practically to the kinetic energy of the electron, as its mass is much less than the mass of the third body. It is precisely this fact that explains the interaction of the laser radiation with the free electrons in gas. Such "collisional" absorption mechanism of the electromagnetic wave by the electron gas was called inverse Bremsstrahlung absorption or absorption by the inverse braking effect (as it is inverse relative to the electron Bremsstrahlung mechanism by collision with a heavy particle).

In the model of a classic Lorentz oscillator the inverse Bremsstrahlung absorption coefficient can be represented as [44]:

$$K_{ib} = \frac{2\sqrt{2}\pi}{\lambda_0} \left[- \left(1 - \frac{\omega_p^2}{\omega^2 + \nu_c^2} \right) + \sqrt{\left(1 - \frac{\omega_p^2}{\omega^2 + \nu_c^2} \right)^2 + \left(\frac{\nu_c}{\omega} \cdot \frac{\omega_p^2}{\omega^2 + \nu_c^2} \right)^2} \right]^{1/2} \quad (2.7)$$

where λ , ω is the wavelength and the frequency of the incident radiation, respectively; ω_p is the Langmuir plasma frequency, which is connected with the free electron density in

the plasma n_e as follows: $\omega_p^2 = \frac{n_e e^2}{\varepsilon_0 m_e}$ (m_e , e are the mass and the electrical charge of electron, respectively; ε_0 is the dielectric permittivity of free space); ν_c is collision frequency embracing the electron-atom ν_{ea} and the electron-ion ν_{ei} collisions:

$$\nu_c = \nu_{ea} + \nu_{ei} \quad (2.8)$$

$$\nu_{ea} = \frac{8}{3\sqrt{\pi}} \sigma_c n_0 \sqrt{\frac{2k_b T_e}{m_e}} \quad (2.9)$$

$$\nu_{ei} = \frac{e^4 \ln(12\pi n_e^{-1/2} e^{-3} (\varepsilon_0 k_b T_e)^{3/2})}{3\varepsilon_0^2 \sqrt{m_e}} \cdot (2\pi k_b T)^{-3/2} (N^+ + N^{++} + \dots) \quad (2.10)$$

where k_b is the Boltzmann constant; T is the temperature; σ_c is described by the classical expression $\sigma_c = \pi(\eta_1 + r_2)^2$ for a cross-section of the collisions between the particles with radii η_1 and r_2 ; n_0 is the number density of neutral atoms; N^+ , N^{++} , ... – the number densities of singly-, doubly- etc. ionized atoms. Under the condition $\omega \gg \omega_p$, which is practically fulfilled for any plasmas induced during material processing by both CO₂- and fiber lasers, Eq. (2.7) can be simplified using the expansion into a series with a small parameter $\frac{\omega_p^2}{\omega^2 + \nu_c^2} \ll 1$. In this case:

$$K_{ib} \approx \frac{v_c}{c} \cdot \frac{n_e e^2}{\epsilon_0 m_e \omega^2} \sim \lambda^2 n_e^2 T_e^{-3/2} \quad (2.11)$$

For practical numerical calculation of the inverse Bremsstrahlung absorption coefficient at the wavelength of 1.07 μm a simplified expression is used:

$$K_{ib} \approx 3,3 \cdot 10^{-41} n_e^2 T_e^{-3/2} \quad (2.12)$$

where n_e and T_e are expressed in m^{-3} and K, respectively.

In Fig. 2.5, the dependency of the plasma plume temperature and electron density on the incident laser radiation power is shown. The presented temperature values were obtained by means of the Boltzmann plotting method, whereas the electron density was calculated from Eq. (2.5). The measurements were carried out for the point at the axis of the fiber laser beam with 2 mm distance to the metal surface. The spot size on the metal surface was 0.56 mm. It can be seen that even with the maximal laser power of 20 kW (corresponding beam power density on the metal surface is about 8 MW/cm^2) the welding plume temperature does not exceed the value of 4500 K and the electron density value remains lower than 10^{15}cm^{-3} . The maximal ionisation degree of the metal vapour was calculated to be about 10^{-3} . The obtained results correspond to the theoretical predictions made in Sec. 1.1 where the reasons for such low values of the ionisation degree and the temperature were described and discussed.

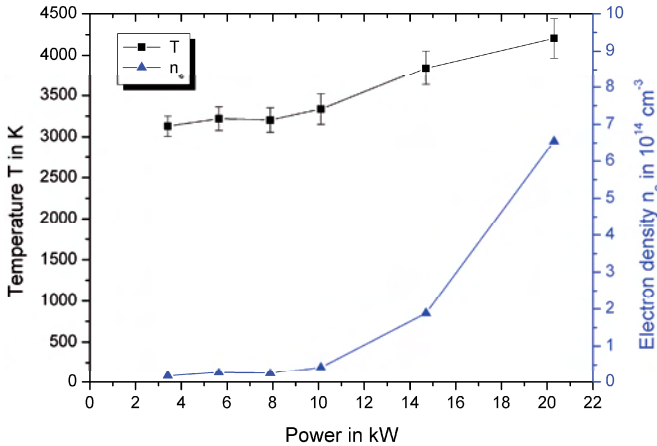


Fig. 2.5. Dependency of welding plasma temperature and electron density on laser beam power; plume height is 2 mm

From the obtained values of the welding plasma parameters the coefficient of the inverse Bremsstrahlung absorption for the solid-state laser radiation with 1.07 μm wavelength can be calculated using Eq. (2.12). The resulting value was about $K_{ib} \approx 0.6 \text{m}^{-1}$. The attenuation of a fiber laser beam, when it propagates through the typical plasma plume length of $L_{pl} = 1 \text{cm}$, can thus be expressed by:

$$\frac{I_0 - I_t}{I_0} = 1 - e^{-\alpha_{ab}L} \approx 6 \cdot 10^{-3} \quad (2.13)$$

where I_0 and I_t are the intensities of the incident and transmitted radiation, respectively.

In other words, a small attenuation value proves the assumption that during high power solid-state laser metal welding process with the radiation wavelength of $1.07 \mu\text{m}$ the direct influence of the welding plasma on the welding process can be fully neglected.

2.4. Influence of the shielding gas on the welding plume

Besides the influence of the welding plume temperature on laser power, the change of the temperature with increasing height above the metal surface was identified as well (see Fig. 2.6). The plasma temperature in case of welding in air reaches the maximal value of $T = 3500 \text{ K}$ at the short distance (about 0.5 mm) from the metal surface, after that it falls down slowly. However, starting from the height of $3\text{-}4 \text{ mm}$ stabilization of the temperature occurs and its value remains at the constant level of about 2500 K .

In case of welding under Ar-shielding, significant cooling of the welding plume takes place near the metal surface as it was already mentioned above. However, after some slight reduction, starting from the same height of $3\text{-}4 \text{ mm}$ the temperature stabilizes at the same constant level as in case of welding in air.

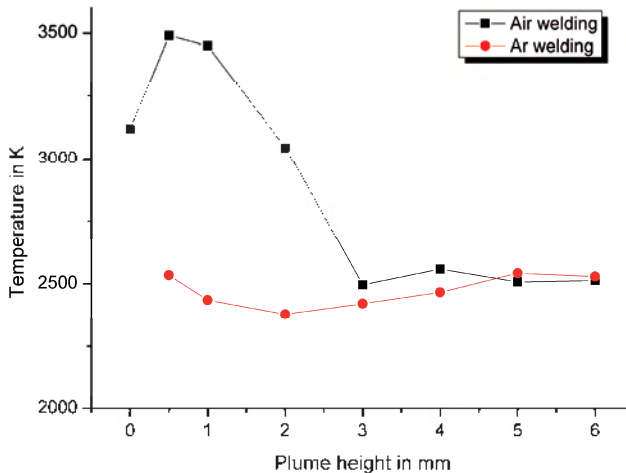


Fig. 2.6. Dependency of the welding plasma temperature on the plume height (calculated from the Boltzmann plotting method; incident laser radiation power 4 kW)

As it will be shown in Sec. 2.5.2 by the spectral pyrometry method, the welding plume temperature in the upper part continues to remain almost constant right up to the plume height of $40\text{-}50 \text{ mm}$.

It can be seen from Fig. 2.6 that, whereas the lower part of the welding plume adjoining directly the keyhole outlet is cooled down significantly by the shielding gas, influence of the

ambient atmosphere type in the higher plume area is negligible. Accordingly, the plume temperature rises again above the cooled area and then keeps its value constant. This fact indicates that there is another energy source which is not connected with the erosive vapour-plasma jet ejected from the keyhole. This is to say that warming up of the upper part probably does not occur owing to the ejection of hot metal vapour, but due to the absorption of the propagating laser radiation. As follows from Sec. 1.3, the reason of such absorption can be only small condensed metal particle cloud which is studied experimentally in Chapter 4.

This supposition is confirmed by the high-speed video observations of the welding plume shown in Fig. 2.7. The presented images were recorded when the welding plume was illuminated by a continuous external source of white light placed opposite to the video camera, resulting in a much higher spectral brightness than that of the welding plasma only.

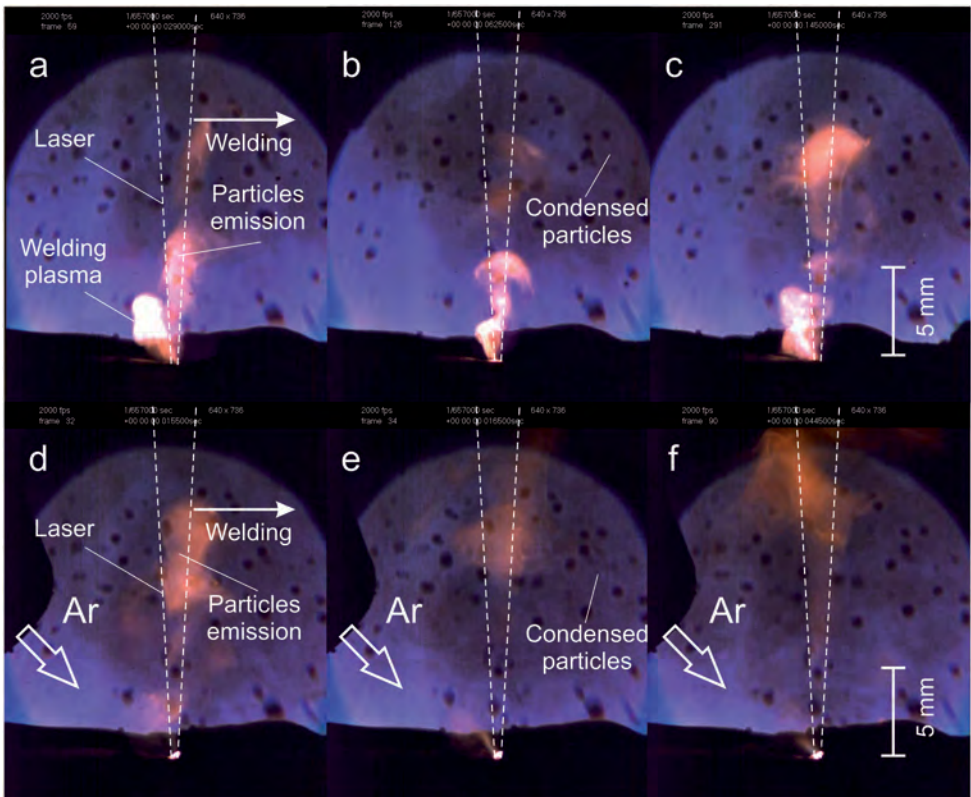


Fig. 2.7. Disappearance of the welding plasma by Ar-supply: (a-c) – welding in air, (d-f) – welding under Ar

In addition, some black-out areas can be seen in all frames in Fig. 2.7, which correspond to the areas where the illumination lamp light is absorbed. This absorption seems to be caused by the small condensed metal vapour particles (see Chapter 4). When the particles get under the fiber laser beam, they are heated up and emit the thermal radiation, which is

seen as the upper part of the welding plume. That is why the emission spectra of the upper part have no intensive spectral lines (in contrast to the welding plasma emission), but mainly consist of the continuum.

When Ar-shielding is applied, the erosive jet (welding plasma) almost fully disappears (see Fig. 2.7), but the upper part remains almost without any changes. This fact can be in good agreement with the measured temperature dependency on plume height (see Fig. 2.6), when it is taken into account that only the area $h \leq 3$ mm corresponds to the welding plasma.

It should additionally be noted that the average darkening of the light transmitted from the illumination lamp is also increased with Ar-supply. This can be linked with the intensification of the metal vapour condensation effect, while the temperature of the medium above the keyhole becomes about 1000 K lower.

2.5. Welding plume study in the upper part

As seen from Fig. 2.6, while the temperature value itself remains high enough, the measurement of the temperature by means of the Boltzmann plotting method in the higher plume areas becomes impossible. In the registered emission spectra from the upper part of the welding plume the spectral line intensity cannot be measured, since it is getting lower than the intensity of the continuous spectra emission. Therefore, temperature measurement in the upper part of the welding plume was carried out using the spectral pyrometry method, which is generally able to give quite accurate values for the low-ionized plumes in this temperature range [113].

2.5.1. Spectral pyrometry method

The spectral pyrometry method [114] is based on the description of different real objects using an emittance function $0 \leq \varepsilon(\lambda, T) \leq 1$. This function represents a generalization of the grey-body emittance ($\varepsilon = \text{Const}$) to an arbitrary case taking into account the deviation of the emission spectrum from the Planck-function form. Thereby, it is supposed that the thermal emission of any object can be characterized by the product $\varepsilon(\lambda, T) \cdot R(\lambda, T)$ where R is the Planck-function describing the black-body emission spectrum.

In order to measure the temperature with the spectral pyrometry method compact diffraction spectrometers with silicon-CCD photo arrays are used which have a spectral registration range from near UV to near IR. Such spectrometers offer an opportunity for fast emission intensity registration with a few hundreds or a few thousands of pixels simultaneously, i.e. almost continuous spectrum with a wavelength width of about 1000 nm is detected. This allows it to check the correlation between the registered and the Planck spectra in order to find the spectral regions with the best correlation in every experiment. This innovation has opened up great new measurement possibilities in conventional optical pyrometry [115].

The value of the thermal emission spectral intensity $I_s(\lambda, T)$, i.e. the radiation power emitted by a surface unit in the spectral range unit, is given by the following expression:

$$I_s(\lambda, T) = \frac{\varepsilon C_1 \lambda^{-5}}{\exp\left(\frac{C_2}{\lambda T}\right) - 1} \quad (2.14)$$

where: $C_1 = 37418 \text{ W}\cdot\mu\text{m}^4/\text{cm}^2$; $C_2 = 14388 \mu\text{m}\cdot\text{K}$; ε is the emittance of the diagnosed object; the wavelength and the spectral intensity are expressed in μm and in $\text{W}\cdot\text{cm}^{-2}/\mu\text{m}$, respectively.

The influence of the indeterminacy $\Delta\varepsilon$ on the measurement result is considerably different for two areas of the Planck diagram. In the Wien range (short wavelengths) where $\frac{C_2}{\lambda T} \gg 1$, the condition $\Delta\varepsilon/\varepsilon = \frac{C_2}{\lambda T} \cdot \frac{\Delta T}{T}$ is fulfilled, while in the Rayleigh-Jeans area (long wavelengths) where $\frac{C_2}{\lambda T} \ll 1$, the expression $\Delta\varepsilon/\varepsilon = \Delta T/T$ is correct.

This means that the relative emittance indeterminacy $\Delta\varepsilon/\varepsilon$ leads to the same relative indeterminacy of the temperature to be measured in the Rayleigh-Jeans area and to a much lower one (by a factor of $C_2/\lambda T$) in the Wien area. Therefore, since there is no exact data concerning the welding plume emittance values, measurements should be carried out rather in the Wien area of the thermal emission spectra.

In this area Eq. (2.14) can be transformed as:

$$\ln(\lambda^5 I_s) - \ln(\varepsilon C_1) = -\frac{C_2}{\lambda T} \quad (2.15)$$

When $\varepsilon = \text{const}$, this spectral section should become straight in the coordinate plane (X_w, Y_w) where $X_w = \ln(\lambda^5 I)$ and $Y_w = \frac{C_2}{\lambda}$, and the inclination angle of this straight line determines the emission temperature. The dependency $\varepsilon(\lambda)$ is normally logarithmical. Therefore, if the emittance value is constant or changes slowly in the chosen spectral range, its influence will result in a parallel shift of the straight line along the X_w -axis, while the inclination angle and consequently the temperature to be measured remain the same.

2.5.2. Plume temperature in the upper part

Thermal emission spectra of the upper part of the welding plume were measured almost in the same experimental configuration and conditions as those described in Sec. 2.2.1 (see Fig. 2.3).

However, in this case a grating spectrometer with a fiber-optic input and a silicon CCD array with the spectral range of 200-1160 nm were used for the registration. The spectral resolution of the spectrometer was about 1.4 nm.

Measured emission spectra of the upper welding plume part are shown in Fig. 2.8a for welding in air and under Ar or He shielding atmosphere. Fig. 2.8b shows the same spectra in the Wien coordinate plane (X_w, Y_w) . As it was mentioned before (see Sec. 2.2.2, Sec 1.1),

the emission intensity was drastically reduced by applying Ar- and especially He-shielding. Therefore, the spectrometer integration time in these cases was increased from 100 ms up to 500 ms and 1000 ms, respectively.

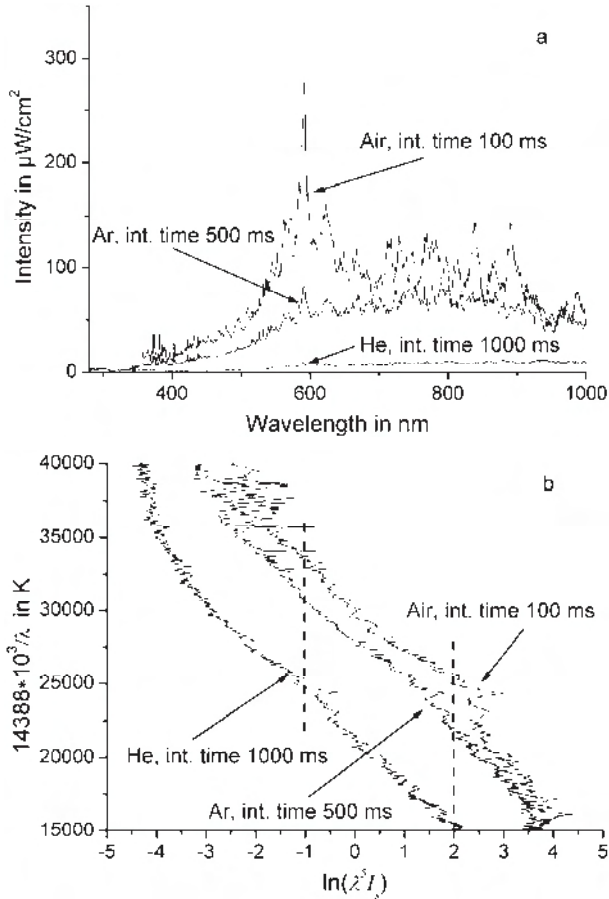


Fig. 2.8. Panoramic emission spectra of the upper welding plume part in case of welding in air, under Ar and He shielding atmosphere in normal (a) and Wien (b) coordinates

In the initial spectra some emission lines obviously corresponding to the electron transitions in neutral Fe-atoms (like in Sec 2.2.2) could be found. However, since the spectrometer wavelength measurement accuracy was no more high enough, these lines were not resolved.

It is seen that all three presented spectra have a quite straight section in the Wien-coordinate plane (e.g.: $-1 \leq \ln(\lambda^5 I_s) \leq 2$) which can be used for temperature calculation. The results of such calculation for different welding plume heights are collected in the diagram shown in Fig. 2.9. The temperature values in the diagram are combined with the

results of the welding plasma temperature measurements by means of the Boltzmann plots method presented in Fig. 2.6.

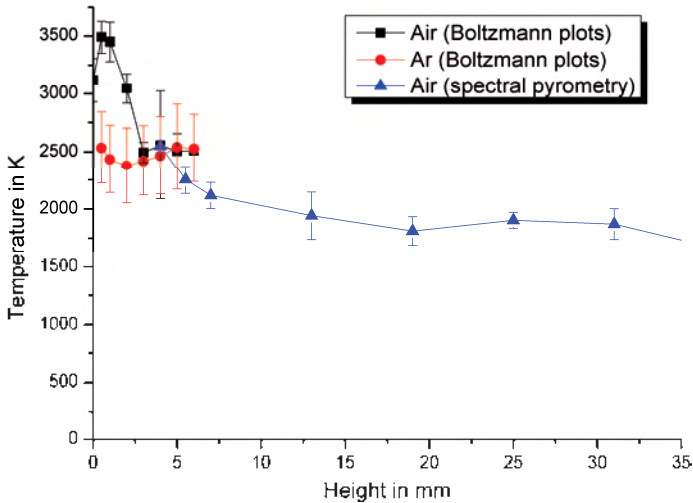


Fig. 2.9. Plume temperature in the lower part (determined using Boltzmann plots) and the upper part (measured with spectral pyrometry)

A quite good correlation between these two measurements is seen. In addition, the upper part temperature does not drop down to zero and remains at an almost constant level with increasing height up to 30-40 mm. First, this means that in the upper part of the welding plume there is some other energy source which maintains the constant temperature. Second, the constant temperature value is near the iron evaporation temperature and the emission spectra look more like a thermal radiation, i.e. there is almost no narrow plasma emission line. Both of these factors can easily be explained by the supposition made in Sec. 1.1, namely that the upper part emission is formed by thermal emission of the small condensed metal vapour particles irradiated by the high-power fiber laser beam.

2.5.3. High-speed video observation

As it was mentioned before, the emission of the welding plume in the upper part has much lower brightness than the welding plasma emission. Therefore, in order to observe the upper part it was necessary to use an external illumination light source [116].

Fig. 2.10 shows the images of the upper part of the welding plume, which were recorded with transillumination of the welding area by an opposite high-brightness white light source. Besides the emitting areas of the welding plume, which were already observed before, some areas with absorbed or scattered illumination light were also definitely seen in such configuration. These areas can be seen more clearly in the high-contrasted images in Fig. 2.10.c-d. They display the upper plume part surrounded by a cloud of small absorbing particles which are apparently the condensate of the metal vapour. Initially the metal vapour ejection is performed by the erosive jet (i.e. by the lower part of the welding plume) mainly in the direction opposite to welding. However, the metal vapour is then picked up by the

stream directed to the fume exhaust system. Thereby, when the condensed particles get under the fiber laser beam, they are heated up and perhaps evaporated, which produces the visible emission in the upper part of the welding plume (see Fig. 2.10.c).

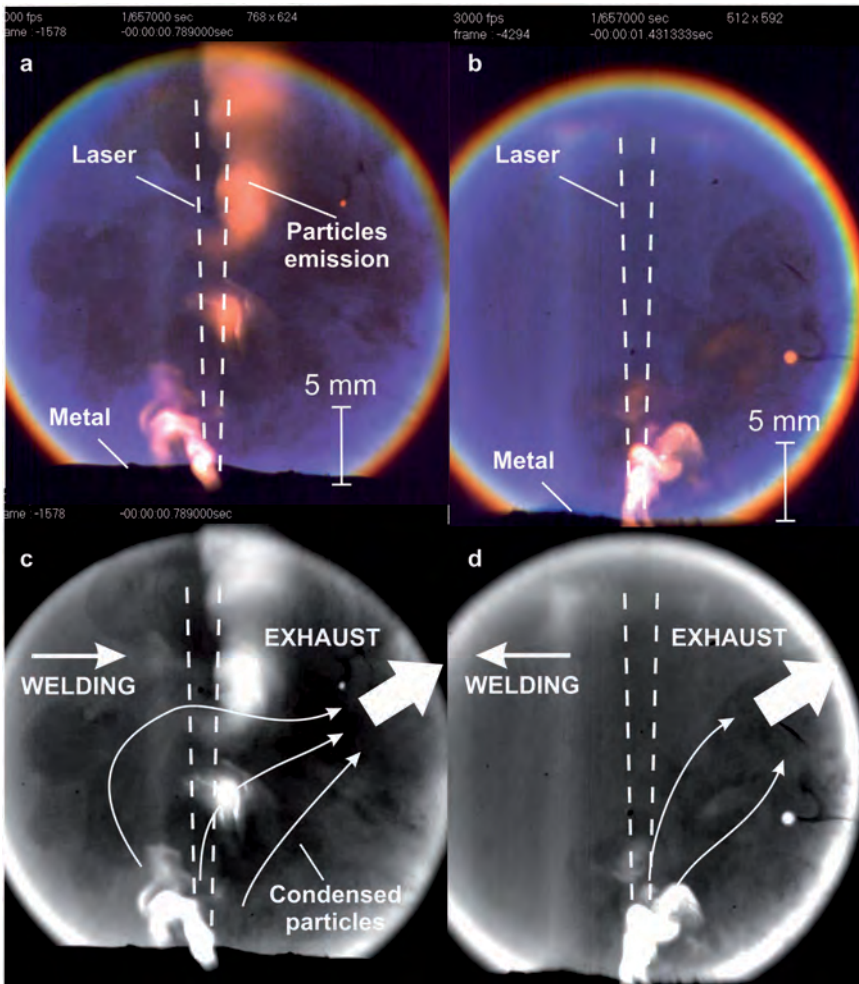


Fig. 2.10. Images of the upper part of the welding plume during welding with front-exhaust (a) and rear-exhaust (b) (original images); (c,d) – highly contrasted images

When the exhaust stream direction is opposite to the welding direction, the particles, which are ejected together with the erosive jet, fly directly to the exhaust tube. As they are immediately carried away from the laser beam caustic area, there is practically no visible emission in the upper part of the welding plume in this case (see Fig. 2.10.d). This fact has an applied importance, as it shows that, in order to remove the negative influence of the welding plume, it is not necessary to take the whole plume away using a fan or an additional gas jet (such method is known to stabilize the welding process and to increase

laser penetration depth). Instead of this, only an appropriate optimisation of the gas flow configuration (like in the simple example shown in *Fig. 2.10*) can be enough.

The presented results demonstrate also that the upper part of the welding plume consists of the cloud of small condensed metal particles which are able to absorb laser radiation. When the particles of this cloud get inside the high-power laser beam caustic, they warm up and generate the visible emitting plume area, whereas the geometrical form of the area is very close to the laser beam caustic form. This fact explains the observed effect that Ar supplied to the welding area has a drastic influence on the welding plasma, while the upper part of the welding plume remains at the same time almost uninfluenced. In addition, the mutual configuration of the erosive jet from the keyhole and the fume exhaust direction greatly impacts the condensed particle cloud.

By placing the exhaust tube straight behind the welding plume, direct and immediate removal of the condensed particle cloud is provided preventing the particles from returning into the interior of the fiber laser beam. In this case there is almost no emission observed in the upper part of the welding plume.

Summary of Chapter 2

The most important results of this Chapter can be formulated as follows:

1. During high-power solid state laser welding of metals the welding plume has two different parts with different brightness, dynamics, temperature and geometrical form.
2. The lower part of the welding plume (welding plasma) exhibits bright emission with a sharp boundary and reaches 3-4 mm in height. It corresponds to the flow of the low-ionized metal vapour from the keyhole with the ionisation degree $\alpha_i \approx 10^{-3}$ and a temperature not exceeding 4500 K. The welding plasma temperature above the keyhole corresponds to the theoretical predictions given in Chapter 1. Due to the low free electron concentration ($n_e < 10^{15} \text{ cm}^{-3}$) absorption of the fiber (or thin disc) laser radiation with the wavelength of 1.07 μm (or 1.03 μm) in such plasma plume is negligibly low. The inverse Bremsstrahlung absorption coefficient was calculated to be $K_{ib} < 0.6 \text{ m}^{-1}$. The welding plasma performs fast oscillations with a frequency of up to a few kHz in the welding plane and mainly inclines toward the direction opposite to welding direction.
3. The upper part of the welding plume corresponds to the weak light emittance and reaches up to 40-50 mm in height. Its geometrical form is very close to the laser beam caustic form. The light-emitting areas move up from the metal surface at a velocity of about a few meters per second, whereas their brightness reduces gradually and no sharp boundaries are observed.

4. Supply of Ar shielding gas to the welding area removes the emission of welding plasma almost completely, even at small flow rates of Ar. This causes the temperature of the welding plasma to drop down to the average temperature in the welding plume medium (about 2500 K). However, the upper part of the welding plume remains practically in the same state, or in some cases the light emission becomes even brighter.
5. Supply of Ar shielding gas to the welding area removes the emission of welding plasma almost completely, even at small flow rates of Ar. This causes the temperature of the welding plasma to drop down to the average temperature in the welding plume medium (about 2500 K). However, the upper part of the welding plume remains practically in the same state, or in some cases the light emission becomes even brighter.
6. Results of high-speed video observation indicate the presence of a cloud consisting of small condensed metal vapour particles in the welding plume area. These particles absorb or scatter some part of the transmitting high power fiber laser radiation. When the particles get inside the laser beam caustic, they warm up and generate the visible light emission which forms the upper part of the welding plume. Formation of the upper part of the welding plume is strongly dependent on the gas flow configuration in the area above the keyhole.

Chapter 3.

Measurement of the probe radiation extinction in the welding plume

- 3.1. Thermal refraction measurement of the transversally propagated probe beam**
 - 3.1.1. Formation of the thermal refraction effect in the welding plume**
 - 3.1.2. Determination of the thermal refraction influence degree on the extinction of probe radiation**
- 3.2 Measurement of the 1.3 μm wavelength IR-laser radiation extinction**
 - 3.2.1. Experimental technique**
 - 3.2.2. Temporal dynamics of the probe beam extinction**
 - 3.2.3. Spatial distribution of the probe beam extinction**
 - 3.2.4. Spatial distribution of the extinction coefficient**

Summary

As it was established in the previous Chapter, the laser-induced plasma in the lower part of the welding plume should have almost no influence on the process of mild steel deep penetration welding with high power high brightness solid state lasers. Only the upper part of the welding plume can exert a considerable influence on the welding quality. This part seems to consist of small particles from condensed metal vapour. It was shown that these particles are able to absorb laser radiation when it propagates through the plume. This effect heats up the condensed particles and at the same time reduces the power of the radiation which reaches the metal surface. However, it is still not clear how much energy is absorbed and which influence on the whole welding process stability has such attenuation.

The present Chapter is devoted to the quantitative description of laser radiation absorption by the cloud of small condensed particles in the upper part of the welding plume.

In order to tackle the tasks defined, the methods were chosen based on optical transparency measurement during transversal propagation of the collimated probe beams through the welding plume medium. Since it was ascertained in Chapter 2 that the temperature of the upper plume part can be quite high, the influence of the thermal refraction effect has to be estimated before carrying out the measurements. The possible contribution of this effect to the measured extinction should be known. The time-averaged distribution of the extinction coefficient in the whole medium above the keyhole was experimentally determined together with the temporal extinction characteristics. These results were used to calculate the integral influence of the whole welding plume on the high power laser radiation.

3.1. Thermal refraction measurement of the transversally propagated probe beam

3.1.1. Thermal refraction effect formation in the welding plume

Light beam trajectories in the medium with inhomogeneous refractive index distribution $n(r)$ obey the Fermat principle. This means that the optical length of the real beam between any two points P_1 and P_2 is shorter than the optical length of any other curve which connects these points and lies in some regular neighbourhood of the beam (i.e. the

integral $\int_{P_1}^{P_2} n(r) ds = c \int_{P_1}^{P_2} dt$ along the beam trajectory has a stationary value). According to the

Fermat principle, propagation of the laser beam in the welding plume is described by the following equation [116]:

$$\frac{d}{ds} \left(n \frac{d\vec{r}}{ds} \right) = \text{grad}(n) \quad (3.1)$$

where n – complex refractive index of medium in the point of radius-vector \vec{r} ; s – coordinate along the beam trajectory. In the Cartesian coordinate system Eq. (3.1) can be divided into a couple of equations [118]:

$$\frac{d^2x}{dz^2} = \frac{1}{n} \frac{dn}{dx}, \quad \frac{d^2y}{dz^2} = \frac{1}{n} \frac{dn}{dy} \quad (3.2)$$

which in the paraxial approximation ($\tan \theta \approx \theta$, $\theta_x = dx/dz$, $\theta_y = dy/dz$) can be written as [92]:

$$\frac{d\theta_x}{dz} = \frac{1}{n} \frac{dn}{dx}, \quad \frac{d\theta_y}{dz} = \frac{1}{n} \frac{dn}{dy} \quad (3.3)$$

or in radial coordinates:

$$\frac{d\theta}{dz} = \frac{1}{n} \frac{dn}{dr} \quad (3.4)$$

The Eq. (3.4) shows that the value of the beam deviation is determined by the refractive index gradient in the plane, perpendicular to the beam propagation direction.

From the results of the previous Chapter it follows that in the upper part of the welding plume the refraction of a probe beam can take place due to the presence of some areas with refractive index gradients which are formed by inhomogeneous temperature distribution. In this case it can be supposed that the medium above the keyhole consists of atmospheric air. Indeed, a change of the refractive index due to the presence of metal vapour flying out of the keyhole is negligibly small. The refractive index of dry atmospheric air in standard conditions (pressure $P = 760$ torr, temperature $t_{air} = 15^\circ \text{C}$) is described by the Edlen equation [119]:

$$n_{air} = 1 + \frac{1}{10^6} \left[64,328 + \frac{29498,1}{146 - 10^6/\lambda^2} + \frac{255,40}{41 - 10^6/\lambda^2} \right] \quad (3.5)$$

where λ is the wavelength of the radiation.

When the air is heated up and its density is decreased, the refractive index is reduced as:

$$n_{t_{air};P} - 1 = (n_{15;760} - 1) \frac{P \left[1 + (1,049 - 0,0157t_{air}) \cdot 10^{-6} P \right]}{720,883(1 + 0,003661t_{air})} \quad (3.6)$$

With the typical values of the upper part temperature (up to 2000 K) and atmospheric pressure, the air refractive index difference can reach values of up to 10^{-4} . This is two or three orders of magnitude higher than the refractive index difference due to the absence of free electrons in the welding plasma (lower part of the welding plume). Such value is comparable with the refractive index difference in the plasma plume during the CO₂-laser beam welding process [120].

In [121],[122] theoretical and experimental study of the thermal refraction effect in the process of short-wavelength laser radiation metal welding was carried out. It was shown that the laser beam profile can change considerably when it propagates through the hot medium of the welding plume.

3.1.2. Determination of the thermal refraction influence degree on the extinction of probe radiation

In order to measure the thermal refraction in the welding plume, a He-Ne laser with a radiation wavelength of 632 nm was used as a probe radiation source. During the welding process the collimated laser beam was transmitted through the axis of the welding plume in the transversal direction (parallel to the metal surface). After that the beam hit a target plate on which a calibrated mesh was plotted (see Fig. 3.1).

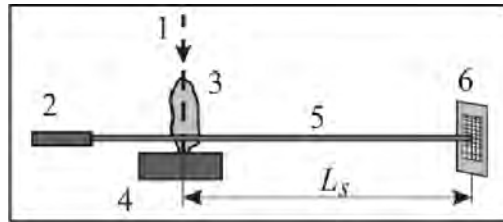


Fig. 3.1. Scheme of the experiment for probe beam thermal refraction measurement when transmitting transversally through the welding plume: 1 – fiber laser beam; 2 – He-Ne laser; 3 – welding plume; 4 – specimen; 5 – probe beam; 6 – target

The refraction angle of the probe beam in the welding plume was measured from the deflection of the spot on the target surface, which was registered with a high-speed video camera (20000 fps rate). Distance L_s from the welding plume to the target was chosen to be about 2.5 m, which permitted the detection of small probe beam inclination angles. The height of the probe laser beam over the metal surface was about 10 mm.



Fig. 3.2. Deviation of the probe beam spot position on the target surface due to the thermal refraction in the welding plume

The video recording allowed to identify fast oscillations (with frequencies up to 5 kHz) of the spot position simultaneously with strong distortions of its round shape (see Fig. 3.2). However, the maximal angle of deviation was less than 0.5 mrad. The aim of these measurements was to determine the importance of a thermal refraction effect for full extinction of the probe beams, which will be used in the following experiments in the same geometry (transversal propagation through the welding plume). As those experiments were carried out not only with infrared laser at 1.3 μm wavelength but also with white light as a probe radiation, it is necessary to estimate the thermal refraction influence not only for the

radiation at the wavelength of the He-Ne laser, which is already measured, but also for other spectral ranges.

Using Eq. (3.4), Eq. (3.5) and Eq. (3.6), dependency of the thermal refraction angle on the radiation wavelength can be expressed as:

$$\frac{d\theta_r}{dz}(\lambda) = \frac{1}{n(\lambda)} \frac{dn(\lambda)}{dr} = \frac{1}{n(\lambda)} \frac{dn(\lambda)}{dT} \frac{dT}{dr} = \frac{n(\lambda)-1}{n(\lambda)} C \quad (3.7)$$

where T is the medium temperature and C is a constant independent of the wavelength λ .

Therefore, for a couple of different wavelengths λ_1, λ_2 :

$$\frac{\frac{d\theta_r}{dz}(\lambda_1)}{\frac{d\theta_r}{dz}(\lambda_2)} = \frac{n(\lambda_2) n(\lambda_1) - 1}{n(\lambda_1) n(\lambda_2) - 1} \approx \frac{n(\lambda_2)}{n(\lambda_1)} \quad (3.8)$$

Calculated from Eq. (3.6) and Eq. (3.8) dependencies of the relative thermal refraction angles $\theta_1 = \frac{\theta(\lambda)}{\theta(1000 \text{ nm})}$ and $\theta_2 = \frac{\theta(\lambda)}{\theta(400 \text{ nm})}$ on the radiation wavelength are presented in Fig. 3.3.

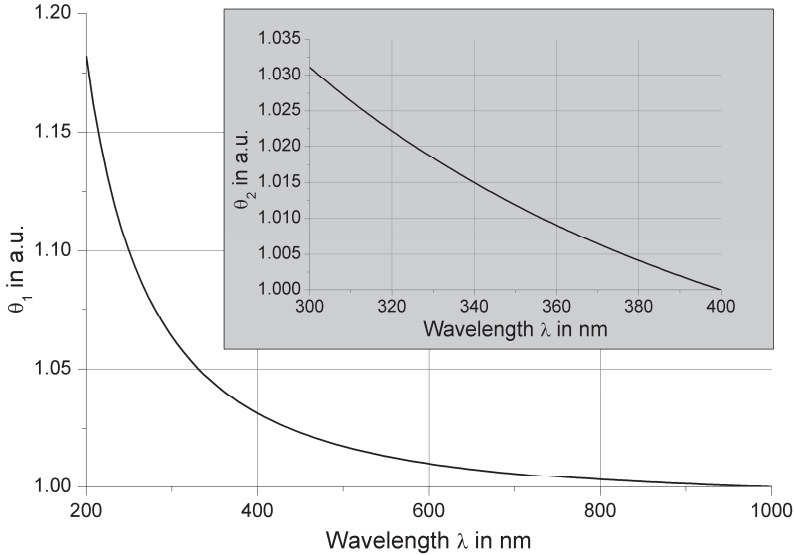


Fig. 3.3. Dependency of the relative thermal refraction angle on the radiation wavelength

Since these dependencies are monotone decreasing, the measured value of the maximal thermal refraction angle could be considered as the higher limit in the first experiment (with the probe radiation wavelength in the IR spectral range). In the second experiment the ratio between the thermal refraction angles for two chosen wavelengths will be important, as the calculation of the particle parameters will be carried out from the ratio between the

extinctions at these two wavelengths (see Sec. 4.1.2). In other words, it has to be guaranteed that the beams with two different wavelengths propagate through the welding plume in exactly the same way.

In the experiment described in Chapter 4 the wavelengths of $\lambda_1 = 300 \text{ nm}$ and $\lambda_2 = 400 \text{ nm}$ were chosen for the calculations. The relative difference between the thermal refraction angles for these two wavelengths was about 3% (see insertion in Fig. 3.3). As the measured value of the maximal refraction angle for the wavelength of $\lambda = 632 \text{ nm}$ does not exceed 0.5 mrad, the absolute difference between the inclination angles for the chosen wavelength couple should be no more than 20 μrad , i.e. negligibly small.

The presented data indicate that in both experiments (described in this Chapter and in the next one) the effect of the thermal refraction can be ignored in fact, when the probe radiation propagates through the welding plume in transversal direction. However, this does not mean that the influence of this effect is small also for the radiation of the high power fiber laser. The thermal refraction angle value is strongly dependent on the mutual configuration of the laser beam and the refractive index gradients in the medium. Hence, it is evident that when the laser beam propagates along the welding plume axis, the situation can be very different from that described above. This is the reason why only within the scope of this experiment, the question regarding the influence of the thermal refraction effect on the high power fiber laser beam is still open.

3.2. Measurement of the 1.3 μm wavelength IR-laser radiation extinction

In order to ascertain the influence of the welding plume on laser radiation, measurement of the probe laser beam radiation was carried out. The probe radiation with the wavelength of 1.3 μm was transmitted through the welding plume in transversal direction like in the previous experiment with the thermal refraction measurement. The probe radiation wavelength λ_p was chosen for the following reasons. First, λ_p has to be different from the ytterbium fiber laser radiation wavelength (1.07 μm) in order to enable spectral discrimination of the radiation from the probe and the high-power lasers. Second, since probe radiation absorption and scattering on the small sub-micron condensed metal particles is supposed, it is possible to recalculate the extinction coefficient for the wavelength of 1.07 μm in the Rayleigh approximation ($\pi a / \lambda_p \ll 1$), whereas the scattering effects can be neglected in comparison with the absorption. Third, due to the corresponding small absorption cross-sections the extinction coefficient can be also considered as small. In this case, the Lambert-Beer law equation can be reduced to the following form for interpretation of the measured extinction:

$$I = I_0 \exp\left(-\int_0^L K_{ext} dl\right) \approx I_0 \left(1 - \int_0^L K_{ext} dl\right) \quad (3.9)$$

Though this method does neither allow it to determine the reason for the extinction nor the parameters of the process of interaction between probe radiation and medium, it was nonetheless chosen as a relatively simple way to achieve the following aims:

- direct check of the interaction of laser radiation in IR spectral range with the welding plume medium during the metal welding process with high power high brightness solid-state lasers,
- determination of the temporal interaction characteristics,
- determination of the spatial interaction characteristics,
- recalculation of the spatial distribution of the extinction coefficient in the whole space of the upper part of the welding plume.

3.2.1. Experimental technique

A schematic diagram of the experiment is shown in Fig. 3.4. The investigation was carried out using a 6-axis anthropomorphic welding robot and a 10 kW ytterbium fiber laser (1) with 1.07 μm radiation wavelength. Specimens (6) prepared from mild tool steel plates with thicknesses from 5 mm to 10 mm were used. The investigations were made during in either the full-penetration or the partial-penetration welding mode. The welding speed was set from 0.5 m/min to 5 m/min. The speed value was chosen on the basis of the optimal material penetration achieved with every concrete welding parameter set as well of the specimen thickness.

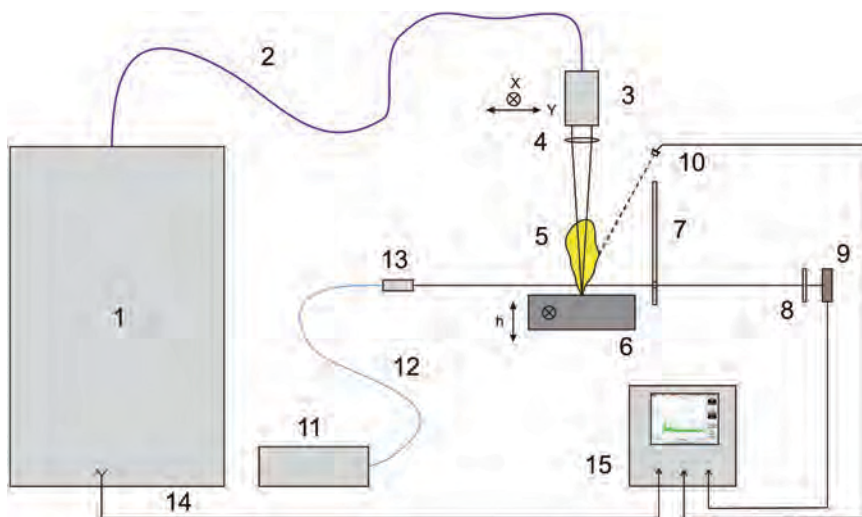


Fig. 3.4. Scheme of the experiment for the measurement of IR probe radiation extinction in the welding plume: 1 – fiber laser; 2 – optical delivery fiber; 3 – collimator; 4 – focusing lens; 5 – welding plume; 6 – specimen; 7 – shielding screen; 8 – optical interference filter; 9 – photo receiver; 10 – optical fiber; 11 – IR probe laser; 12 – optical fiber; 13 – collimator; 14 – synchronisation; 15 – oscilloscope

In all experiments the fiber laser beam as well as all other measurement devices were stationary fixed, whereas welding was carried out by moving the metal specimen which was

mounted on a servo-driven linear moving platform. A robotic arm holding the optical welding head provided the movement of the laser beam focus spot along the metal surface in two mutually perpendicular directions of the horizontal plane (x,y) as well as the movement of the whole welding head in vertical direction (h) synchronously with the specimen on the moving platform with an accuracy of 0.1 mm. This opened up the possibility of shifting the welding point in all three dimensions independently of the probe beam in order to determine the spatial characteristics of the measured values.

The fiber laser radiation was delivered to the welding area by an optical transport fiber (2) with 200 μm core diameter, after that it was focused on the metal surface by a lens (4) with 200 mm focus distance. The beam diameter in the focal plane (beam waist) was about 0.35 mm in such configuration.

As a probe radiation source a semiconductor laser (11) was used generating the continuous-mode radiation with a power of 1 mW at 1300 nm wavelength. The probe laser beam was delivered to the welding area by a single-mode optical fiber (12) with 9 μm core diameter. A collimator (13) at the end of the optical fiber collected the probe radiation into a parallel beam with a diameter of about 0.5 mm. After the transmission through the welding plume the intensity of the probe radiation was registered with a photo receiver (9) based on a germanium-doped photo element with 5 mm sensitive surface diameter and 200 kHz spectral bandwidth. In order to suppress the influence of the welding plasma emission radiation an interference optical filter (8) with a bandpass of 1300 ± 20 nm was placed at the front of the photo receiver.

3.2.2. Temporal dynamics of the probe beam extinction

Fig. 3.5 shows a typical form of the measured signal after passage of the probe beam through the welding plume. It can be seen that after fiber laser switch-on ($t=0$ s) the intensity of the probe radiation is reduced.

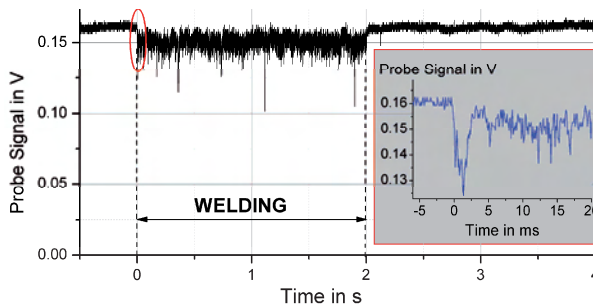


Fig. 3.5. Typical form of the probe beam transmission signal during welding

For numerical description of the welding plume influence on probe radiation the value of the relative extinction was used:

$$E = \frac{I_0 - I_t}{I_0} \quad (3.10)$$

where I_0 , I_t are the initial probe radiation intensity and the intensity of the transmitted beam, respectively.

Due to high non-stationarity of the processes in the keyhole (condensation, re-evaporation, gas dynamics and ambient conditions) the relative extinction value changes rapidly during the welding time. The diagram in Fig. 3.6 shows the temporal distribution of the extinction in the whole welding process, i.e. total relative duration (normalized to the total welding time) of the period when the extinction has the given value.

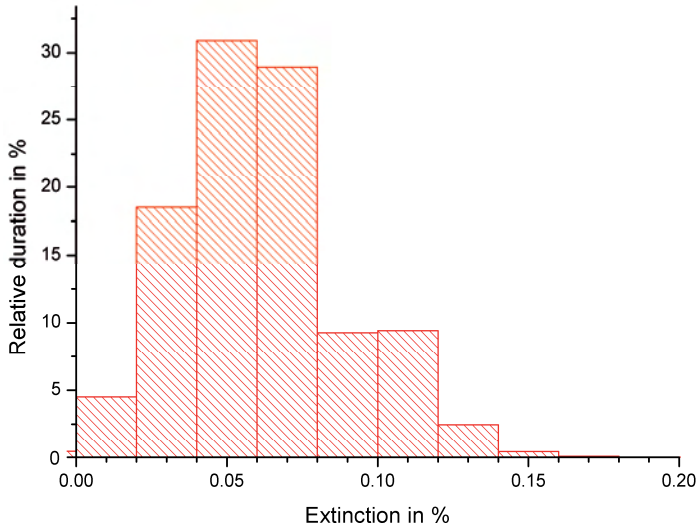


Fig. 3.6. Temporal parameters of the extinction signal

From this it follows that the extinction value for most of the welding time is about 4%-7%, however short jumps up to 15% and more are possible. Spectrum of the probe beam essential oscillations has frequencies up to 2-3 kHz and by registration of the probe signal with high spatial resolution short pulses with about 1 ms duration can be found (see inset in Fig. 3.5). The signal from the photodiode registering the plasma plume emission intensity indicated similar dynamics, but a direct correlation between the welding plasma emission and the extinction signal was not found. The mean-square deviation of the probe signal during the welding process was measured to be about 2%-3%.

3.2.3. Spatial distribution of the probe beam extinction

By shifting the laser beam focus area orthogonally to the probe beam direction as well as changing the specimen moving direction relative to the welding and probe beams the spatial distributions of the extinction were measured. Fig. 3.7 shows the spatial extinction distribution in the longitudinal $E(x) \equiv E(x, y=0)$ and the transversal $E(y) \equiv E(x=0, y)$ directions (relative to the welding direction) at different height h of the probe beam above the metal surface. The results of the numerous experiments show that the extinction distribution in transversal direction is almost symmetric relative to the high power laser

beam axis, as it is shown in Fig. 3.7.b, and changes slightly with increasing height. On the other hand, the distribution in longitudinal direction reveals a characteristic shift backwards (relative to the welding direction), which intensifies with increasing height. At low height ($h < 10$ mm) this shift leads only to the displacement of the maximum extinction point, but with increasing height a “stretching” of the backward distribution branch, as it is shown in Fig. 3.7.a, is also noticeable. The full extinction area width at half maximum near the metal surface is about 10-15 mm.

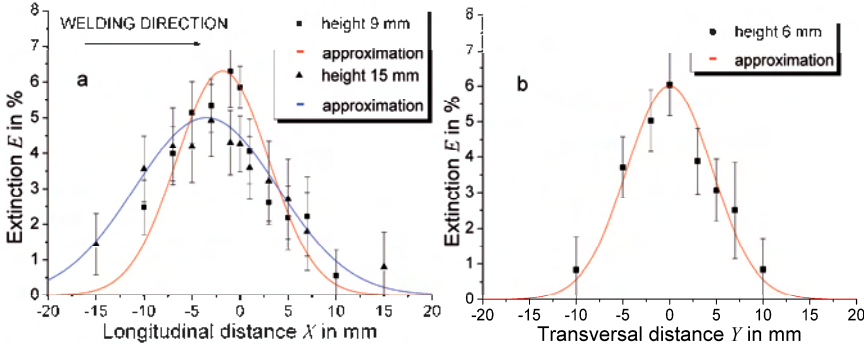


Fig. 3.7. Spatial distributions of the probe beam extinction in longitudinal (a) and transversal (b) direction for different plume heights

From Fig. 3.7 it can be seen furthermore that not only the longitudinal but also the transversal extinction distribution near the laser beam axis can be approximated in the error bound as Gaussian functions, and that the asymmetrical behaviour with increasing height can be considered as a shift of the Gaussian function center. Thereby, due to the high distribution width, the difference between the extinction values at the laser beam axis (at $x = 0$) and in the distribution function center are insignificant at low h .

According to the described considerations, in order to simplify further interpretation of the measured results the spatial extinction distribution was finally approximated as following symmetrical Gaussian function:

$$E(x, h) = A_1(h)e^{-\frac{x^2}{W_1(h)^2}}, \quad E(y, h) = A_2(h)e^{-\frac{y^2}{W_2(h)^2}} \quad (3.11)$$

where $A_{1,2}(h)$ and $W_{1,2}(h)$ are the distribution parameters depending on plume height.

3.2.4. Spatial distribution of the extinction coefficient

Using Eq. (3.9) and Eq. (3.10) the measured distributions of the probe radiation extinction can be described by the following expressions:

$$E(x, h) = 1 - \exp \left[- \int_{-\infty}^{\infty} K_{ext}(x, y, h) dy \right] \quad (3.12)$$

$$E(y, h) = 1 - \exp \left[- \int_{-\infty}^{\infty} K_{\text{ext}}(x, y, h) dx \right] \quad (3.13)$$

where x, y, h are the spatial coordinates shown in Fig. 3.4 and Fig. 3.7.

Taking into account the supposition about the axial symmetry of the extinction distribution functions $E(x, h)$ and $E(y, h)$ (i.e. $A_1(h) \equiv A_2(h) = A(h)$; $W_1(h) \equiv W_2(h) = W(h)$), the distribution $K_{\text{ext}}(x, y, h)$ in Eq. (3.12) and Eq. (3.13) can also be considered as axially symmetrical. In this case the experimentally measured functions $E(x, h)$ and $E(y, h)$ become identical and the integration can be transformed to the coordinate $r = \sqrt{x^2 + y^2}$ as follows:

$$\int_{-\infty}^{\infty} K_{\text{ext}}(x, y, h) dx = 2 \int_y^{\infty} K_{\text{ext}}(r, h) \frac{r dr}{\sqrt{r^2 - y^2}} = F(y, h) \quad (3.14)$$

where $F(y, h) = -\ln[1 - E(y, h)]$ (see Eq. (3.13)).

Since the extinction value is small ($E \ll 1$), the expression for the function $F(y, h)$ can be expanded to a series with $E(y, h)$ as a small parameter:

$$F(y, h) \approx E(y, h) + \frac{1}{2} E^2(y, h) + \frac{1}{3} E^3(y, h) + \dots \quad (3.15)$$

With an error no more than the measurement inaccuracy Eq. (3.15) can be reduced to only the first expansion term. Hence, when the probe laser beam propagates along the x -axis at the height h and along the line which is the value of y distant from the welding plume axis, its extinction value is described by the following expression:

$$E(y, h) \approx 2 \int_y^{\infty} K_{\text{ext}}(r, h) \frac{r dr}{\sqrt{r^2 - y^2}} = A(h) e^{-\frac{y^2}{W^2(h)}} \quad (3.16)$$

where parameters A and W can be measured experimentally for different plume heights h .

In this case the subintegral function of the extinction coefficient distribution can be expressed in the explicit form applying the inverse Abel transformation [123] in Eq. (3.14):

$$K_{\text{ext}}(r, h) = -\frac{1}{\pi} \int_r^{\infty} \frac{\partial E(y, h)}{\partial y} \frac{dy}{\sqrt{y^2 - r^2}} = \frac{1}{\sqrt{\pi}} \frac{A(h)}{W(h)} e^{-\frac{r^2}{W^2(h)}} \quad (3.17)$$

Therefore, in order to rebuilt the full spatial distribution of the probe radiation extinction coefficient the form of the dependencies $A(h)$ and $W(h)$ has to be ascertained. On the basis of the experimentally measured values of these two parameters, the dependencies $A(h)$ and $W(h)$ were assumed to be linear and exponential, respectively.

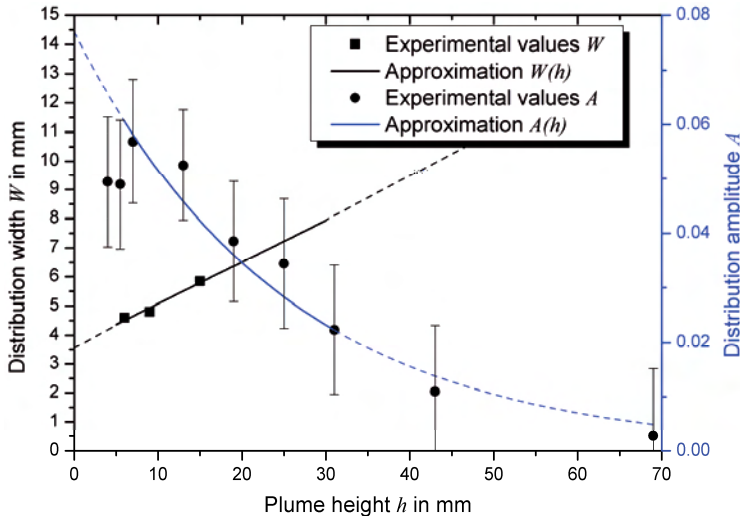


Fig. 3.8. Parameters of spatial distribution of the probe radiation extinction over the keyhole

As can be seen from Fig. 3.8, such assumption correlates quite well with the experimentally measured points in the plume height area $5 \text{ mm} < h < 30 \text{ mm}$ which is the most interesting one for numerical estimation of the welding plume influence on high power fiber laser radiation. When the plume height h is more than 30 mm, the extinction becomes small and the deviation of the real distribution function from the chosen approximation does not considerably change the integral attenuation of the fiber laser beam which propagates along the welding plume axis through its whole height. On the other hand, when h is less than 5 mm, i.e. in the area close to the keyhole outlet, the situation can be very different from that observed in the welding plume volume far enough from the metal surface. Supposedly, in this area the process of metal vapour condensation takes place when the hot vapour flies out of the keyhole and meets the cold ambient gas (see Sec. 1.3.1). This effect is the most probable reason for the measured probe radiation extinction. However, experimental measurement of the extinction in the plume height area $h < 5 \text{ mm}$ was hindered by spattering of macroscopic liquid metal drops from the weld pool.

Because of these reasons the plume height area $h < 5 \text{ mm}$ will not be taken into account in the integration during the calculation of full attenuation of the high power fiber laser radiation propagating along the welding plume axis. It should be also noted that such simplification lowers the resulting value of the integral attenuation, i.e. the real value can be higher than the calculated one.

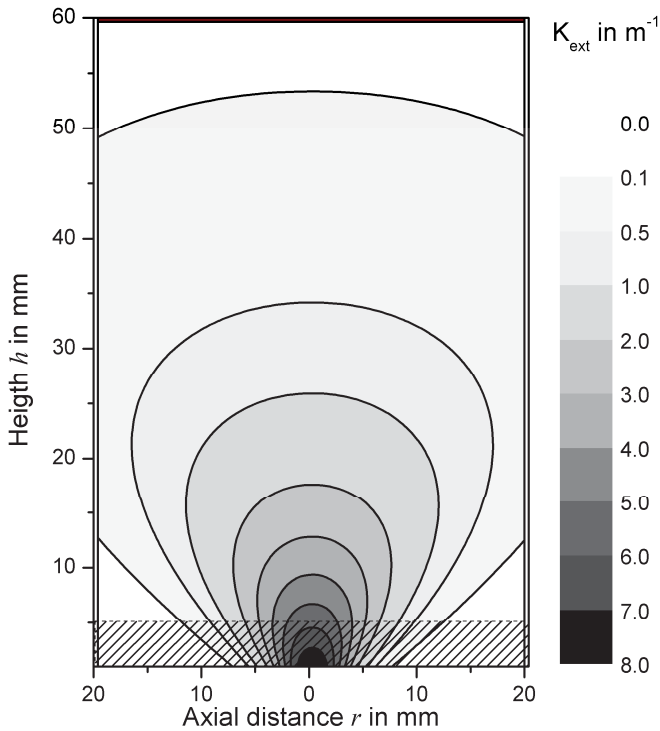


Fig. 3.9. Spatial distribution of the probe radiation extinction coefficient above the keyhole; hatched area corresponds to the lower part of the welding plume (welding plasma)

Fig. 3.9 illustrates the spatial distribution of the extinction coefficient calculated from Eq. (3.17) under the conditions described above. It should be remembered that this results were obtained without concretisation of the reason causing the observed extinction. However, the most probable reasons in this case is the influence of the small condensed metal vapour particles. Therefore, the investigation presented in Chapter 4 was devoted to the study of the condensation process and allowed it to draw some conclusions about the parameters of small absorbing particles.

Summary of Chapter 3

1. The thermal refraction of the beam propagating transversally through the welding plume is negligibly low for all spectral ranges of the probe radiation used in both this and the next Chapter. At the radiation wavelength of 632 nm the maximal refraction angle is less than 0.5 mrad. Therefore, any extinction of the probe beams can be caused only by either absorption or scattering in the welding plume medium.
2. The upper part of the welding plume attenuates the laser radiation propagating through it in transversal direction. The probe radiation extinction is not stable and changes during the welding process in characteristic intervals of about a few milliseconds.
3. The spatial distribution of the whole welding time-averaged extinction coefficient has almost symmetrical form relative to the laser beam axis and can be approximated as a Gaussian function.
4. The value of the extinction coefficient at the wavelength of 1.3 μm is much higher than the inverse Bremsstrahlung absorption coefficient (for the same radiation wavelength) and can reach up to a few units per meter.

Chapter 4.

Metal vapour condensation effect in fiber laser welding plume medium

4.2. Measurement of the condensed particle parameters in the welding plume

4.2.1. Experimental technique

4.2.2. Multi-wavelength method

4.2.3. Transmission spectra of the welding plume

4.2.4. Measurement of the averaged condensed particle parameters

4.3. Estimation of the welding plume influence on the high power fiber laser radiation

4.3.1. Metal vapour condensation under the influence of high power laser radiation

4.3.2. Estimation of the high power fiber laser beam attenuation when propagating through the welding plume medium

Summary

“In the previous chapters it was ascertained that during high power high brightness fiber laser beam welding of low-alloyed mild steel a cloud of small condensed metal vapour particles is produced in the upper part of the welding plume. It was shown that these particles are able to absorb a considerable part of the laser beam energy and lead to welding process destabilization. This chapter is devoted to the measurement of such parameters of the small condensed metal particle cloud like average particle size or spatial distribution of the particle concentration. The theoretical preconditions of the condensation process in the welding plume medium and a review of the applied methods of condensed particle diagnostics were presented in *Sec. 1.3*. Using the condensed particle cloud parameters measured by the multi-wavelength method, numerical calculation of the extinction coefficient was carried out as proposed by the Mie-scattering theory. The comparison between the calculated value and the value measured experimentally in *Chapter 3* allowed it to conclude that the observed extinction of the probe radiation is generally caused by the absorption in the small condensed metal vapour particles.

4.1. Measurement of the condensed particle parameters in the welding plume

Using probe radiation with a continuous wavelength spectrum instead of single-wavelength monochrome laser radiation for the extinction measurement in the welding plume allows it to obtain information about the properties of the object causing the extinction. The experiment was based on the multi-wavelength method of parameter measurement of dusty mediums and aerosols [125],[126],[127]. This method consists in extinction measurement for probe radiation at two or three different wavelengths. The ratio between the relative

extinction values $E = \frac{I_0 - I_t}{I_0}$ (where: I_t and I_0 are intensities of the transmitted and initial

light, respectively) for two different probe radiation wavelengths is independent of the particle concentration in a cloud and of the optical beam path length. The ratio is determined only by the proportion between the extinction efficiencies corresponding to these two wavelengths, i.e. it is a function of small particle size. Since such function in some cases can be non-monotone, sometimes measurement of the extinction ratio for a few (three or more) different wavelength couples is required in order to calculate the particle size unequivocally. In the described experiment the extinction measurement was carried out in the continuous wavelength spectrum of the probe radiation, which has the following additional advantages:

- simultaneous measurement of the welding plume transparency at different wavelengths which takes into account the influence of the welding plume non-stationarity,
- detection of the absorption lines corresponding to the metal vapour and to the shielding gas,
- consideration of the plasma plume emission spectrum influence on the measured extinction signals,
- possibility of arbitrary choice of the wavelength couple for calculating the extinction ratio and choice of the spectral area which is free from emission or absorption lines,

- qualitative comparison between the dependency of the extinction signal on the probe radiation wavelength which is calculated using the Mie-theory on the one hand and the measured corresponding extinction coefficient dependencies on the another hand.

4.1.1. Experimental technique

The scheme of the experimental setup which allowed it to measure the welding plume extinction of the probe radiation in a wide frequency spectrum is shown in Fig. 4.1. The principle of the experiment is similar to that described in Sec. 3.1.2, however, instead of the fiber laser and the photo receiver a laser driven light source (LDLS) (9) and a spectrometer (13) were used, respectively. The light source had a wide spectral composition and a high radiation brightness (value of radiance remains constant at about $10 \text{ mW}/(\text{mm}^2 \cdot \text{nm} \cdot \text{srad})$ in the wavelength range from 170 nm to 850 nm)

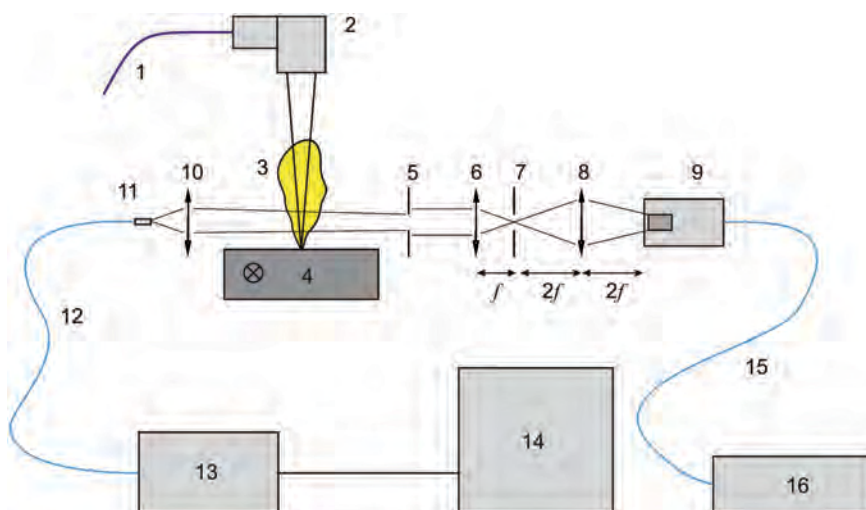


Fig. 4.1. Scheme of experimental setup for welding plume extinction measurement in continuous frequency spectrum: 1 – fiber delivery; 2 – optical welding head; 3 – welding plume; 4 – specimen; 5, 7 – apertures; 6, 8, 10 – lenses; 9 – laser driven light source; 11 – fiber end; 12, 15 – optical fiber; 13 – spectrometer; 14 – PC; 16 – laser

The experiments were carried out with a 20 kW power ytterbium fiber laser. The laser radiation was delivered by a transport fiber (1) to the welding optical head (2) and focused on the metal specimen surface (4). The focused spot size on the metal surface was about $560 \mu\text{m}$. Radiation of a laser-induced discharge in LDLS was collimated by an optical system (5-8) into a parallel beam with a diameter near 1 mm. After the probe beam passed through the welding plume, it was collected with a lens (10) into an optical fiber (12). For probe radiation registration two different spectrometers were used which had a spectral registration range in the near-UV (range I: 198–432 nm) and in the visible (range II: 381–588 nm) range, respectively. Taking into account the dynamical characteristics of the probe laser radiation extinction (see Sec. 3.2.2), measurements of the transmission spectra

were carried out in a series of 10-20 snapshots during every single welding process with durations of about 2-3 s. The spectrometer integration time for every measurement snapshot was about 4 ms. Like in the previous experiment, such procedure allowed it to make statistical averaging of the measured results within the welding time.

4.1.2. Multi-wavelength method

Size determination of the scattering particle using the multi-wavelength method is based on the measurement of the ratio between two extinction or scattering efficiencies corresponding to different wavelengths. Like in the previous experiment, where the extinction of a monochrome probe laser radiation was measured (see 1.1), in case of the continuous wavelength spectrum of the probe radiation the relative extinction value can be used as well. However, in this case this value is obviously dependent on the wavelength in the following way:

$$E(\lambda) = \frac{I_0(\lambda) - I_t(\lambda)}{I_0(\lambda)} \quad (4.1)$$

where:

$$I_t(\lambda) = I_0(\lambda) \exp \left[- \int_L K_{ext}(\lambda) dl \right] \quad (4.2)$$

$$K_{ext}(\lambda) = \frac{\pi}{4} C_n \int_0^{\infty} Q_{ext}(a, \lambda) N(a) a^2 da \quad (4.3)$$

(see Eq. (1.9)-(1.10)).

In this experiment it is supposed that all condensed metal vapour particles in the welding plume are spherical and have some average diameter a_0 , i.e. the size-distribution function of particles has a delta-function form: $N(a) = \delta(a - a_0)$. In this case, using Eq. (4.1)-(4.3), the logarithmic extinction function can be expressed as follows:

$$\ln[1 - E(\lambda)] = \frac{\pi a_0^2}{4} Q_{ext}(a_0, \lambda) \int_L C_n dl \quad (4.4)$$

where $Q_{ext}(a_0, \lambda)$ is the extinction efficiency which can be unequivocally calculated for any given values of a_0 and λ from the equations of the Mie-scattering theory (Eq. (1.11)-(1.14)).

As it was shown in Sec. 3.1, when a white light beam passes through the welding plume in the transversal direction parallel to the metal surface, the dispersion effects which are mainly connected with the thermal refraction can be neglected. It can hence be considered that beams with different wavelengths pass along the welding plume absolutely in the same trajectory. This means that the integral in the right part of Eq. (4.4) is independent of the radiation wavelength, and that the ratio of the extinction efficiencies for a wavelength couple λ_1, λ_2 can be written as:

$$\frac{Q_{ext}(a_0, \lambda_1)}{Q_{ext}(a_0, \lambda_2)} = \frac{\ln[1 - E(\lambda_1)]}{\ln[1 - E(\lambda_2)]} \quad (4.5)$$

The right hand part of Eq. (4.5) can be measured experimentally by selecting only two values corresponding to λ_1 and λ_2 from the whole white light extinction spectrum, whereas the left hand part of this equation is a function of the average particle size a_0 only. Therefore, Eq. (4.5) serves as a basis for determining the a_0 value in the multi-wavelength method.

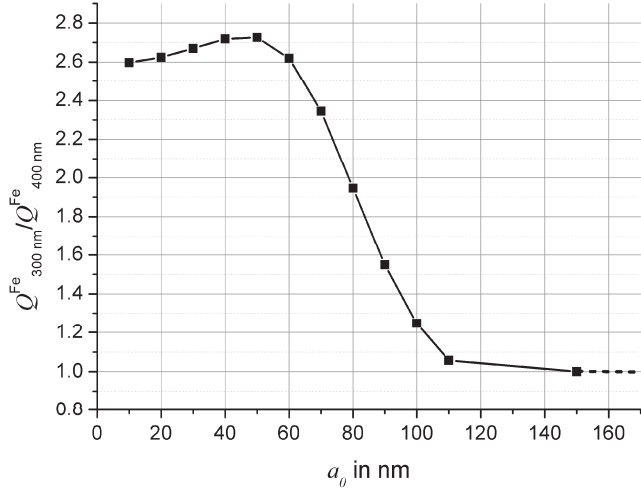


Fig. 4.2. Characteristic dependency of the iron particle extinction efficiency ratio on the average particle diameter a_0 for the wavelengths of $\lambda_1 = 300$ nm and $\lambda_2 = 400$ nm on the average particle diameter a_0

The characteristic form of the dependency of the left hand part in Eq. (4.5) on the a_0 value is presented in Fig. 4.2, where it is assumed that the scattering particles consist of pure iron. In this case the values of the complex refractive particle index n_p necessary for consequent calculation were taken from the experimental data [128] (see Table 4.2), with linear interpolation of the values between the experimentally measured points.

When the a_0 value is low, the extinction efficiency can be described by the Rayleigh-approximation $Q_{ext}(a_0, \lambda) \sim \lambda^{-1} \text{Im} \left(\frac{m^2 - 1}{m^2 + 2} \right)$ [130], whereas high a_0 values correspond to the geometrical optics and the ratio in this case becomes 1.

Therefore, the dependency of the extinction efficiency ratio (in the right part of Eq. (4.5)) on the particle size becomes apparent only in the middle-size area (in our case this area is $20 \text{ nm} < a_0 < 150 \text{ nm}$). However, since this function is not always monotonic (e.g. the area $a_0 \leq 60 \text{ nm}$), measurement of several (three or more) ratios for different wavelength couples is sometimes necessary in order to determine the particle diameter.

Table 4.2. Values of the complex refractive index for iron particles at different wavelengths [128],[129]

λ in nm	150	250	410	490	550	580	600	700	750	800	850	900	950	1000	1100	1300
n	0.94	1.14	1.88	2.41	2.59	2.75	3.16	2.89	2.86	2.69	2.81	2.93	3.15	3.1	3.0	3.41
k	1.18	1.87	3.12	3.55	3.62	3.65	3.92	3.83	3.92	3.88	4.13	4.24	4.51	4.4	4.4	5.19

4.1.3. Transmission spectra of the welding plume

Characteristic forms of probe white light transmission spectra with (I_t) and without (I_0) the welding plume influence are shown in Fig. 4.3. From the difference between the upper and the lower curves it is seen that the probe laser radiation extinction in the welding plume in visible and especially in near-UV spectral range is much higher than the probe laser radiation extinction in the IR-range which was described in Sec. 1.1. Spectra of the transmitted through the welding plume probe radiation have also some absorption lines (mainly in the range I) which correspond to the electron energy transitions in neutral atoms of iron.

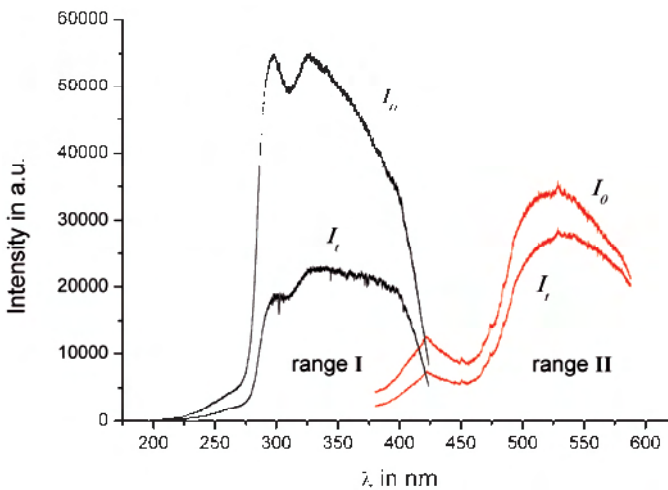


Fig. 4.3. Characteristic transmission spectra of the welding plume in near-UV and visible wavelength ranges

Another effect which deserves to be noted is the behaviour of the absorption line intensity. These lines superpose the continuous absorption spectra of the small condensed metal vapour particles and correspond to the electron transitions in neutral iron atoms. It is obvious that these lines arise from the presence of iron vapour over the keyhole, and consequently the absorption line amplitude correlates with the iron vapour concentration. As can be seen from Fig. 4.4 and Fig. 4.5, the relative intensity of the absorption lines remains almost constant in different time points of the welding process independently of the continuous extinction spectrum amplitude.

Fig. 4.4 shows the characteristic statistical set of the welding plume transmission spectra (in range I).

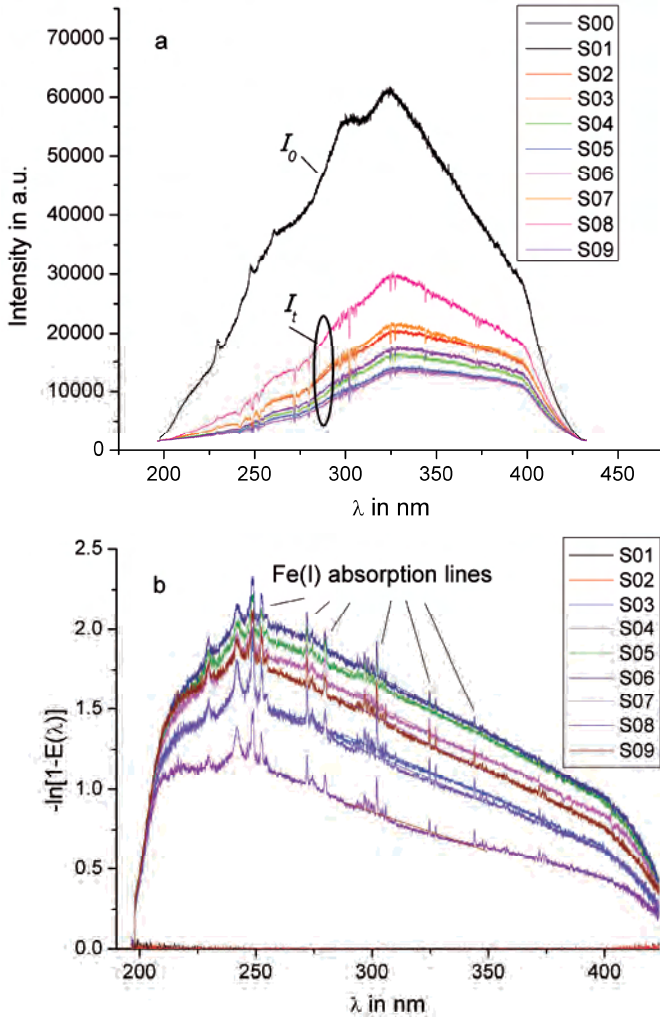


Fig. 4.4. Statistical set of transmission spectra (a) and corresponding logarithmic extinction functions (b) during a single welding process

These curves were detected in a single welding process with 250 ms time interval between each other. Like in Sec. 3.2.2 a strong non-stationarity of the absolute extinction value can be noted here too. Nevertheless, the corresponding recalculated logarithmic extinction functions remain qualitatively similar to each other and have almost the same inclination angle, i.e. the ratio $\frac{\ln[1-E(\lambda_1)]}{\ln[1-E(\lambda_2)]}$ remains practically constant during the whole welding process. This fact means that the observed non-stationarity of the welding plume transmission is not connected with changing particle size (or in general case with optical

particle properties), but with decreasing or increasing particle concentration along the optical probe beam path.

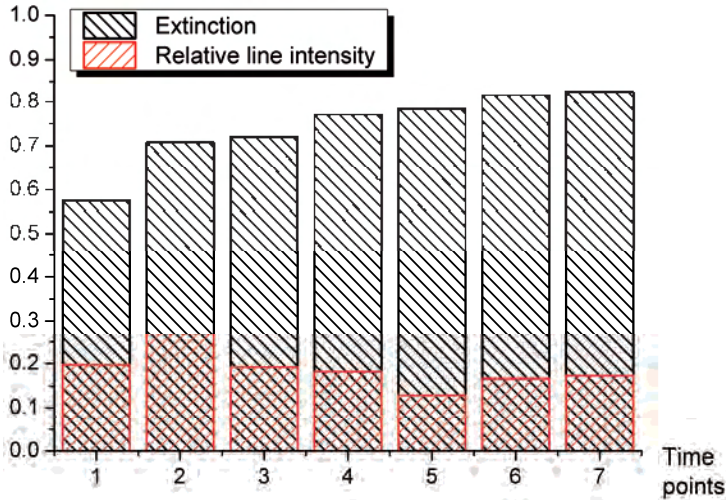


Fig. 4.5. Comparison of the extinction amplitude in continuous (condensed particles) and in linear (metal vapour) spectrum for a measurement series 1-7

This means that there is a stationary vapour cloud over the metal surface which has a constant concentration during welding process and is not connected dynamically with the behaviour of the condensed metal vapour particle cloud.

4.1.4. Measurement of the averaged condensed particle parameters

Fig. 4.6 shows the characteristic values of the calculated average diameter of small condensed metal vapour particles in the welding plume. The calculations were carried out by means of numerical solution of Eq. (4.5) using the white light probe beam extinction spectra measured at different plume height. The probe beam trajectory met the welding plume axis ($r=0$) at different heights over the metal surface). The errors in Fig. 4.6 correspond to the mean-square deviations of the particle diameter values during the welding process.

Generally, the average particle size values varied within a quite broad scope ranging from 60 nm to 110 nm depending on the measurement point and on the welding parameters. This dispersion does not seem to be connected with the change of the condensed particle parameters. On the contrary, this is probably a consequence of the used experimental technique, since the spatial particle distribution in the welding plume volume can be inhomogeneous and the average particle size value can be significant depending on the part of the whole welding plume volume which mainly contributed to the full extinction of the probe beam along its whole path.

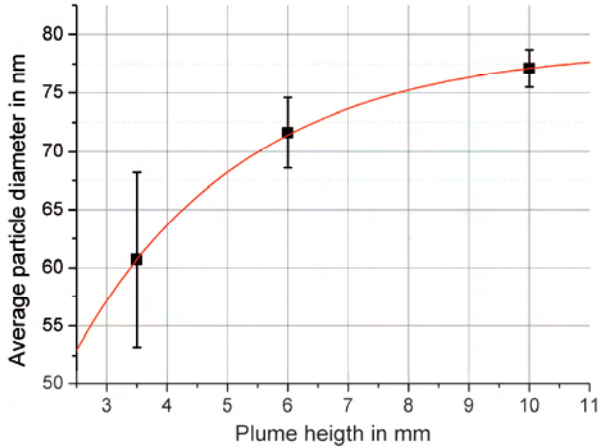


Fig. 4.6. Values of the average particle diameter a_0 at different plume height

Nevertheless, a qualitative correlation was observed between the spectra of the logarithmic extinction function $\ln[1 - E(\lambda)]$ and the extinction efficiencies which were calculated for the obtained particle size values. A good correlation was not only found at the measurement wavelengths λ_1 , λ_2 , but also in the rest of the wavelength spectrum in both range I and range II (see Fig. 4.7). All dependencies in Fig. 4.7 are built in relative units with normalization on the corresponding values at the wavelength $\lambda = 300$ nm .

Using the obtained a_0 values, it is possible to determine the condensed metal vapour particle concentration in the welding plume volume. Since the particles are supposed to be mono-sized at a fixed plume height, the extinction distribution functions which were measured in Sec. 3.2.3 should remain correct independently of the spectral composition of the used probe radiation. The only difference may be the change of the whole extinction amplitude as a constant factor. Hence, from Eq. (3.17) and Eq. (4.3) the spatial extinction coefficient distribution function can be obtained as:

$$K_{ext} = \frac{1}{\sqrt{\pi}} \frac{A(h, \lambda)}{W(h)} e^{-\frac{r^2}{W(h)^2}} = \frac{\pi a_0^2}{4} Q_{ext}(a_0, \lambda) \cdot C_n(r) \quad (4.6)$$

From this equation the spatial distribution function of the condensed particle volume concentration can be derived:

$$C_n(r) = \frac{1}{\sqrt{\pi}} \frac{A(h, \lambda)}{W(h)} \frac{4}{\pi a_0^2} \frac{1}{Q_{ext}(a_0, \lambda)} e^{-\frac{r^2}{W(h)^2}} \quad (4.7)$$

The results of the calculations using Eq. (4.7) carried out for the characteristic particle diameter value $a_0 = 77$ nm at the plume height $h = 10$ mm are plotted in the diagram presented in Fig. 4.8. It is seen that the condensed particle concentration on the welding plume axis reaches the value of about 10^{10} cm⁻³.

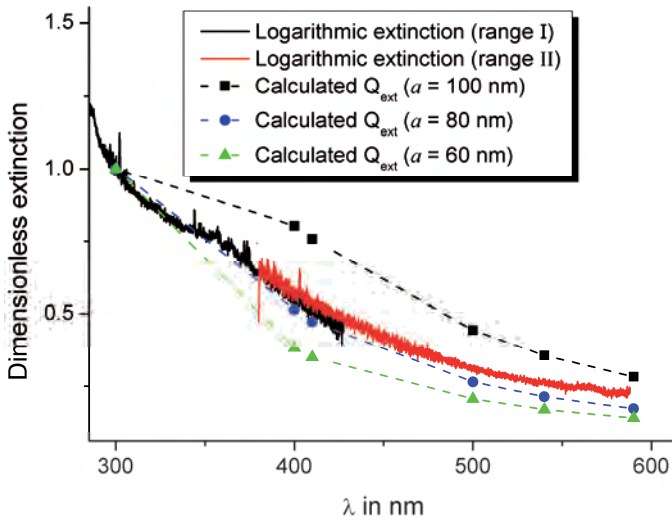


Fig. 4.7. Logarithmic extinction function spectra corresponding to Fig. 4.3 and extinction efficiency spectra calculated for different particle diameter values a_0 (measured a_0 value is about 80 nm)

Inserting the obtained condensed particle cloud parameters into Eq. (4.6), it is possible to calculate the extinction coefficient for a probe radiation wavelength of $1.3 \mu\text{m}$ and to compare this value with that measured experimentally in Sec. 1.1. Since the extinction efficiency for the chosen parameters calculated based on the Mie-scattering theory was found to be $Q_{ext}(a_0 = 77 \text{ nm}, \lambda = 1.3 \mu\text{m}) \approx 0.0889$, the corresponding extinction coefficient value is $K_{ext}(\lambda = 1.3 \mu\text{m}) \approx 4.9 \text{ m}^{-1}$. On the other hand, the value of K_{ext} in the corresponding welding plume point ($h = 10 \text{ mm}, r = 0$) is about 3.8 m^{-1} , as measured experimentally in Sec. 1.1 (see Fig. 3.9). Quite good coincidence is thus seen between these two values of the extinction coefficient, whereas the former was directly measured with no concretization of the extinction coefficient, and the latter was calculated from only the measured condensed metal vapour particle cloud parameters. This fact confirms two suppositions. Firstly, the measurement of the condensed particle parameters (average particle diameter and particle volume concentration) gave correct results, and the secondly, the observed probe radiation extinction in the welding plume is mainly caused by absorption and scattering on the small condensed metal vapour particles.

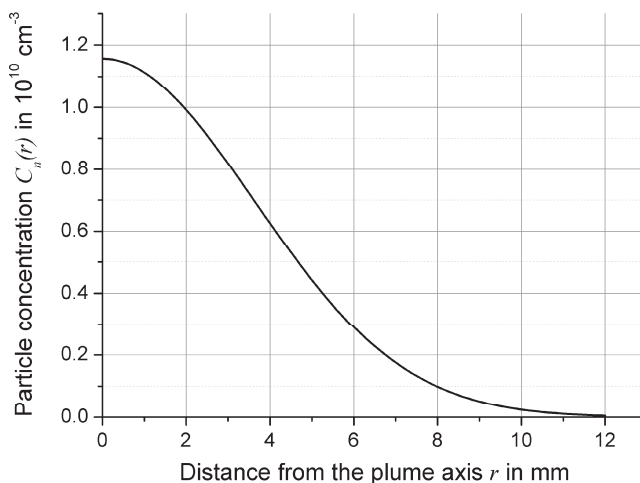


Fig. 4.8. Spatial distribution of the condensed metal particle concentration in welding plume at a height of 10 mm

It should be noted that full absolute coincidence of the results of these two experiments (especially the spatial distributions of particle concentration) was initially not expected. Small deviation of the measured and calculated extinction coefficient values may be explained by difference in the experimental conditions (laser source, mechanical configuration, specimen material etc.).

4.2. Estimation of the welding plume influence on the high power fiber laser radiation

The results of high-speed video observation of the welding plume given in *Chapter 2* indicated that the upper part of the welding plume is formed due to thermal emission of the small condensed metal vapour particles which are irradiated and heated up by the laser beam. In such case, the particle size will decrease if the particle surface temperature exceeds the vaporization temperature of the specimen material. At the same time, the absorption cross-section of the particle will also be reduced. Hence, the part of the absorbed laser radiation energy will become smaller too. Thereby, the influence of high-power laser radiation on the particle condensation process can either entail total particle evaporation (when the radiation power density is extremely high) [105] or some stable particle size providing equilibrium between the particle condensation and the particle evaporation processes (with moderate radiation power density values).

4.2.1. Metal vapour condensation under the influence of high power laser radiation

Presence of condensed metal vapour particles in the welding plume directly inside the high-power fiber laser beam caustic was examined experimentally with the method of probe light scattering. For this purpose, probe radiation from a second harmonic solid-state Nd:YAG

laser with a wavelength of $0.532 \mu\text{m}$ and a power of up to 200 mW was used. The laser had a free optical output with a collimated beam diameter of about 1.5 mm.

As opposed to the previous experiments, the probe radiation in this case was coupled directly into the optical tract of the high-power fiber laser via the optical fiber combiner (see Fig. 4.9).

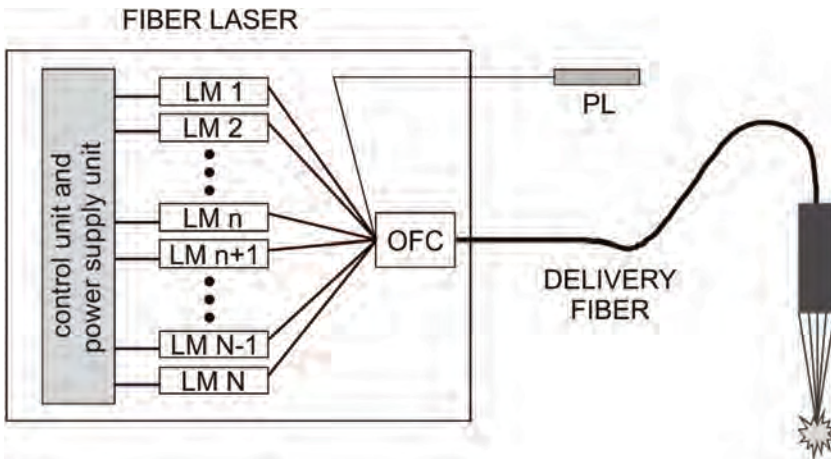


Fig. 4.9. Scheme of probe laser radiation coupling into the optical tract of a high-power fiber laser: LM – laser module; PL – probe laser; OFC – optical fiber combiner

Such probe radiation input provided full coincidence between the high-power and the probe laser beam trajectories. Therefore, registration of the probe radiation scattering signal gave the information which was not averaged along the whole welding plume like in the previously described measurements. This was the information from only that part of the welding plume where the interaction between high-power fiber laser beam and condensed particle cloud really takes place.

Since all input optical fibers in the optical fiber combiner (OFC) were prepared for a radiation wavelength of $1.07 \mu\text{m}$ and have a core diameter of only $10 \mu\text{m}$ (single-mode fibers), the probe radiation coupling efficiency was very low (a few percent). For that and some other reasons, exact numerical determination of particle size and particle concentration appeared to be impossible. Therefore, the probe radiation scattering was registered only at a qualitative, but not at a quantitative level. In such conditions, the multi-wavelength method could be the most suitable for particle sizing, but it requires coupling of two probe laser beams with different wavelengths into the single-mode input fibers of the optical fiber combiner.

Probe radiation scattering was detected using an experimental setup configured as shown in Fig. 4.10. With a help of a lens (4) the scattered probe radiation was collected from the interaction area between the high-power fiber laser beam (1) and the welding plume (2). By using a collimator (5) the collected scattered probe radiation was coupled into an optical fiber (6) with a core diameter of $750 \mu\text{m}$.

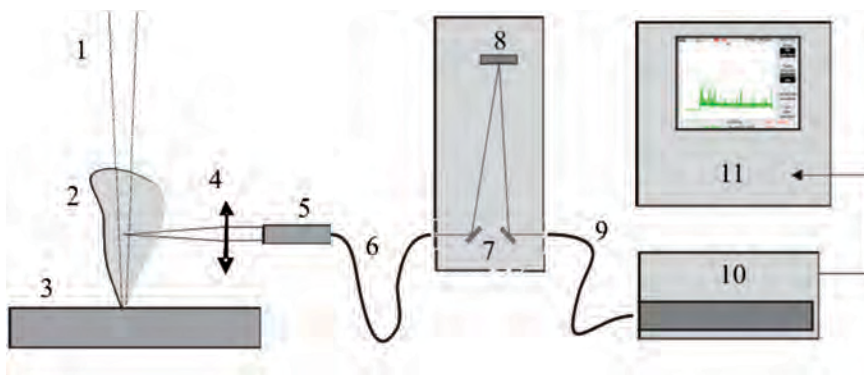


Fig. 4.10. Scheme of the scattered probe radiation registration: 1 – high-power and probe laser beams; 2 – welding plume; 3 – specimen; 4 – lens; 5 – collimator; 6,9 – optical fibers; 7 – mirrors; 8 – diffraction grating; 10 – photoelectric multiplier; 11 – oscilloscope

The emission spectra of the welding plume (with the scattered probe radiation) shown in Fig. 4.11 clearly show a narrow laser line at the wavelength of the probe laser radiation (532 nm). However, this line could be registered only on the background of a continuous spectrum of the welding plasma thermal emission (see Sec. 1.1).

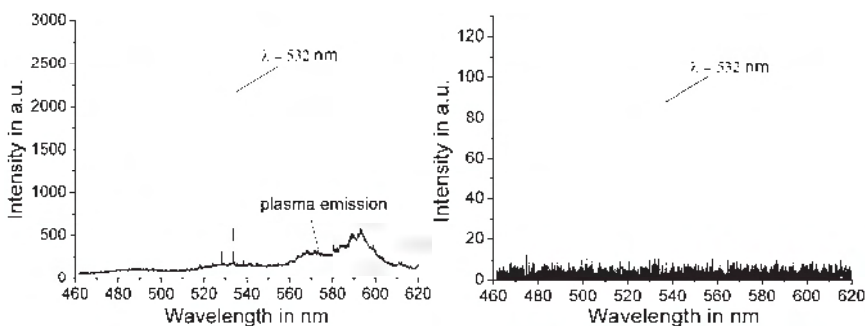


Fig. 4.11. Emission spectrum of the welding plume with the scattered probe laser radiation line (left) and spectrum of registered signal after monochromator (right)

Therefore, a monochromator with a diffraction grating (8) was used for spectral discrimination of the scattered probe radiation from the emission of the upper part of the welding plume. Since the amplitude of the useful part of the scattering signal was strongly reduced after the monochromator (see Fig. 4.11, right), the collected radiation was delivered by an optical fiber (9) to a photoelectric multiplier (10) and then registered with an oscilloscope (11). Such configuration enabled it to register the scattered probe laser radiation without any influence of the welding plasma plume emission on the one hand, and to save sufficiently high amplitude of the useful signal on the other hand.

The registered probe radiation scattering signal revealed similar dynamics to the signal of the probe radiation extinction described in Sec. 1.1. At a quite long distance from the metal surface (30-50 mm and more) single peaks with a duration time of a few milliseconds could

be noted in the signal structure (see Fig. 4.12), whereas with decreasing height the peaks become more frequent and finally blend with each other. In this case such behaviour is revealed more clearly than in case of the probe radiation extinction signal measured by transversal propagation of the probe beam through the whole welding plume medium, because the scattering signal is measured locally, whereas the extinction signal measurement is always an integral along the whole path length of the probe beam.

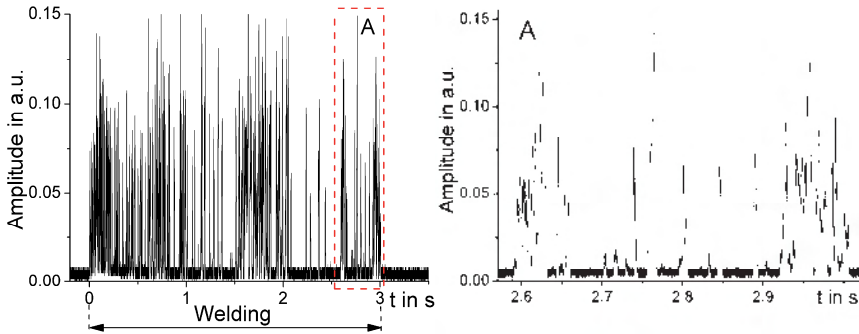


Fig. 4.12. Characteristic form of the scattered probe laser radiation signal at plume height of 25 mm; A – peaks in the time interval 2.6-3.0 seconds with a high temporal resolution

The fact that the probe radiation scattering was persistently observed at plume heights of up to 50 mm indicates that the condensed metal vapour particles are not evaporated totally under the high-power fiber laser beam influence. However, it is possible that the average particle size is reduced to a greater or lesser degree. Together with some theoretical preconditions, this gives reason to use the spatial distribution of the extinction coefficient observed experimentally in Sec. 3.2.4 in order to estimate the total attenuation of the high-power ytterbium fiber laser beam propagating through the whole welding plume height. In other words, it may be supposed that the particle size distribution in the welding plume volume is uniform in the transversal direction (i.e. when the plume height h is fixed). Hence, it can be considered also that the condensed metal vapour particle parameters inside the high-power fiber laser beam caustic are completely the same as those measured in average in the whole welding plume medium. Based on such supposition it is obvious that this should be an upper-bound estimation.

4.2.2. Estimation of the high power fiber laser beam attenuation when propagating through the welding plume medium

Using the Mie-scattering theory, the scattering efficiency and the total extinction efficiency for fiber laser radiation with the wavelength of $1.07 \mu\text{m}$ were calculated numerically for different values of the particle diameter. Fig. 4.13 shows these dependencies in the measured average particle diameter range $60 \text{ nm} \leq a_0 \leq 120 \text{ nm}$. From the given picture it is seen that the absorption prevails over the scattering in the whole range of a_0 , i.e. almost the whole energy taken from the laser beam is absorbed by small condensed metal vapour particles.

With measured spatial distribution of the extinction coefficient $K_{ext}(r, h)$ the total attenuation of the high-power fiber laser beam propagating along the welding plume axis can be calculated as:

$$E_A = 1 - \exp \left[\int_5^{\infty} K_{ext}(r=0, h) dh \right] \approx 0.075 \quad (4.8)$$

where the integration begins from the plume height $h_0 = 5$ mm (the reason is described in Sec. 3.2.4).

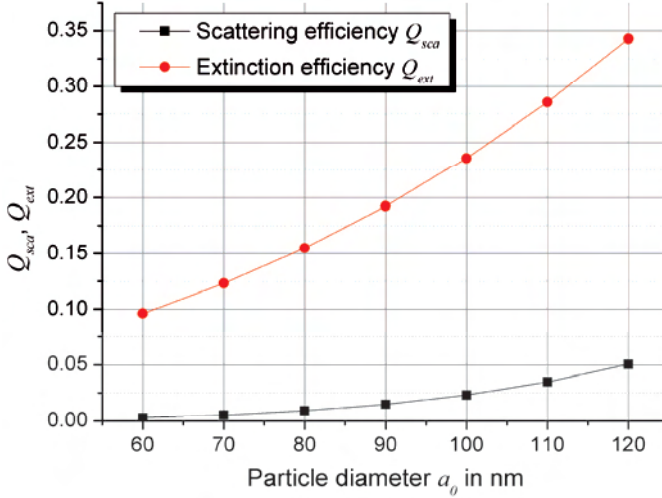


Fig. 4.13. Dependency of the scattering and the extinction efficiencies on the iron particle diameter for the radiation wavelength of $1.07 \mu\text{m}$ calculated from the Mie-scattering theory

However, it should be taken into account that the measurement of the extinction coefficient was carried out with the probe radiation wavelength of $1.3 \mu\text{m}$ while the ytterbium fiber laser radiation wavelength is $1.07 \mu\text{m}$. Since in Sec. 4.1.4 the supposition was confirmed that the observed extinction effect is caused by the small condensed metal vapour particle absorption, the dependency of the total attenuation on the wavelength can be expressed using the light scattering theory:

$$\begin{aligned} E(\lambda) &= 1 - \exp \left[- \int_L K_{ext} dl \right] \approx \int_L K_{ext} dl = \\ &= \frac{\pi}{4} \int_L \int_0^{\infty} C_n(Q_{abs} + Q_{sca}) N(a) a^2 da dl \sim Q_{abs}(\lambda) \end{aligned} \quad (4.9)$$

For radiation wavelengths in a range of $1 \div 1.3 \mu\text{m}$ and the characteristic condensed particle size $a \sim 80$ nm the so-called Rayleigh approximation ($\pi a / \lambda \ll 1$) can be applied:

$$Q_{abs}(\lambda) \sim \text{Im} \left[\frac{m^2(\lambda) - 1}{m^2(\lambda) + 2} \right] \cdot \lambda^{-1} \quad (4.10)$$

For particles consisting of pure iron:

$$m(\lambda_1 = 1.07 \mu\text{m}) = 3.25 + 4.38i, \text{ and } m(\lambda_2 = 1.3 \mu\text{m}) = 3.41 + 5.19i \text{ (see Table 4.2).}$$

Then:

$$\frac{E(\lambda_1)}{E(\lambda_2)} = \frac{\text{Im} \left[\frac{m^2(\lambda_1) - 1}{m^2(\lambda_1) + 2} \right]}{\text{Im} \left[\frac{m^2(\lambda_2) - 1}{m^2(\lambda_2) + 2} \right]} \cdot \frac{\lambda_2}{\lambda_1} \approx 1.63 \quad (4.11)$$

When the ytterbium fiber laser beam with the wavelength of 1.07 μm passes through the whole welding plume height during deep penetration metal welding, the value of its total attenuation E_L should be about 12%. This means that the welding plume can change the parameters of a laser beam propagating through it, and that the radiation power near the keyhole inlet can deviate from the output fiber laser power considerably. However, for deep penetration high power laser metal welding not the average extinction amplitude is most important, but its dynamical characteristics, since it is known that even small variations of the laser beam power can generate of resonance oscillations in the weld pool [59],[60]. The results of high-speed video observation of the welding plume described in Chapter 2 showed that the dynamics of the probe radiation extinction signal established in Sec. 3.2.2 corresponds to the dynamics of the vapour-plasma phase ejections from the keyhole. Therefore, the attenuation of the high-power fiber laser beam has probably similar oscillations and changes at frequencies of about a few kilohertz in the range of a mean-square band with 3%-5% width.

Summary of Chapter 4

1. The experimentally measured average condensed metal vapour particle diameter in the welding plume volume ranges from 80 nm to 110 nm depending on the welding plume height and on the welding process parameters. The particle volume concentration at the welding plume axis has a value of about 10^{10} cm^{-3} and corresponds in general to the predicted values according the models described in Chapter 1.
2. Observed probe radiation extinction is mainly caused by absorption in the cloud of small condensed metal vapour particles.
3. The energy absorbed by the condensed particles is not high enough to cause instantaneous particle evaporation. Therefore, the condensed metal vapour particle cloud is able to attenuate the high-power fiber laser beam propagating through its whole height. Presence of the condensed particles during welding was proved experimentally, not only in the whole welding plume volume but also directly inside the high-power fiber laser beam caustic.

4. Without consideration of the repeated particle evaporation under the influence of laser radiation, the total attenuation of the high-power ytterbium fiber laser beam propagating from the optical welding head down to the metal surface through the whole welding plume height can have a value of more than 10%. Taking into account the temporal dynamics, it can be concluded that this effect is able to cause a significant worsening of the laser beam power stability when the beam reaches the metal surface and enters the keyhole.

Conclusions

The most important results of the dissertation are:

1. Systematic experimental investigations of the vapour-plasma plume generated during deep penetration high-power (10÷20 kW) ytterbium fiber laser beam welding of low-alloyed mild steel plates were carried out.
2. It was confirmed experimentally that free electron temperature and concentration in the laser-induced welding plasma plume are negligibly low ($T < 4500$ K, $n_e < 10^{15}$ cm⁻³). On the basis of these values it can be affirmed that absorption and refraction of high power fiber laser radiation in the welding plasma plume are not able to influence the welding quality in this case.
3. It was shown that the vapour-plasma welding plume is composed of the welding plasma generated in a relatively small area (5-10 mm height) near the metal surface and of an extensive upper part (up to 60-70 mm height) which consists of a small condensed metal vapour particle cloud and is able to absorb electromagnetic radiation.
4. Average condensed metal vapour particle diameter in the welding plume was measured experimentally to vary from 80 nm to 110 nm depending on the welding plume height as well as on the welding process parameters. Volume particle concentration in the cloud on the welding plume axis has a value of about 10^{10} cm⁻³.
5. Extinction of the probe laser radiation in the upper part of the welding plume is mainly caused by absorption in the small condensed metal vapour particles. The extinction coefficient at the probe radiation wavelength of 1.3 μm was measured experimentally to have a value of about a few units per meter which is much higher than the inverse Bremsstrahlung absorption coefficient in the welding plasma plume calculated for this radiation wavelength.
6. Shielding gas (Ar or He) supplied to the welding area leads to intensive cooling of the welding plasma in the lower part of the welding plume down to its complete suppression. However, due to the more intensive metal vapour condensation process in the colder medium above the keyhole, the upper part influence can become even stronger.
7. Total attenuation of the high-power fiber laser beam propagating through the whole welding plume height to the metal surface was estimated to be about 10%. Considering the spatial dynamics of the probe light extinction signals it was concluded that the effect of metal vapour condensation over the keyhole during deep penetration high-power fiber laser metal welding is able to significantly worsen of the laser beam power stability when the beam reaches the keyhole inlet.

Zusammenfassung

Die wichtigsten Ergebnisse der Dissertation sind:

1. Experimentelle Untersuchungen der Dampf-Plasma-Fackel wurden beim Schweißen von niedriglegierten Stählen großer Blechdicke unter Einsatz der Strahlung eines Hochleistungsfaserlasers (10÷20 kW) durchgeführt.
2. Experimentell wurde festgestellt, dass die Temperatur sowie die Volumenkonzentration der freien Elektronen im laserinduzierten Schweißplasma vernachlässigbar gering sind ($T < 4500$ K, $n_e < 10^{15}$ cm⁻³).
3. Es wurde gezeigt, dass neben dem Schweißplasma, das mit einem relativ kleinen Volumen (5-10 mm) nahe der Metalloberfläche entsteht, die Schweißfackel einen größeren Teil (bis 60-70 mm) im oberen Bereich einnimmt, welcher aus der Wolke der kleinen Partikel aus kondensiertem Metalldampf besteht und die Laserstrahlung absorbieren kann.
4. Die experimentell gemessene durchschnittliche Größe der kondensierten Metallpartikel in der Schweißfackel beträgt je nach Fackelhöhe bzw. Schweißprozessparameter 80 nm bis 110 nm. Die Volumenkonzentration der Partikel in der Wolke an der Fackelachse beträgt ca. 10^{10} cm⁻³.
5. Die Extinktion der Prüfstrahlung im oberen Teil der Schweißfackel wird zum großen Teil von der Absorption der kleinen kondensierten Partikel verursacht. Der experimentell gemessene Extinktionskoeffizient für eine Prüfstrahlungswellenlänge von 1.3 µm hatte einen Wert von etwa einigen m⁻¹ und ist damit wesentlich größer als der Koeffizient der inversen Bremsstrahlungsabsorption im Schweißplasma.
6. Schutzgaszufuhr (Ar, He) beim Schweißprozess führt zur effektiven Abkühlung des Schweißplasmas im unteren Teil der Fackel bis zur vollen Unterdrückung. Infolge des intensiveren Kondensationsprozesses über der Dampfkapillare kann aber dabei der Einfluss des oberen Teiles noch stärker werden.
7. Die Gesamtleistungsabschwächung des Hochleistungsfaserlaserstrahls, der durch die Schweißfackel zur Metalloberfläche gelangt, kann variierend einen Wert von bis zu 10% haben. Mit Rücksicht auf die zeitliche Dynamik kann dieser Effekt zu einer erheblichen Verschlechterung der Leistungsstabilität der Laserstrahlung führen, die den Dampfkapillareingang erreicht.

Literature

- [1] V.P. Gapontsev
Fiber lasers burst a laser industry
Proc. of the 12th International Laser Physics Workshop, Hamburg, Germany,
August 25-29, 2003 (LPHYS'03), Paper PS3.
- [2] V. Gapontsev
Ten Years of Ultra-High Power Fiber Laser Era
13th Conference on Laser Optics, St. Petersburg, Russia, 2008.
- [3] M. Larionov, F. Dausinger, S. Sommer, A. Giesen
Thin disc lasers: operation principles and applications (in Russian)
Photonica 3, 2-7, 2009.
- [4] A. Giesen, J. Speiser
Fifteen years of work on thin disc lasers: Results and scaling laws
IEEE Journal of Sel. Topics in Quantum Electronics 13, 598, 2007.
- [5] A. Giesen
Thin Disc Lasers – Power Scalability and Beam Quality
Laser Technik Journal, 2, 42-45, 2005.
- [6] W. Köchner
Thermal lensing in a Nd:YAG laser rod
Appl. Opt. 9(11), 2548, 1970.
- [7] L. Quintino, A. Costy, R. Miranda, D. Yapp
Welding with high power fiber lasers – a preliminary study
Materials & Design, Vol. 28(4), 2007, 1231-1237.
- [8] B. Shiner
High power fiber lasers impact material processing
Industrial Laser Solutions, February 2003, pp 9-11.
- [9] B. Kessler
Power Development and Application of Ultra High Power Lasers
International Colloquium High Power Laser Welding, BAM Berlin, Germany,
2009.
- [10] N.N.
Laser: Jede Aufgabe perfekt lösen
TRUMPF Laser GmbH + Co. KG, Prospekt, 2009.
- [11] K. Löffler
New Development of High Power Laser and their Applications
International Colloquium High Power Laser Welding, BAM Berlin, Germany,
2009.
- [12] A. Giesen, H. Hügel, A. Voß et al
Scalable concept for diode-pumped high-power solid-state lasers
Appl. Phys. B 58, 365, 1994.
- [13] H. Hügel
New solid-state lasers and their application potentials
Optics and lasers in engineering, Volume 34 (2000), 213-239.

- [14] N.N.
Einführung in die industrielle Lasermaterialbearbeitung
Rofin-Sinar Laser GmbH, 2002.
- [15] N.N.
Single Mode Fiber Lasers for Industrial and Scientific Applications
IPG Photonics Brochure,
http://german.ipgphotonics.com/Collateral/Documents/English-US/sm_ipgbrochure.pdf, link from 24.08.2011.
- [16] N.N.
High Power Fiber Lasers for Industrial Applications
IPG Photonics Brochure,
http://german.ipgphotonics.com/Collateral/Documents/English-US/HP_Brochure.pdf, link from 24.08.2011.
- [17] C. Thomy
Laserstrahlschweißen im Dickblechbereich – Herausforderungen und Lösungen
7. Lasertage Weser-Ems, 11-12 Mai, 2011, Papenburg, Germany.
- [18] S. Katayama
Fundamentals of Fiber Laser Welding, International Colloquium High Power Laser Welding, BAM Berlin, Germany, 2009.
- [19] Y. Gainand, J. Mas, J.P. Jansen, J.C. Coiffier, J.C. Dupont, and C. Vautiner
Laser orbital welding applied to offshore pipeline construction
Proc. of 3rd International Conference “Pipeline Technology”, Ostend, Belgium, 21-24 May, 342-372, 2000.
- [20] A. Gumenyuk, S. Gook, M. Rethmeier
Orbitalschweißen im Pipelinebau – Neue Möglichkeiten durch die Anwendung von Hochleistungslasern
Proc. of 8th International Conference on Beam Technology, Halle, Germany, April 14-15, 74-79, 2010.
- [21] A. Sanderson, C.S. Punshon, J.D. Russel
Advanced welding process for fusion reactor fabrication
Fusion Engineering and Design, vol. 49-50, 2000, 77-78.
- [22] M Onozuka, et al.
Manufacturing and maintenance technologies developed for a thick-wall structure of the ITER vacuum vessel
Fusion Engineering and Design, 55 (2001) 397-410.
- [23] U. Jasnau, A. Sumpf
High power fibre laser – new prospects for welding and cutting in shipbuilding
DVS Workshop „Fiber Laser“, Bremen , Germany, May 24, 2005.
- [24] F. Roland, T. Reinert
Laser Welded Sandwich Panels for the Shipbuilding Industry
Advanced Composite Sandwich Steel Structures, Bremen, Germany, September 21, 2000.
- [25] A.G. Grigoryants, I.N. Shiganov, A.I. Misyurov
Technological laser treatment processes (in Russian)
Moscow, MGTU im N.E. Bauman, 2008.

- [26] N.N.
CO₂-Slab laser – Industrielaser zum Laserschneiden
Laserschweißen und Laserbeschriften,
<http://www.rofin.de/index.php?id=161&L=0>, link from 24.08.2011.
- [27] W. Suder, S. Williams, P. Colegrove
Absolute spot size effect on penetration depth in laser welding
Proceedings of the Fifth International WLT-Conference on Lasers in
Manufacturing 2009, Munich, 53-58.
- [28] R. Poprawe, H. Weber, G. Herziger
Fundamentals of laser-induced processes
Institut für Strahlwerkzeuge (IFSW), Universität Stuttgart, Germany, 2004.
- [29] M.F. Zaeh, R. Daub, A. Mahrle, E. Beyer
Influence of the CO₂ in the Ar Process-Gas on the Heat-Conduction Mode Laser
Beam Welding Process with Nd:YAG and Diode Lasers
Proceedings of the Fifth International WLT-Conference on Lasers in
Manufacturing 2009, Munich, 45-52.
- [30] V.S. Mayorov
Effect of capillary thermo-concentration instability during interaction of laser
radiation with matter (in Russian)
Modern laser-information and laser technologies, collected articles of IPLIT RAN
ed. by V.Ya. Panchenko and V.S. Golubev, 2004, 236-248.
- [31] V.S. Golubev
Models of deep penetration of laser radiation in materials (in Russian)
Modern laser-information and laser technologies, collected articles of IPLIT RAN
ed. by V.Ya. Panchenko and V.S. Golubev, 2004, 199-220.
- [32] A.P. Streltsov, V.N. Petrovskiy
Laser parameter choice for high-quality cutting (in Russian)
Journal "RITM" 26, 2007, 44-45.
- [33] H. Pleteit
Analyse und Modellierung der Keyhole-Dynamik beim Laserstrahlschweißen von
Aluminiumlegierungen
Dissertation, Universität Bremen, 2001.
- [34] Z. Szymanski, J. Kurzyzna, W. Kalita
The spectroscopy of the plasma plume induced during laser welding of stainless
steel and titanium
J. Phys. D.: Appl. Phys.30 (1997) 3153.
- [35] Y. Arata, I. Miyamoto
Some fundamental properties of high-power CO₂-laser beam as a heat source
(2) – CO₂-laser absorption characteristics of metal
Trans Japan Welding Society 3(1), 152, 1972.
- [36] A. Poueyo, G. Deshors, R. Fabbro, A.M. de Frutos, J.M. Orza
Study of Laser Induced Plasma in Welding Conditions with Continuous High
Power CO₂-Lasers
Proc. Intl. Conf. on Laser Advanced Materials Processing LAMP'92 (Nagaoka,
Niigata, Japan), Osaka: High Temperature Society of Japan (1992) 323.

- [37] T.J. Rockstroh, J. Mazumder
Spectroscopic studies of plasma during cw laser materials interaction
J. Appl. Phys. 61(3), 1987, 917.
- [38] K.R. Kim and D.F. Farson
CO₂ laser-plume interaction in materials processing
J. Appl. Phys 89(1), 2001, 681-688.
- [39] R. V. Arutyunyan, V.Yu. Baranov, L.A. Bol'shov
Influence of laser radiation on materials (in Russian)
Moscow, Nauka, 1970, 367.
- [40] Yu.P. Raizer
Physics of gas discharge (in Russian)
2-nd ed. Moscow, Nauka, 1992.
- [41] A.A. Vedenov, G.G. Gladush
Physical processes of laser material processing (in Russian)
Moscow: Energoatomizdat, 1985.
- [42] Yu.P. Raizer
Laser spark and spreading of discharges (in Russian)
Moscow, Nauka, 1974.
- [43] A.N. Gresev
Plasma formation during deep penetration laser welding (in Russian)
Modern laser-information and laser technologies, collected articles of IPLIT RAN
ed. by V.Ya. Panchenko and V.S. Golubev, 2004, 228-235.
- [44] M. van Allmen
Laser-Beam Interactions with Materials
Materials Science 2, Berlin: Springer, 1987.
- [45] S. Katayama, S. Oiwa, N. Matsumoto, M. Mizutani and Yo. Kawahito
Fundamentals of fiber laser remote welding and deep penetration welding
Proceedings of the Fifth International WLT-Conference on Lasers in
Manufacturing 2009, Munich, 829-835.
- [46] V.M. Yermachenko, A.P. Kuznetsov, V.N. Petrovskiy, N.M. Prokopova, A.P.
Streltsov and S.A. Uspenskiy
Peculiarities welding of the metals by radiation of powerful laser
19th International Laser Physics Welding, 2010, Foz do Iguaçu, Brazil.
- [47] S.H. Lee, J. Mazumder
Characteristics of disc laser-induced plasma
Proc. of 29th International Congress on Applications of Lasers & Electro-Optics
(ICALEO-2010), September 27-30, Anaheim, USA, 2010.
- [48] I.V. Krivtsun
Simulation of thermal- and mass exchange processes in melt pool, keyhole and
plasma plume during deep penetration laser welding (in Ukrainian)
Project report No. F28.7/028, Paton Welding Institute NASU 2009.
- [49] I.V. Krivtsun, S.B. Sukhorukov, V.N. Sidoretz, O.B. Kovalev
Modelling of the processes of evaporation of metal and gas dynamics of metal
vapour inside a keyhole in laser welding
Paton Welding Journal 10, 16-21, 2008.

- [50] S.I. Anisimov, Ya.A. Imas, G.S. Romanov, Yu.V. Hodyko
Influence of high power radiation on metals (in Russian)
Moscow, Nauka, 1970.
- [51] G. Turichin, E. Zemlyakov, E. Pozdeeva, E. Norman
Volume condensation in plasma plume (in Russian)
Photonics 1/2009(13), 12-14.
- [52] G.A. Turichin, E.V. Zemlyakov
Kinetics of condensed phase nano-cluster formation in plasma plume during
hybrid laser-arc influence on metals (in Russian)
Proceedings of the IV International Conference Beam Technologies and Laser
Application, Saint-Petersburg, Russia, 2009.
- [53] H.C. Van De Hulst
Light Scattering by Small Particles
Dover Publications Inc., 1982.
- [54] C.E. Bohren, D.R. Huffman
Absorption and Scattering of Light by Small Particles
Wiley-Interscience, New York, 1988.
- [55] R.R. Lettfulin
Solid-state aerosols in strong laser field (in Russian)
Journal of Samara Technical University, Phys.-Math. Sciences, No. 4, 1996.
- [56] A. Mutsanawa, H. Yoshida, S. Katayama
Beam-Plume Interaction in Pulsed YAG Laser
Proc. of ICALEO, 1984, 35-42.
- [57] A. Matunawa and T. Ohnawa
Beam-Plume Interaction in Laser Materials Processing
Trans Japan Welding Society, 20(1), 1991.
- [58] Y. Kawahito, K. Kinoshita and S. Katayama
Interaction between YAG or Fiber Laser Beam and Laser-Induced Plume
Proc. ICALEO, 2005.
- [59] T. Klein, M. Vicanek, J. Kroost, I. Decker and G. Simon
Oscillations of the keyhole in penetration laser beam welding
J. Phys. D, 27(1994), 2023-2030.
- [60] T. Klein, M. Vicanek and G. Simon
Forced oscillations of the keyhole in penetration laser beam welding
J. Phys. D, 29(1996), 322-332.
- [61] W. Jüptner, Th. Franz, J. Sikau and G. Sepold
Laser Interaction with Plasma during Material Processing
Laser Physics, Vol.7, No.1, 1997, 202-207.
- [62] Z. Scymanski, J. Kurzyna
Spectroscopic measurements of laser induced plasma during welding with CO₂-
laser
J. Appl. Phys. 76(12), 1994, 7750-7756.
- [63] D.C. Smith and R. Brown
Aerosol-induced air breakdown with CO₂-laser radiation
J. Appl. Phys., Vol.46, No.3, 1975.

- [64] I.A. Bakulin, V.S. Kazakevitch, S.Yu. Pichugin
Pulse CO₂-laser beam attenuation in Ar-medium with fine dispersed Al-particles
(in Russian)
Journal of Technical Physics 76 (11), 2006.
- [65] C. Courteille, Ch. Hollenstein, J.-L. Dorier, P. Gay, W. Schwarzenbach, A.A. Howling, E. Bertran, G. Viera, R. Martins and A. Macarico
Particle agglomeration study in rf-silane plasmas: In situ study by polarization-sensitive laser light scattering
J. Appl. Phys. 80(4), 1996, 2069-2078.
- [66] W. Samenfink, A. Tremmel, R. Dittmann, S. Wittig, K. Schaber, A. Schenkel
Multiple Wavelength Extinction Measurements in Highly Concentrated Aerosols under Industrial Conditions
J. Aerosol Sci., Vol. 25, Suppl. 1, 1994, 565-566.
- [67] A. Michalowski, A. Heß, A. Ruß, F. Dausinger
Plume attenuation under high-power Yb:YAG laser material processing
Proceedings of the Fourth International WLT-Conference on Lasers in Manufacturing 2007, Munich, 357-361.
- [68] J. Greses, P.A. Hilton, C.Y. Bartlow and W.M. Stehen
Plume attenuation under high power Nd:yttrium-aluminium-garnet laser welding
Journal of Laser Appl. (2004) 16, 9-15.
- [69] D. Lacroix, G. Jeandel and C. Boudot
Solution of the radiative transfer equation in an absorbing and scattering Nd:YAG laser-induced plume
J. Appl. Phys. 84(5), 1998, 2443-2449.
- [70] P.Yu. Shcheglov, M. Rethmeier, A. Gumenyuk
Study of dusty plasma influence on radiation of ytterbium fiber laser during deep metal penetration (in Russian)
Proc. of "Scientific Session MEPhI-2010" vol.2, p.194.
- [71] V.N. Petrovskiy, N.M. Prokopova, P.Yu. Shcheglov, A.P. Streltsov, Yu.A. Vdovin, and V.M. Yermachenko
Detection of radiation of powerful fiber lasers reflected back from metals in course of laser processing
Laser Physics Letters Vol. 7, No. 5, 2010, pp. 396-401.
- [72] V.N. Petrovskiy, S.A. Uspenskiy, P.Yu. Shcheglov
Study of shielding gas influence on vapour-plasma plume during high-power fiber laser welding (in Russian)
Proc. of "Scientific Session MEPhI-2011" vol.2, p.87.
- [73] P.Yu. Shcheglov, S.A. Uspenskiy, V.N. Petrovskiy, A.V. Gumenyuk, M. Rethmeier
Study of vapour-plasma plume during high-power fiber laser welding (in Russian)
Proc. of "Scientific Session MEPhI-2011" vol.2, p.90.
- [74] P.Yu. Shcheglov, S.A. Uspenskiy, V.N. Petrovskiy, A.V. Gumenyuk, M. Rethmeier
Laser beam attenuation by plasma plume during high-power fiber laser welding (in Russian)
Proc. of "Scientific Session MEPhI-2011" vol.2, p.91.

- [75] P.Yu. Shcheglov, S.A. Uspenskiy, A.V. Gumenyuk, V.N. Petrovskiy, M. Rethmeier, and V.M. Yermachenko
Plume attenuation of laser radiation during high power fiber laser welding
Laser Physics Letters Vol. 8, No. 6, pp. 475-480.
- [76] V.N. Petrovskiy, S.A. Uspenskiy, P.Yu. Shcheglov, A.V. Gumenyuk, M. Rethmeier
Investigation of vapour-plasma plume during high-power fiber laser welding (in Russian)
Nuclear physics and engineering, vol.2, No.2, 2011, p.159-165.
- [77] P.Yu. Shcheglov, A.V. Gumenyuk, M. Rethmeier, S.A. Uspenskiy, V.N. Petrovskiy
Study of welding plume during high-power fiber laser metal welding (in Russian)
Proceedings of 5th International Conference „Laser Technologies in Welding and Materials Processing“, May 24-27, Katsiveli, Ukraine, 2010, p.142-147.
- [78] P.Yu. Shcheglov, A.V. Gumenyuk, M. Rethmeier, S.A. Uspenskiy, V.N. Petrovskiy, V.M. Yermachenko
Influence of the Welding Plume on Laser Radiation during High Power Fiber Laser Welding
Book of Abstracts “20th International Laser Physics Workshop (LPHYS’11), July 11-15, 2011, Sarajevo, Bosnia and Herzegovina, Paper 08.05.04.
- [79] P.Yu. Shcheglov, S.A. Uspenskiy, V.M. Yermachenko, A.P. Kuznetsov, V.N. Petrovskiy, A.P. Streltsov
Line and Continuum Emission Spectroscopy of the High Power Ytterbium Fiber Laser Welding Plume under Ar and He Shielding Atmosphere
Book of Abstracts “20th International Laser Physics Workshop (LPHYS’11), July 11-15, 2011, Sarajevo, Bosnia and Herzegovina, Paper 08.P.01.
- [80] A.V. Gumenyuk, V.N. Petrovskiy, M. Rethmeier, P.Yu. Shcheglov
Condensed metal particles influence during the high power fiber laser welding
Proc. of XII International science and technology conference „Lasers in Science, technology, medicine“, September 20-23, Gelendzik, Russia, 2011, p.170-177.
- [81] P.Yu. Shcheglov, S.A. Uspenskiy
Peculiarities of vapor-plasma plume during the high power fiber laser metal welding
Proc. of XII International science and technology conference „Lasers in Science, technology, medicine“, September 20-23, Gelendzik, Russia, 2011, p.178-183.
- [82] P. Shcheglov, A. Gumenyuk, I. Gornishkin, M. Rethmeier
Experimental Investigation of the Laser-Plume Interaction during High Power Fiber Laser Welding
Proceedings of the 30th International Congress on Applications of Lasers & Electro-Optics (ICALEO-2011), 23-27 October, Orlando, FL, USA, Paper 1606.
- [83] P.Yu. Shcheglov, A.V. Gumenyuk, I.B. Gornushkin, M. Rethmeier and V.N. Petrovskiy
Vapor-plasma plume investigation during high power fiber laser welding
Laser Physics 7, 2012 (accepted manuscript).
- [84] V.M. Yermachenko, V.S. Mezhevov, V.N. Petrovskiy, and P.Yu. Shcheglov
Peculiarities of regimes generation powerful single-mode fiber laser
Proc. of 17th International Laser Physics Workshop (LPHYS’08), June 30 – July 4, 2008, Trondheim, Norway.

- [85] A.N. Oraevskiy
Gaussian beams and optical resonators
Moscow, MEPhI, 1987.
- [86] C. Wandera
Laser cutting of austenitic stainless steel with a high quality laser beam
PhD Dissertation, Lappeenranta University of Technology, 2006.
- [87] G. Caquot
Remote scanner applications in automotive industry
Journée soudage par faisceau laser, 16 March 2011, Villepinte, France.
- [88] M. Dupenthaler
Systemvergleich Laser: Faser zu CO₂,
7. Lasertage Weser-Ems, 11-12 Mai, 2011, Papenburg, Germany.
- [89] D.T. Swift-Hook and A.E. F. Gick
Welding Research Supplement
Weld. J., 492-S, 1973.
- [90] M. Rethmeier, A. Gumenyuk, S. Grünenwald, F. Vollertsen, S. Olschok, U. Reisgen, H. Kohn
New approaches of welding thick steel plates with fibre lasers
13th Conference on Laser Optics, St. Petersburg, Russia, 2008.
- [91] C. Thomy, T. Seefeld, F. Vollertsen
Humping effect in welding of steel with single-mode fibre laser
Welding in the World, Vol. 52, 5/6, 2008, 9-18.
- [92] M. Rethmeier, S. Gook, M. Lammers, A. Gumenyuk
Laser-Hybrid Welding of Thick Plates up to 32 mm Using a 20 kW Fibre Laser
Journal of the Japan Welding Society 27(2), 2009, 74s-79s.
- [93] A.F. Kaplan and G. Wiklund
Advanced welding analysis methods applied to heavy section welding with a 15 kW fiber laser
Advances in Welding and Allied Technologies, Singapore, 2009.
- [94] S. Gook, A. Gumenyuk, M. Rethmeier
Orbital laser-hybrid welding of pipelines using a 20 kW fibre laser
Proceedings 5th International WLT-Conference on Lasers in Manufacturing, Munich, Germany, 2009.
- [95] G.A. Turichin, I.A. Tsibul'skiy, E.A. Valdaytseva, M.V. Karasev
Theory and technology of thick metal hybrid welding
Beam Technologies and Laser Applications, Proc. of the VI Int. Conference, 2009, 11-18.
- [96] N.B. Delone
Basics of interaction of laser radiation with matter
Editions Frontières, 1993.
- [97] Y. Kawahito, N. Matsumoto, M. Mizutani and S. Katayama
Characterisation of plasma induced during high-power fiber laser welding of stainless steel
Science and Technology of Welding and Joining, 2008 Vol.13, No. 8, 144-748.

- [98] M. Schellhorn, A. Eichhorn, B. Hohenberger
Frühjahrstagung der DPG (Mainz, Germany)
Verhandl. DPG (VI) 32 (1997) 221.
- [99] A.V. Bondarenko, A.P. Kuznetsov, V.N. Petrovskiy, A.P. Streltsov, S.A. Uspenskiy
Peculiarities of metal welding with high-power fiber laser radiation (in Russian)
Proc. of "Scientific Session MEPhI-2010", vol.2, p.185.
- [100] D. Lacroix and G. Jendei
Spectroscopic characterisation of laser-induced plasma created during welding with a pulsed Nd:YAG laser
J. Appl. Phys. 81(10), 1997, 6599-6606.
- [101] Y. Kawahito, K. Kinoshita, N. Matsumoto, M. Mizutani and S. Katayama
Effect of weakly ionised plasma of penetration of stainless steel weld produced with ultra high power density fibre laser
Science and Technology of Welding and Joining, 2008 Vol.13, No. 8, 749-753.
- [102] C. Börner, K. Dilger, V. Rominger, T. Harrer, T. Kruessel, T. Löwer
Influence of Ambient Pressure on Spattering and Weld Seam Quality in Laser Beam Welding with the Solid-State Laser
Proceedings of the 30th International Congress on Applications of Lasers & Electro-Optics (ICALEO-2011), 23-27 October, Orlando, FL, USA, Paper 1604.
- [103] S. Katayama, Y. Abe, R. Ido, M. Mizutani, Y. Kawahito
Deep Penetration Welding with High Power Disk Lasers in Low Vacuum
Proceedings of the 30th International Congress on Applications of Lasers & Electro-Optics (ICALEO-2011), 23-27 October, Orlando, FL, USA, Paper 1614.
- [104] E. Stoffels, W.W. Stoffels, G.M.W. Kroesen
In situ powder diagnostics in low temperature plasmas
Rep. Eindhoven University of Technology.
- [105] L. Boufendy, J. Hermann, A. Bouchoule, B. Dubreuil, E. Stoffels, W.W. Stoffels and M.L. de Giorgi
Study of initial dust formation in an Ar-SiH₄ discharge by laser induced particle explosive evaporation
J. Appl. Phys. 76(1), 1994, 148-153.
- [106] E. Stoffels, W.W. Stoffels, D. Vender, G.M.W. Kroesen, F.J. de Hoog
Laser-particulate interactions in a dusty RF plasma
IEEE Trans. Plasma Sci. 22, 116, 1994.
- [107] G. Mie
Beitrage zur Optik trüber Medien speziell kolloidaler Metallösungen
Ann. Phys., 1908, 25, 377-445.
- [108] Ya.B. Zel'dovich, Yu.P. Raizer
Physics of Shock Waves and High-Temperature Hydrodynamic Phenomena I
New York, NY: Academic Press, 1966.
- [109] V.E. Zuev
Atmosphere transparency for visible and infra-red beams (in Russian)
Moscow, 1966.
- [110] V.S. Letochov
Laser photo-ionisation spectroscopy (in Russian)
Moscow, 1987.

- [111] W. Heitler
The quantum theory of radiation
Oxford University Press, London 1949.
- [112] L.D. Landau, E.M. Lifshitz
The classical theory of fields
Vol. 2, Butterworth-Heinemann 1975.
- [113] V.M. Yermachenko, A.P. Kuznetsov, V.N. Petrovskiy, N.M. Prokopova, A.P. Streltsov, and S.A. Uspenskiy
Specific Features of the Welding of Metals by Radiation of High-Power Fiber Laser
Laser Physics, 8(21), 1530-1537, 2011.
- [114] V.A. Kop'ev, I.A. Kosygi, A.N. Magunov, N.M. Tarasova
Thermometry of intensity distribution in thermal emission spectra (in Russian)
Experimental equipment and technics, 3, p. 1-4, 2006.
- [115] A.N. Magunov
Spectral pyrometry (in Russian)
Experimental equipment and technics, 4, p.5-28, 2009.
- [116] A.P. Kuznetsov, R.O. Buzhinskiy, K.L. Gubskiy, A.S. Savelov, S.A. Sarantsev, A.N. Terehin
Visualisation of plasma-induced processes by projecting system with Cu-vapour laser as brightness (in Russian)
Plasma physics, 4(36), p.1-10, 2010.
- [117] M. Born, E. Wolf
Principles of Optics
7th (expanded) edition I, Cambridge Univ. Press, 2005.
- [118] B.E. A. Saleh, M.C. Teich.
Fundamentals of Photonics
John Wiley & Sons, Inc, 1991.
- [119] I.K. Kikoin
Tables of physical constants (in Russian)
Moscow, Atomizdat, 1976.
- [120] M. Schellhorn
CO-Hochleistungslaser: Charakteristika und Einsatzmöglichkeiten beim Schweißen
Ph.D. thesis, Univ. of Stuttgart, Germany, Munich: Herbert Utz Verlag, 2000.
- [121] Y. Kawahito, K. Kinoshita, N. Matsumoto, S. Katayama
Visualisation of refraction and attenuation of near-infrared laser beam due to laser-induced plume, Journal of Laser Applications
Vol 21 (2), 2009, 96-101.
- [122] M. Mizutani and S. Katayama
Effect on Laser Beam Deflection of Plume and Induced Hot Air above Specimen during Laser Welding
Proc. of ICALEO 2009, LIA, p. 600.
- [123] S.L. Ma, H.M. Gao, G.J. Zhang, and L. Wu
A Versatile Analytical Expression for the Inverse Abel Transform Applied to Experimental Data with Noise
Appl. Spectrosc. 62, p. 701, 2008.

-
- [124] F. Hansen and W.W. Duley
Attenuation of laser radiation by particles during laser materials processing
Journal of Laser Appl. (1994) 6, 137-143.
- [125] N. Ladommatos and H. Zhao
Optical diagnostics for soot and temperature measurement in diesel engines
Progress in Energy and Combustion Science, Vol.24 (3), 221-255, 1998.
- [126] R. Zahoranski, H.-J. Feld, R. Dittmann, W. Samenfink, E. Laile
Das optische Dispersionsquotienten-Verfahren für die on-line/in-situ
Partikelanalyse
Beitrag in der Festschrift: Prof. Dr.-Ing. Dr. h.c. Sigmar Wittig zum 60.
Geburtstag, erschienen am Institut für Thermische Strömungsmaschinen
Universität Karlsruhe (T.H.), Februar 2000.
- [127] R. Dittmann, H.J. Feld, W. Samenfink, S. Wittig
Multiple Wavelength Extinction Technique for Particle Characterisation in Dense
Particle Clouds
Part. Part. Syst. Charact. 11 (1994) 379-384.
- [128] I.E. Leksina, I.V. Penkina
Optical properties of iron in visible and infra-red spectral range (in Russian)
-FMM, 1967, vol.23, p.344.
- [129] K.H. Clemens, J. Jaumann
Magnetooptische und optische Eigenschaften von ferromagnetischen Schichten
im Ultraroten
Zeitschrift für Physik 173, 135-148, 1963.
- [130] M. Kerker, P. Scheiner, D.D: Cooke
The range of validity of the Rayleigh and Thomson limits for Lorenz-Mie
scattering
J. Opt. Soc. Am., 1978, 68, 135-237.

Acknowledgments

This dissertation is compiled from the results of my employment as a member of the research staff at BAM Federal Institute for Materials Research and Testing in Berlin in close collaboration with the Laser Centre of the National Research Nuclear University “MEPhI” in Moscow.

I would like to express my deepest gratitude for excellent guidance to my supervisors Prof. Dr.-Ing. Michael Rethmeier from BAM who approved my initiative for research cooperation between Berlin and Moscow as well as Dr. Viktor Petrovskiy who gave me great support in all experiments and in my defence procedure at MEPhI.

I gratefully acknowledge Dr.-Ing. Andrey Gumenyuk as the head of my working group and a good friend for having always been willing to help me and give me his best suggestions. I was really pleased to have been on friendly terms with him and his family all this time.

I would like to thank all the people in Division 9.3 “Welding Technology” and Division 9.4 “Weld Mechanics” of BAM, especially Florian Tölle for his advices and nice lessons in German, Sören Hähnel and Marco Lammers for the technical help with laser machines and equipment. My special thanks go to Mrs. Margit Bauer for the huge help with the text correction.

I would also like to thank the companies NTO “IRE-Polus” (Fryazino, Moscow), Lasertechnik Berlin, OOO “Lasers and Devices” (Zelenograd, Moscow) and the International Company of Optical Innovations MKOI (Moscow) which have provided their equipment for the experimental part of the work. My special gratitude I would like to show Dr. Alexander Streltsov from NTO “IRE-Polus”, Department of Complex Systems, for a number of useful advices and great organisational help in the experiments at MEPhI.

Collective and individual acknowledgments are also owed to all my colleagues and friends who were daily making my work impressive and unforgettable, in particular to Marcel Bachmann, Sergej Gook, André Schneider, Andrey Vilyanskij and Sergej Uspenskiy.

Last but not least, I would like to thank my parents Olga Shcheglova and Yuriy Shcheglov as well as my brother Alexander Shcheglov for loving me and encouraging me in all my deeds.

Thank you!

Berlin, May 2012

Pavel Shcheglov

Curriculum Vitae

Pavel Shcheglov

Date of Birth: 25 May 1986
Place of Birth: Divnomorskoe, Russia
Nationality: Russian

Education

1993-2001 Divnomorsk Secondary School, Krasnodar
2001-2003 Odinzovo Gymnasium, Moscow
2003-2009 Study: Moscow Engineering Physics Institute (State University)
Faculty: Experimental and theoretical physics
Speciality: Physics of condensed matter
Specialization: Interaction of concentrated radiation fluxes with matter
Certificate: Diplom
2009-2012 Postgraduate study: National Research Nuclear University
"MEPhI", Moscow, Russia
Faculty: Experimental and theoretical physics
Speciality: Laser physics
2009-2012 Postgraduate study: Technical University of Berlin, Germany
Faculty: Mechanical Engineering and Transport Systems
Speciality: Machine engineering

Professional activity

01/2007 – 09/2007 Internship: Federal State Unitary Enterprise "Gas-Turbine
Engineering Research and Production Center "SALUT", Moscow
09/2007 – 04/2009 Engineer: NTO IRE-Polus (IPG Photonics), Moscow
Department: Complex Systems
Since 09/2009 Engineer: BAM Federal Institute for Materials Research and
Testing, Berlin, Germany
Division: Safety of Joined Components / Welding Technology